

TUNABLE SLOT-RING ANTENNA USING VARACTORS

By

Ileana Carrasquillo Rivera

A thesis submitted in partial fulfillment of the requirements for the degree of

MASTER of SCIENCES

in

Electrical Engineering

UNIVERSITY OF PUERTO RICO

MAYAGÜEZ CAMPUS

2003

Approved by:

José Colom Ustariz, PhD.
Member, Graduate Committee

Date

Sandra Cruz Pol, PhD.
Member, Graduate Committee

Date

Rafael Rodríguez Solís, PhD.
President, Graduate Committee

Date

Pedro Vásquez, PhD.
Representative of Graduate Studies

Date

José L. Cruz, PhD.
Chairperson of the Department

Date

Abstract

A dual mode rectangular slot-ring antenna fed with a coplanar waveguide transmission line was tuned over a band of frequencies using varactors. The analysis demonstrated that when varactors are attached to the side slots of the 2.4-GHz rectangular slot-ring antenna, the second resonant frequency could be tuned over a 22 % bandwidth around 3.7 GHz while the first resonance remains unchanged. The first resonant frequency could be tuned over a 4.4 % bandwidth around 2.25 GHz when varactors were connected across the bottom slot. Consequently, varactors were placed across both side slots and across the bottom slot on the same antenna configuration. Results showed that both frequencies could be independently tuned when both sets of varactors are separately biased. A 7.3 % frequency shift around 2.18 GHz and a 12.3 % frequency shift around 4.05 GHz were registered. Agreements between simulations and prototypes results were achieved.

Resumen

Una antena de anillo de ranura rectangular de dos bandas alimentada a través de una guía de onda coplanar fue sintonizada a lo largo de dos bandas de frecuencias usando diodos. El análisis demostró que al colocar un diodo en cada una de las ranuras laterales de una antena de anillo diseñada a una frecuencia de operación de 2.4 GHz, la segunda resonancia puede ser sintonizada en un ancho de banda de 22 % alrededor de 3.7 GHz sin afectar la primera resonancia en absoluto. La primera resonancia fue sintonizada en un ancho de banda de 4.4 % alrededor de 2.25 GHz cuando las diodos fueron colocados a través de la ranura inferior. Además, los diodos fueron colocados tanto a través de la ranura inferior como de las ranuras laterales en una misma configuración. Los resultados demostraron que ambas frecuencias pueden ser sintonizadas de manera independiente cuando ambos pares de diodos son alimentados independientemente. La primera resonancia fue sintonizada en un ancho de banda de 7.3 % alrededor de 2.18 GHz mientras que la segunda resonancia fue sintonizada alrededor de 4.05 GHz con un ancho de banda de 12.3 %. Los resultados simulados y los medidos fueron aproximados.

To my Lord and Savior Jesus Christ for in Him all the treasures of wisdom, knowledge, and enlightenment are hidden.

To Rafael Antonio for he has been not only an excellent professor, but also a wonderful friend

Acknowledgements

Thanks to Dr. Zoya Popovic from the University of Colorado at Boulder for her helpful comments, suggestions, and for letting me be part of her laboratory group for a summer period. I would also like to thank her for providing the SMV1405 tuning varactors. Thanks to Dr. Félix Fernández for providing the gold bonding wire. In addition, thanks to Amada Castro and Néstor D. López for their valuable help and patience.

Special thanks to, Dr. Rafael A. Rodríguez Solís, Dr. José Colom, Dr. Sandra Cruz Pol, Dr. Miguel Vélez, and Dr. Luis O. Jiménez for sharing with me their valuable knowledge in electrical engineering. This work was sponsored by a CAREER award granted by the National Science Foundation.

Chapter 4. Results and Discussions	29
Section 4.1 Partial Characterization of Rectangular Slot-Ring Antennas	29
Section 4.1.1 Effect Produced by Variations to the Width of the Four Slots	30
Section 4.1.2 Effects on the Antenna Resonant Frequency due to Variations of λ_g	33
Section 4.1.3 Effects produced by variations in w_1	35
Section 4.1.4 Effects produced by changes to w_2 , w_3 , and w_4	36
Section 4.2 Electrical Tuning on the Rectangular Slot-Ring Antenna	44
Section 4.2.1 Experiment with Varactors Attached at Both Side Slots	44
Section 4.2.2 Experiment with Varactors Attached at the Bottom Slot	48
Section 4.2.3 Experiments with Varactors on a 2.4-GHz Rectangular Slot-Ring Antenna	50
Section 4.2.4 Experiments with Varactors on a 6-GHz Rectangular Slot-Ring Antenna	64
Section 4.3 Effect of a Short and Open-Circuited Stub on a Slot-Ring Antenna ..	71
Section 4.4 Gain, Polarization and Radiation Pattern	80
Section 4.5 Summary	85
 Chapter 5. Conclusions and Recommendations	 87
Section 5.1 Conclusions	87
Section 5.2 Recommendations	89
 References	 90

List of Tables

Table 4.1.1.	Slot-Ring Antennas Dimensions with Same Perimeter and Different Slot Widths	30
Table 4.1.2.	Frequency Shift Calculations for Antennas with Different Slot Widths but Having the Same Perimeter $\lambda_g(w = \lambda/75)$	32
Table 4.1.3.	Slot-Ring Antenna Dimensions with Variations in Width and Perimeter	33
Table 4.1.4.	Description of the Slot-Ring Antenna Dimensions	35
Table 4.1.5.	Slot-Ring Antennas Dimensions	37
Table 4.1.6.	Slot-Ring Antenna Dimensions	40
Table 4.2.1.	Slot-Ring Antenna Dimensions	45
Table 4.2.2.	Slot-Ring Antenna Dimensions	48
Table 4.2.3.	2.4-GHz Slot-Ring Antenna Dimensions	51
Table 4.2.4.	6-GHz Slot-Ring Antenna Dimensions	64

List of Figures

Figure 2.1.1.	Electrical fields in cylindrical coordinates	5
Figure 2.1.2.	Electrical field distribution in a slotline	6
Figure 2.2.1.	Distribution of the magnetic current on a rectangular slot antenna	7
Figure 2.2.2.	Bandwidth enhancement techniques for slot-ring antennas	10
Figure 2.3.1.	Coplanar waveguide	11
Figure 2.4.1.	P-n junction	12
Figure 2.4.2.	Transmission line equivalent circuit	14
Figure 3.1.1.	Description of the rectangular slot-ring antenna dimensions	16
Figure 3.2.1.	Slot-ring antenna configuration without varactors	21
Figure 3.2.2.	Slot-ring antenna configuration with a capacitor	22
Figure 3.2.3.	Slot-ring antenna layout with varactors connected on lateral slots	23
Figure 3.2.4.	Slot-ring antenna layout with varactors connected on bottom slots	24
Figure 3.2.5.	Tunable dual mode slot-ring antenna configuration	26
Figure 3.2.6.	Bias implementation	27
Figure 4.1.1.	Input reactance of slot-ring antennas with the same perimeter but different slot widths	31
Figure 4.1.2.	Input resistance of slot-ring antennas with the same perimeter but different slot widths	32
Figure 4.1.3.	Input reactance for slot-ring antennas with a physical perimeter corresponding to λ for each width	34
Figure 4.1.4.	Return loss for antennas with different perimeters and widths	34

Figure 4.1.5.	Representation of the impedance matching of a slot-ring antenna on a Smith Chart	36
Figure 4.1.6.	Input impedance curves with changes in w	38
Figure 4.1.7.	Graph of bandwidth percent versus ratio between upper slot and remaining slots	39
Figure 4.1.8.	Graph of the input reactance of a slot-ring antenna when variations to w_2 were performed	41
Figure 4.1.9.	Graph of the input resistance for a slot-ring antenna when variations to w_2 were performed	41
Figure 4.1.10.	Graph of the input reactance for a slot-ring antenna when variations to w_3 were performed	42
Figure 4.1.11.	Graph of the input resistance for a slot-ring antenna when variations to w_3 were performed	42
Figure 4.1.12.	Graph of the input reactance for a slot-ring antenna when variations to w_2 and w_4 were performed	43
Figure 4.1.13.	Graph of the input resistance for a slot-ring antenna when variations to w_2 and w_4 were performed	43
Figure 4.2.1.	Graph of the return loss of a rectangular slot-ring antenna when varactors are connected across both side slots	46
Figure 4.2.2.	Graph of the input reactance when varactors are connected at both side slots	46
Figure 4.2.3.	Graph of the input resistance of a slot-ring antenna with varactors connected at both side slots	47
Figure 4.2.4.	Return loss graph of a slot-ring antenna with varactors connected at the bottom slot	49
Figure 4.2.5.	Input resistance curves of a slot-ring antenna with varactors connected at the bottom slot	49
Figure 4.2.6.	Input reactance curves of a slot-ring antenna with varactors connected at the bottom slot	50

Figure 4.2.7.	Graph of the return loss for the 2.4-GHz slot-ring antenna with matching stubs and without varactors	51
Figure 4.2.8.	Graph of the return loss of the 2.4-GHz slot-ring antenna with varactors connected at each side slot	53
Figure 4.2.9.	Graph of the input reactance curves of a 2.4-GHz slot-ring antenna with varactors connected at each side slot	53
Figure 4.2.10.	Graph of the input resistance curves of a 2.4-GHz slot-ring antenna with varactors connected at each side slot	54
Figure 4.2.11.	Graph of the measured return loss of the 2.4-GHz slot-ring antenna with varactors connected at each side slot	55
Figure 4.2.12.	Graph of the measured reactance of the 2.4-GHz slot-ring antenna with varactors connected at each side slot	55
Figure 4.2.13.	Graph of the measured resistance of the 2.4-GHz slot-ring antenna with varactors connected at each side slot	56
Figure 4.2.14.	Graph of the return loss of the 2.4-GHz slot-ring antenna with varactors connected to the bottom slot	57
Figure 4.2.15.	Graph of the input reactance curves of a 2.4-GHz slot-ring antenna with varactors connected at the bottom slot	57
Figure 4.2.16.	Graph of input resistance curves of a 2.4-GHz slot-ring antenna with varactors connected at the bottom slot	58
Figure 4.2.17.	Graph of the measured return loss of the 2.4-GHz slot-ring antenna with varactors connected to the bottom slot	59
Figure 4.2.18.	Graph of the measured reactance of the 2.4-GHz slot-ring antenna with varactors connected to the bottom slot	59
Figure 4.2.19.	Graph of the measured resistance of the 2.4-GHz slot-ring antenna with varactors connected to the bottom slot	60
Figure 4.2.20.	Input reactance curves for a 2.4-GHz slot-ring antenna having a 3-pF capacitance at the bottom slot while the varactors on the sides varied from 1 pF to 3 pF	61

Figure 4.2.21. Input resistance curves for a 2.4-GHz slot-ring antenna having a 3-pF capacitance at the bottom slot while the varactors on the sides varied from 1 pF to 3 pF	62
Figure 4.2.22. Return loss curves for a 2.4-GHz slot-ring antenna having a 3-pF capacitance at the side slots while the varactors on the bottom slot varied from 1 pF to 3 pF	63
Figure 4.2.23. Input resistance curves for a 2.4-GHz slot-ring antenna having a 3-pF capacitance at the side slot while the varactors on the bottom varied from 1 pF to 3 pF	63
Figure 4.2.24. Graph of the return loss for the 6-GHz slot-ring antenna without varactors	65
Figure 4.2.25. Resistance and reactance curves of the 6-GHz slot-ring antenna without varactors	66
Figure 4.2.26. Graph of the return loss of the 6-GHz slot-ring antenna with varactors connected at each side slot	67
Figure 4.2.27. Graph of the input reactance curves of a 6-GHz slot-ring antenna with varactors connected at each side slot	67
Figure 4.2.28. Graph of the input resistance curves of a 6-GHz slot-ring antenna with varactors connected at each side slot	68
Figure 4.2.29. Graph of the return loss of the 6-GHz slot-ring antenna with varactors connected to the bottom slot	69
Figure 4.2.30. Graph of the input reactance curves of a 6-GHz slot-ring antenna with varactors connected to the bottom slot	70
Figure 4.2.31. Graph of the input resistance curves of a 6-GHz slot-ring antenna with varactors connected to the bottom slot	70
Figure 4.3.1. 2.4 GHz antenna layout matched to 50 Ω with a short-circuited stub	72
Figure 4.3.2. Return loss curves of a slot-ring antenna with different short-circuited stub lengths	72
Figure 4.3.3. Input resistance curves of a slot-ring antenna with different short-circuited stub lengths	73

Figure 4.3.4.	Input resistance curves around the first resonant frequency of a slot-ring antenna with different short-circuited stub lengths	73
Figure 4.3.5.	Input reactance curves of a slot-ring antenna with different short-circuited stub lengths	74
Figure 4.3.6.	Return loss curves of a slot-ring antenna with different short-circuited stub widths	75
Figure 4.3.7.	Input resistance curves of a slot-ring antenna with different short-circuited stub widths	75
Figure 4.3.8.	Return loss curves of a slot-ring antenna with different open stub lengths	76
Figure 4.3.9.	Input resistance of a slot-ring antenna with different open stub lengths	77
Figure 4.3.10.	Input reactance of a slot-ring antenna with different open stub lengths	77
Figure 4.3.11.	2.4 GHz antenna layout matched to 50Ω with an open-circuited stub	78
Figure 4.3.12.	Return loss curves of a slot-ring antenna with different open stub widths	79
Figure 4.3.13.	Input resistance curves of a slot-ring antenna with different open stub widths	79
Figure 4.4.1.	Electric field distribution of the slot-ring antenna at 2.3 GHz	80
Figure 4.4.2.	Gain (dBi) of a slot-ring antenna vs. theta at 2.3 GHz and $\phi = 0^\circ$	81
Figure 4.4.3.	Gain (dBi) of a slot-ring antenna vs. theta at 2.3 GHz and $\phi = 90^\circ$	82
Figure 4.4.4.	Electric field distribution of the slot-ring antenna at 4.15 GHz	83
Figure 4.4.5.	Gain (dBi) of a slot-ring antenna vs. theta at 4.15 GHz and $\phi = 0^\circ$	83

Figure 4.4.6. Gain (dBi) of a slot-ring antenna vs. theta at 2.3 GHz and $\phi = 90^\circ$	84
Figure 4.4.7. Gain (dBi) of a slot-ring antenna vs. theta at 2.3 GHz and $\phi = 45^\circ$	85

Chapter 1. Introduction

1.1 Justification

In the past decades there has been an increasing and unstoppable growth in technology, and wireless communication systems have not been an exception. Wireless communication systems have not only increased in terms of improved technology but also in terms of popularity. Wireless communication services have penetrated our daily lives so fast like no other invention of the past century. The increasing demand for cellular phone services, wireless Internet access, teleconferencing, wireless cable television, among others, will force such systems to provide very large bandwidths as well as simultaneous access to different systems through the same device, which can be accomplished with multiband technology. Hence, it is of great interest to characterize antennas that can be used for antenna array designs, or single antenna elements that can provide wide bandwidth, multiple resonances, or tuning agility.

The need of wide bandwidths will force wireless communications systems to use higher frequency bands in the microwave and millimeter wave regions; frequency bands in which slot antennas are often used. However, slot antennas have limited bandwidth problems and few bandwidth enhancement techniques have been published. This is the reason why this type of antenna has captured the attention of many researchers. One way proposed in [1] to increase bandwidth is by adjusting the antenna dimensions in order to tune the antenna for better reception. For slot antennas, it is inconvenient to physically

change its dimensions; nevertheless, the same effect can be achieved electrically with the help of varactors.

This research focuses on a technique to increase the operating frequency range of a rectangular slot-ring antenna, as a single element, using varactors as the tunable device. The antenna is fed using coplanar waveguide (CPW) transmission lines in order to keep low profile, easier construction, low cost, and small size, desirable characteristics when choosing the antenna element for a commercial design. The antenna proved to be a tunable dual mode antenna. Implementing the slot-ring antenna and measuring its parameters validated these results.

1.2 Objectives

The main goal of this research was to tune a rectangular slot-ring antenna over a wide range of frequencies with varactors, as well as to explain their effect in the antenna. However, before introducing varactors into the antenna configuration, it was intended to perform a partial characterization of the slot-ring antenna in which every dimension was varied to check its effect in the antenna response. The partial characterization suggested the places where varactors must be attached by predicting the dimensions that strongly contribute to a frequency shift. It was desired to construct and measure the antenna parameters to validate simulations.

1.3 Project Description

Slot-ring antennas are often one guided-wavelength in perimeter at the first resonance and designed over a dielectric layer. These antennas can be fed either by electromagnetic coupling with a microstrip line or with a coplanar waveguide (CPW) transmission line. Nevertheless, it is desirable to use CPW in cases where low profile and simple implementation is required. Some researchers have been focusing in different techniques to improve the slot antennas bandwidth since these elements suffer of limited bandwidths. One way of improving bandwidth is by tuning the antenna. It has been found in [2, 3] that single-slot antennas that are electromagnetically fed can be tuned over a wide range of frequencies using variable capacitors. However, a tunable slot-ring antenna fed with a coplanar waveguide transmission line has not yet been found in literature, neither a full characterization of this type of antenna.

This thesis presents a partial characterization of a rectangular slot-ring antenna. The term partial means that only variations made to the widths of each slot that forms the antenna were analyzed, for the widths will be the only dimensions electrically affected by the varactor. The characterization suggested the best places to attach the varactors on a rectangular slot antenna configuration.

Varactors were attached to both side slots and to the bottom slot, as well. When the varactors were connected to both side slots, tuning of the second resonant frequency was achieved, while tuning of the first resonant frequency was accomplished when varactors were attached to the bottom slot. This behavior introduced a novel rectangular slot-ring antenna configuration, which has a set of varactors attached to the side slots and a second set attached to the bottom slot. Simulations proved that it is possible to tune

both resonant frequencies in separate ways, suggesting the implementation of a tunable dual mode slot-ring antenna configuration. This configuration was implemented and tested in order to validate simulations.

Recent research has proven that slot-ring antennas can be implemented in many wireless applications. This tunable slot-ring antenna fed with coplanar waveguide transmission lines keeps low profile, compact, and simple configuration, making it attractive for array designs and single element applications. From amplifiers, mixers, and receivers [4] to digital audio broadcasting, satellite digital audio radio system, and slot arrays for Doppler radar and weather applications, slot-ring antennas promise to offer good performance, fulfilling every requirement including bandwidth enhancement.

1.4 Work Organization

Basic theory about slotlines, antennas, varactors, and coplanar waveguide transmission lines is described in Chapter 2, as well as a brief description of recent studies based on slot-ring antennas and their applications. The third chapter explains in detail how the antenna was partially characterized to establish where to place the varactors. The procedure to simulate the varactors and the methodology used to tune the slot-ring antenna with varactors is also explained in Chapter 3. The simulated and measured results are presented in Chapter 4 followed by an explicit discussion of the results. Finally, Chapter 5 presents conclusions of the partial characterization and the tuning agility of the rectangular slot-ring antenna, including recommendations for future research.

Chapter 2. Theory and Applications

2.1 Slotline Characteristics

A slotline is a planar transmission structure that consists of a dielectric substrate with a narrow slot etched on the ground plane on one side of the substrate. Its geometry is planar, which makes it suitable for microwave integrated circuits. Slotlines can be employed as short circuits, high impedance lines, stubs, and resonant or nonresonant antennas [5].

The slotline electric field contains three components; however, in far field there is only one component in the ϕ -direction as shown in Figure 2.1.1. The major electric field component of the traveling wave along the slot is oriented across the slot in the plane of metallization on the dielectric substrate. If the width of the slot w is much smaller than the free-space wavelength, the electric field across the slot may be modeled by an equivalent line source of magnetic current.

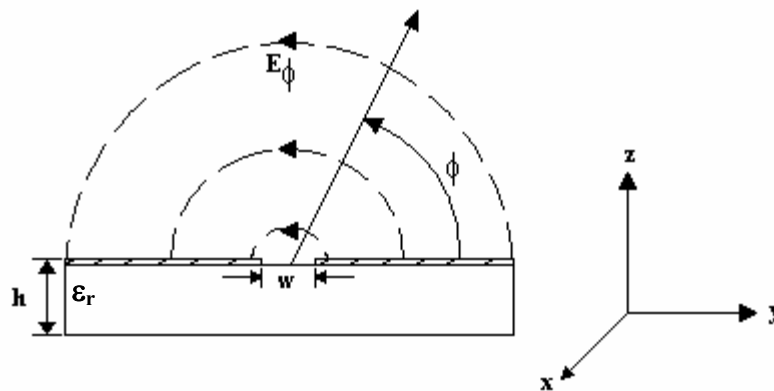


Figure 2.1.1. Electrical fields in cylindrical coordinates

Figure 2.1.2 shows that the field components are not only confined to the substrate. They extend on both sides of the substrate and metallization layer, distributing the energy between the substrate and the air regions. Therefore, the substrate permittivity ϵ_r is greater than the effective dielectric constant for a slotline ϵ_{re} , which is basically the average dielectric constant of the two media.

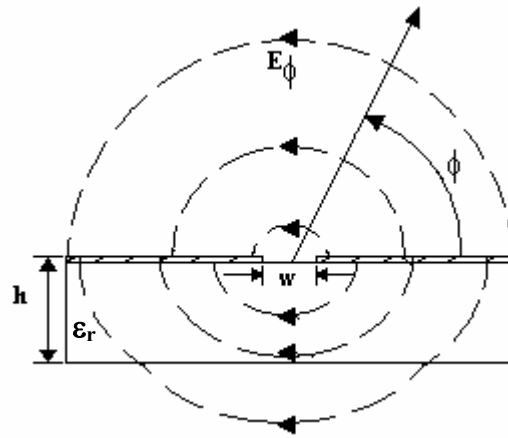


Figure 2.1.2. Electrical field distribution in a slotline

Slotlines can be easily incorporated in microwave circuits by etching the slotline circuit in the ground plane. Besides, many circuit functions that were not possible or easy to construct such as short circuits, balanced circuits and tight coupling can now be achieved. Slotlines also add flexibility in the design by introducing wider range of line impedances, and series and parallel device mounting; features that have given rise to novel microwave circuits consisting of planar antennas directly integrated with amplifiers and mixers.

2.2 Slot-Ring Antennas Applications

An example of a slotline that is employed as a resonant antenna is a slot-ring antenna. A slot-ring antenna is the dual of the microstrip ring antenna [6]. They are usually one guided-wavelength in perimeter at the first resonant frequency and designed on ground plane over a substrate layer. To use the structure as an antenna, the first-order mode must be excited, and the impedance seen by the source must be real at resonance; that is, all the power delivered to the ring will be radiated. Figure 2.2.1 shows the distribution of the magnetic current, J_m , on a rectangular slot-ring antenna.

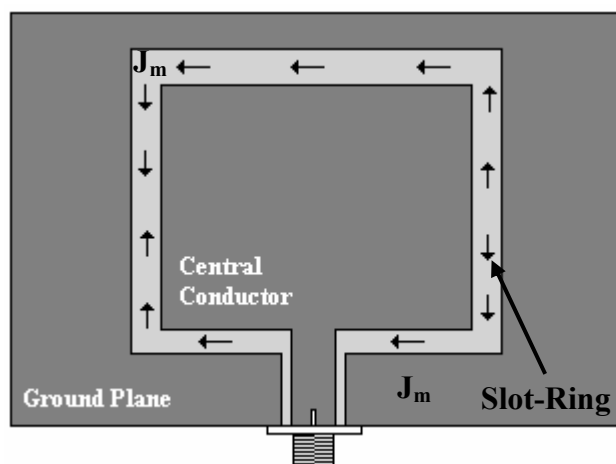


Figure 2.2.1. Distribution of the magnetic currents on a rectangular slot antenna

Researchers choose to analyze slot antennas, including slot-ring antennas, around its second resonance since the real part of the impedance is lower (usually 70-100 Ω) when compared to the impedance at the first resonance, which in some cases is five times higher or more. One disadvantage of the slot-ring antenna is its limited bandwidth and researchers are focusing their investigations in efficient bandwidth improving methods. However, slot-ring antennas are still an attractive alternative for its compact geometry,

potential for polarization diversity, and capability to transmit and receive on both sides of the ground plane. These antennas have also been used in many applications such as millimeter-wave receivers, transmitters, and imaging arrays, as well as aircraft landing systems and automotive anti-collision systems [4].

Second resonance slot antennas can be employed in planar active antenna arrays due to their ability to transmit and receive on both sides of a microstrip plane and to their capability to be orthogonally polarized. The orthogonal polarization characteristic ensures amplifier stability. For example, in [3], a 7 GHz-cross-slot antenna was designed as a mixer/phase detector active antenna. Furthermore, it was electrically tuned over a 10% bandwidth by incorporating a varactor diode into the microstrip feedline.

In [7], Minard and Louzir presented a slot-ring antenna with a λ_s perimeter designed over a 0.81 mm thick substrate with 3.38 of relative permittivity. It was fed by electromagnetic coupling to a microstrip line etched on the opposite side of the substrate. This feeding microstrip line crosses the antenna in two points situated at 90 degrees on the annular slot, and extends $\lambda_m/8$ beyond the second point, where λ_m is the guided wavelength of the microstrip line [7]. The microstrip line length should be located in a position where 90 degrees phase shift are introduced. This technique provided a wide bandwidth since there is a slow variation of the E field magnitude around the two-excitation points. The antenna presented an impedance bandwidth of 19.36%. Besides, it has been reported in [8] that slot-ring antennas also allow switching between linear and left as well as right hand circular polarizations with a single antenna element. Results showed that the antenna in circular polarization mode presented a 30% bandwidth around 2.4 GHz.

An interesting application of slot-ring antennas is presented in [9], in which two conformal, shallow cavity backed, slot antennas are combined into a single configuration to operate at different frequencies and with different electrical characteristics. This combo antenna is intended for use in automobile applications, especially for receiving digital audio broadcasting and satellite digital audio radio system.

Misra and Chowdry presented in [10] a concentric microstrip triangular ring structure designed using the log-periodic principle and also fed with electromagnetic coupling to a microstrip line. The antenna presented a 3.72% bandwidth at a center frequency of 3.76 GHz. The dual structure in slot could be investigated.

Slot-ring antennas can also be excited using coplanar waveguide (CPW) transmission lines. It is desirable to use CPW in cases where low profile and simple implementation is required. The tunable rectangular slot-ring antenna presented in this thesis is fed with coplanar waveguide transmission lines keeping low profile, compact and simple configuration; attractive features for single antenna elements and array designs.

CPW-fed rectangular slot-ring antennas, also called in literature as coplanar patch antennas (CPA), are described as a rectangular patch surrounded by a thin slot. Some research engineers call the slot antennas patch antennas because the design rules for microstrip patch antenna hold for the coplanar patch antenna [11], as well. In [11], it was found that the resonant length of a CPA $L \approx 0.47\lambda_0 / \sqrt{\epsilon_r} \approx 1/2\lambda_0 / \sqrt{\epsilon_r}$ follows the same rule as for the microstrip patch antenna. In addition, microstrip patch antennas and CPA with a back ground conductor have very similar field distribution [11].

Researchers have improved the bandwidth of these antennas by either shortening the upper slot [12] or replacing the rectangular patch for a bow-tie patch [13]. The antenna configuration used in [12] is shown in Figure 2.2.2a. They reported a 40% bandwidth at 10 GHz (4 GHz) for antenna with sh equal to 10 mm. In [13] as the parameters h_1 and h_2 , shown in Figure 2.2.2b, were increased bandwidth enhancement was obtained.

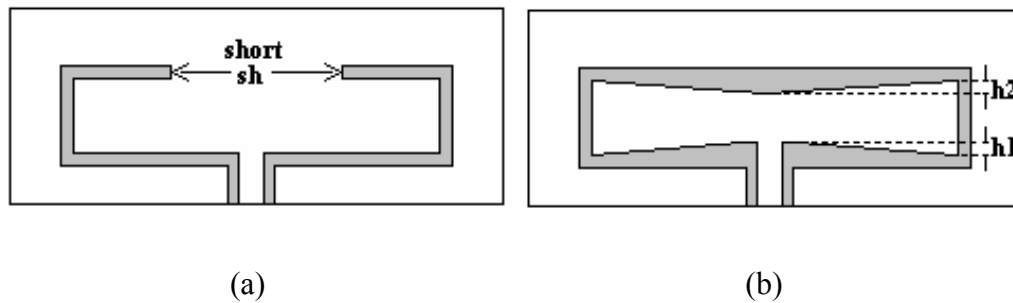


Figure 2.2.2. Bandwidth enhancement techniques for slot-ring antennas: (a) shortening the upper slot and (b) with a bow-tie patch

2.3 Coplanar Waveguide Transmission Lines

Coplanar lines are defined in [14] as those transmission lines where all the conductors are in the same plane. Examples of these lines are slotline, coplanar strip, and coplanar waveguide. The later was used as the feeding line in the design described in this project. Coplanar waveguide transmission lines have gained popularity, due to inherent advantages such as easier construction, no via holes are needed for ground connection, good grounding, less radiation at discontinuities, lower conductor loss, and easier mounting of lumped components in shunt or series configuration [15]. They are low profile, conformal, light in weight, can be easily integrated with active devices and have

found to provide a wider bandwidth when compared with a microstrip line. Furthermore, their performance is comparable, and in some cases better, than microstrip lines in terms of dispersion and losses.

The CPW consists of two slots each of width, s , printed on a dielectric substrate separated by a central conductor of width denoted by w , as shown in Figure 2.3.1a. The electrical and magnetic field configurations are presented in Figure 2.3.1b. A longitudinal component of the magnetic field exists at higher frequencies, reason for which the mode of propagation in this type of lines becomes non-TEM. This characteristic makes it suitable for nonreciprocal ferrite devices.

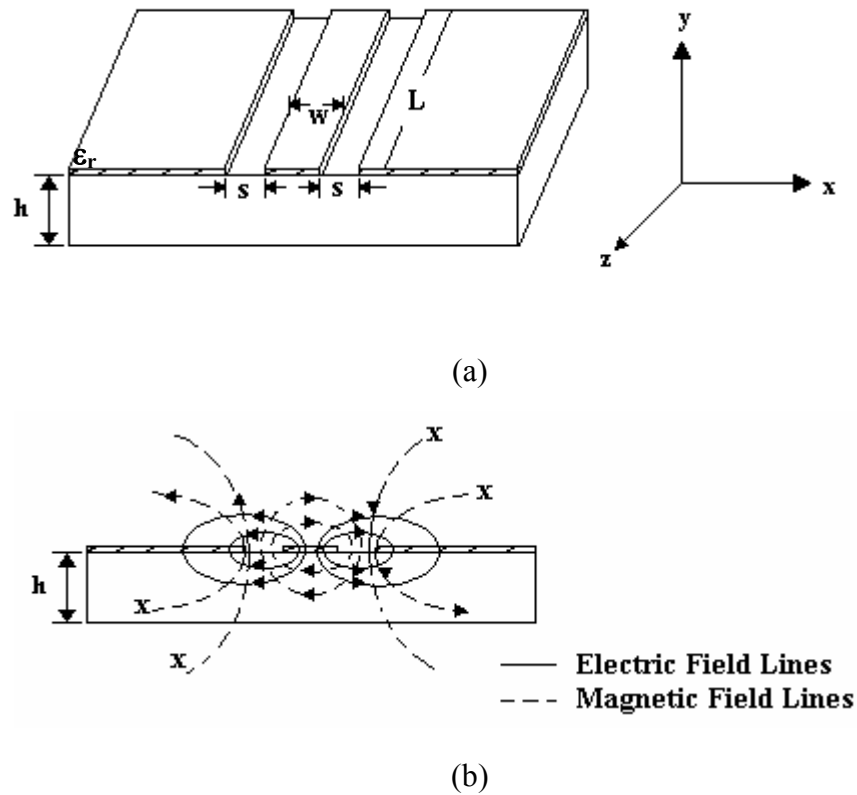
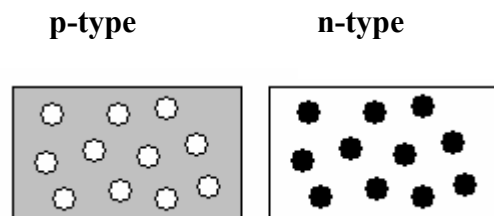


Figure 2.3.1. Coplanar Waveguide: (a) geometry and (b) electric and magnetic field distribution

2.4 Varactors

Researchers have been focusing in different techniques to improve the slot antennas bandwidth since these elements suffer of limited bandwidths. Tuning is considered as a bandwidth improvement technique [1]. In [2, 3], electromagnetically fed single-slot antennas could be tuned over a wide range of frequencies using varactors.

A p-n junction is one of the crucial keys to solid-state electronics. When p-type and n-type materials are placed in contact with each other, the junction behaves very differently than either type of material by itself. Current will flow readily in one direction (forward biased) but not in the other (reverse biased), creating the basic diode. The charge transport process in the two materials determines the one-direction behavior. Figure 2.4.1a shows the open circles in the p-type material, which represents the holes or positive charge carriers. The solid circles on the right of the junction represent the available electrons from the n-type dopant. Near the junction, electrons combine with holes, creating what is called the depletion region, shown in Figure 2.4.1b.



(a)

Figure 2.4.1. P-n junction: (a) geometry and (b) when a reversed voltage is applied.

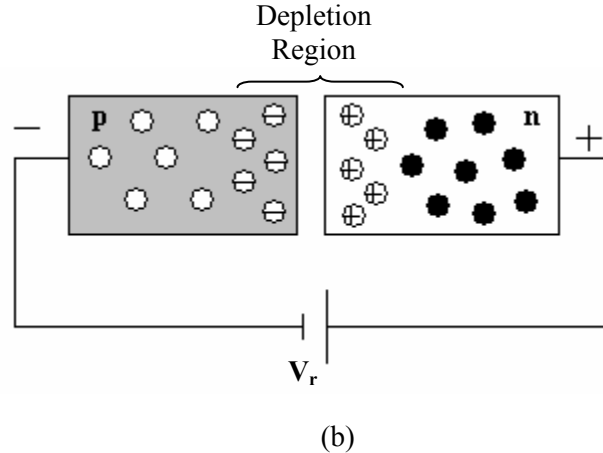


Figure 2.4.1 Continued

In the p-type region there are holes from the acceptor impurities and in the n-type region there are extra electrons. When a p-n junction is formed, some of the electrons from the n-region that have reached the conduction band are free to diffuse across the junction and combine with holes. Filling a hole makes a negative ion and leaves behind a positive ion on the n-side. A space charge builds up, creating a depletion region, which inhibits any further electron transfer unless it is helped by putting a forward bias on the junction [16].

A varactor diode uses a p-n junction in reverse bias and has a structure such that the capacitance of the diode varies with the reverse voltage [17]. When a reverse voltage is applied to a p-n junction, the holes in the p-region are attracted to the anode terminal creating the depletion region where there is little current. This region is practically devoid of carriers and behaves as the dielectric material of a capacitor. As the reversed voltage across the varactor increases, so does the depletion region; and since there is an inversely proportional relationship between the capacitance and the dielectric thickness,

the capacitance will decrease as the voltage across the p-n junction increases. The capacitance-voltage relation is nonlinear.

The use of a varactor in tunable antenna configurations follows from the fact that when a reversed voltage is applied to a variable capacitor connected to a microstrip line, its electrical length will be varied. As the reversed voltage is increased, the depletion region increases and; therefore, the capacitance decreases. As the capacitance decreases the resonant frequency increases. For a better understanding, this concept is explained with a transmission line equivalent circuit of the slot antenna and its feedline. The circuit, presented in Figure 2.4.2, shows the transmission line, L , connected in series with the varactor impedance. When a voltage is applied to the varactor, the reactance of the input impedance, Z_{in} , will be varied, as well as the effective length of the line, changing the resonant frequency and consequently increasing the tunable bandwidth.

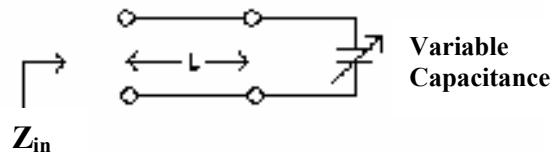


Figure 2.4.2. Transmission line equivalent circuit

Thus, if a varactor is connected to a microstrip feedline of a single slot antenna, as in [3], the lowest capacitance that can be achieved makes the antenna stub electrically smaller, tuning the antenna at the higher frequency possible. In [2], the antenna implemented could be tuned from 4.69 GHz to 4.87 GHz when a varactor was applied at the end of the stub. Therefore, if varactors are applied to a slot-ring antenna, its

dimensions will be changed with voltage variations and; consequently, the resonant frequency will be varied.

2.5 Summary

Researchers have suggested the use of slot-ring antennas in many wireless applications that go from amplifiers, mixers, and receivers to digital audio broadcasting, satellite digital audio radio system, and slot arrays for Doppler radar and weather applications. Furthermore, these antennas can be fed with coplanar waveguide transmission line to keep their planar characteristic, which provides easier construction, and mounting of lumped components, low profile and light weight. Nevertheless, their bandwidth limitation is still under investigation.

To improve the performance of these antennas, engineers have used tuning elements such as varactors in order to increase the antenna operating bandwidth. However, literature presents slot antennas that have been tuned by attaching tunable elements to the microstrip that feeds the antenna. When a reversed voltage is applied to a varactor, the electrical length of the microstrip line changes and so does the resonant frequency. Therefore, if varactors are connected across the slots that form a slot-ring antenna, the slot width will be changed and the antenna will resonate at a different frequency. The idea of implementing varactors into a CPW-fed slot-ring antenna configuration is developed in the following chapters.

Chapter 3. Methodology

3.1 Physical Variations on a Rectangular Slot-Ring Antenna

All simulations for the rectangular slot-ring antenna were performed using Ansoft Ensemble V.8 software. The slot-ring antenna was designed on a substrate with a relative permittivity, ϵ_r , of 6.15 and a thickness, h , of 0.635 mm, and fed with a coplanar waveguide (CPW) transmission line. The advantages of CPW include low profile, conformal, light in weight, no via holes needed for ground connection, good grounding, easier construction, less radiation at discontinuities and lower conductor loss. They can also be integrated with active devices and provide large bandwidth. The dimensions of the CPW transmission line were calculated using ADS LineCalc for a specific resonant frequency of 2.9 GHz since this frequency band is used in cellular communication systems. The antenna perimeter is one guided-wavelength at the first resonance.

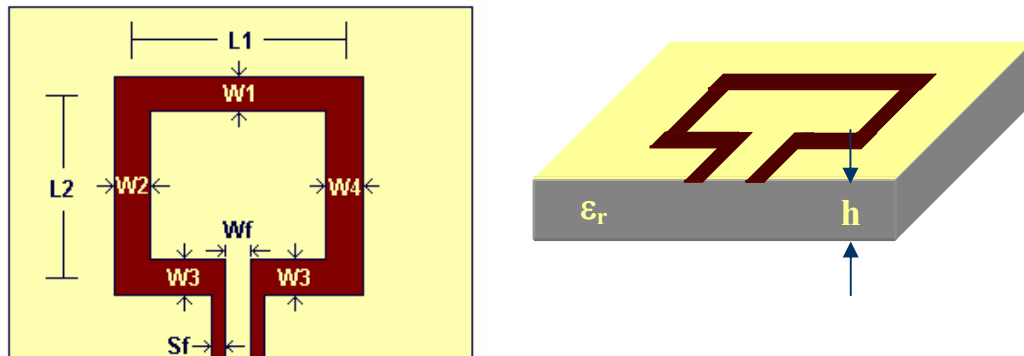


Figure 3.1.1. Description of the rectangular slot-ring antenna dimensions

Keeping in mind our major goal, which is to achieve tuning using varactors, the dimensions of the slot-ring antenna were physically varied. These dimensions, which are described in Figure 3.1.1, were the lengths L_1 and L_2 , and widths of the four slots that form the antenna (w_1 , w_2 , w_3 , and w_4). Varying each dimension of the rectangular slot-ring antenna gives a complete view of the most sensitive antenna physical parameters that will affected the electrical parameters and, therefore, suggests the best place to attach a varactor. These electrical parameters are input impedance, resonant frequency, bandwidth, polarization, and radiation pattern. Changes in the width, w_f , and slot width, s_f , of the transmission line were not taken into account in the analysis.

3.1.1. Width Variations Effects on the Resonant frequency

As a starting point, the rectangular-slot-ring antenna was analyzed leaving the perimeter, λ_g , constant but varying the widths w_1 , w_2 , w_3 , and w_4 all at the same time, where $w_1 = w_2 = w_3 = w_4 = w$. To calculate λ_g , [18] suggests the following approximation for a configuration with $0.0015 \leq w/\lambda_0 \leq 0.075$ and $3.8 \leq \epsilon_r \leq 9.8$.

$$\frac{\lambda_g}{\lambda_0} = 0.9217 - 0.277 \log(\epsilon_r) + 0.0322 \left(\frac{w}{h} \right) \left(\frac{\epsilon_r}{w/h + 0.453} \right)^{1/2} - \frac{3.65}{\epsilon_r^2 \left(w/\lambda_0 \right)^{1/2} \left(9.06 - 100 \left(w/\lambda_0 \right) \right)} \quad (3.1.1)$$

This approximation calculates λ_g with respect to the wavelength in free-space λ_0 , the width of the slot w , the substrate thickness h , and relative permittivity of the substrate ϵ_r . In this experiment, an antenna perimeter λ_g was fixed for a slot width of $\lambda/75$. The slot width, w , was set for three different cases: with the four slots having a width of $\lambda/50$,

$\lambda/75$, and $\lambda/100$ while keeping the perimeter corresponding to a slot width of $\lambda/75$ constant. Only the resonant frequency was analyzed and its results are discussed in Chapter 4.

3.1.2. Rectangular Slot-Ring Antenna with λ_g Corresponding to Each Slot Width

The resonant frequency of the rectangular slot-ring antenna was also analyzed when the four widths were varied along with the corresponding perimeter λ_g . The perimeter was calculated using equation 3.1.1 for w equals to $\lambda/50$, $\lambda/75$, and $\lambda/100$, where $w_1 = w_2 = w_3 = w_4 = w$.

Even though results from this experiment are discussed in the next chapter, there is one observation that leads to the next experiment. Simulations showed that as the slot width is increased, reflections decreased. Leading to the question, could a rectangular slot-ring antenna be matched by only adjusting the widths of the slots?

3.1.3. Input Impedance Matching with Variations in w_1

The experiment in Section 3.1.2 suggested that it might be possible to match the input impedance of a rectangular slot-ring antenna to 50Ω by adjusting the widths of the slots. However, in the latter test all the widths had the same value, and were equally varied, making unclear to establish which of the four dimensions is affecting the input impedance. In [19], the author found that the input impedance of a folded slot antenna was controlled by the width of the upper slot. As the width of the upper slot increased,

the input impedance of the folded slot antenna was matched to 50Ω . Will this technique apply to a rectangular slot-ring antenna?

In order to answer the latter question, the dimension w_1 was increased by one millimeter towards the center of the ring to minimize the overall size of the antenna. The perimeter λ_g was calculated using equation 3.1.1 for an antenna having $w_2 = w_3 = w_4 = \lambda/50$ and $w_1 = \lambda/50 + \delta$, where δ goes from 1 mm to 4 mm. Note that λ_g depends on the width of the slot, but the slots that form the antenna have different width values. For this reason, the perimeter was calculated, by considering that each slot contributes with one-quarter of a wavelength. In other words, the perimeter was adjusted to be one wavelength every time w_1 was increased to make sure that any variation in the results is due only to the upper slot of the rectangular slot-ring antenna.

3.1.4. Effect produced by changes in w_2 , w_3 , and w_4

In the test described in Section 3.1.3, simulations suggested that as the ratio between the width of the upper slot and the width of the remaining slots increases, the input resistance decreases. Therefore, if the upper slot of a rectangular slot-ring antenna is increased and the width of the remaining slots is decreased, then input impedance matching may be achieved, as well as bandwidth enhancement. To verify this assumption, the input impedance of the rectangular slot-ring antenna was matched to 50Ω with an upper slot width of $\lambda/50 + 3$ mm. The remaining dimensions were equally varied ($w_2 = w_3 = w_4 = w$) from 2 mm to 0.5 mm. The perimeter was calculated with equation 3.1.1, considering that each slot contributes with one-quarter of a wavelength.

In addition, the widths of the slots were individually varied in order to examine the effect on the slot-ring antenna parameters; paying special attention to the resonant frequency. A slot-ring antenna with an upper slot width of $\lambda/50 + 4$ mm, and $w_2 = w_3 = w_4 = \lambda/50$ was taken as a reference for three separated tests. First, w_2 and w_3 were independently varied from 2 mm to 1 mm, and finally, w_2 and w_4 were also varied at the same time from 2 mm to 1 mm. The reference antenna perimeter was calculated using equation 3.1.1; nevertheless, adjustments were not performed every time each dimension was altered since frequency shift was desired.

3.2. Electrical Variations on a Rectangular Slot-Ring Antenna

The partial characterization described in Section 3.1 revealed that w_2 , w_3 , and w_4 strongly contribute to a frequency shift. In other words, variable capacitors must be attached across the side and bottom slots in order to achieve tuning, which is the main objective. The Abrupt Junction Tuning Varactor SMV1405 was chosen as the tuning element, since it has an efficient performance from 1 GHz to 4 GHz. Its nominal capacitance varies from 1 pF to 3 pF approximately when a reversed voltage from 0 V to -30 V is applied.

An important observation revealed in Section 3.1 is that an adjustment in the width of the upper slot, w_1 , will result in a $50\text{-}\Omega$ input impedance matching around the second resonant frequency, reason for which no varactor was placed at the upper slot for analysis. Another important observation revealed that equal changes to w_2 and w_4 introduced a frequency shift of the second resonance; meanwhile, when w_3 was changed a

frequency shift was observed at the first resonance. Thus, will a varactor achieve the same tuning effect?

3.2.1. Simulating a Capacitor on Ground Plane Using Ansoft Ensemble

Simulations of the antennas from Section 3.1 were performed using Ansoft Ensemble Simulation Software. The two-layer configuration consists of a substrate layer ($\epsilon_r = 6.15$; $h=0.635$ mm) and a ground plane layer in which the slot-ring antenna was drawn, as shown in Figure 3.2.1.

The next step may sound very simple, which is to connect a capacitor on top of the ground plane. Nevertheless, Ensemble does not allow such a connection; no lumped component can be directly connected to ground plane. To solve the problem, two more layers were added to the slot-ring antenna configuration: a metal layer where the capacitor was attached, and a 0.1 mm-air gap between the metal layer and ground plane, as shown in Figure 3.2.2. A via through the air gap was made, connecting the capacitor in the metal layer to ground plane.

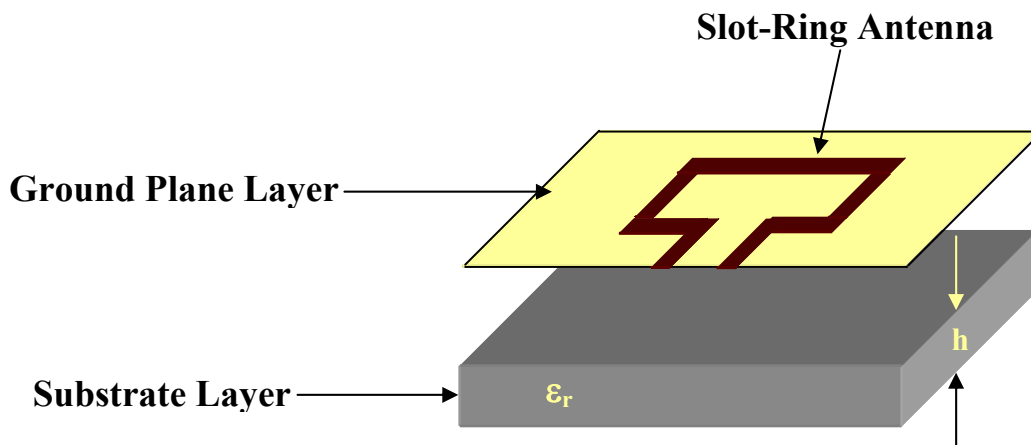


Figure 3.2.1. Slot-ring antenna configuration without varactors

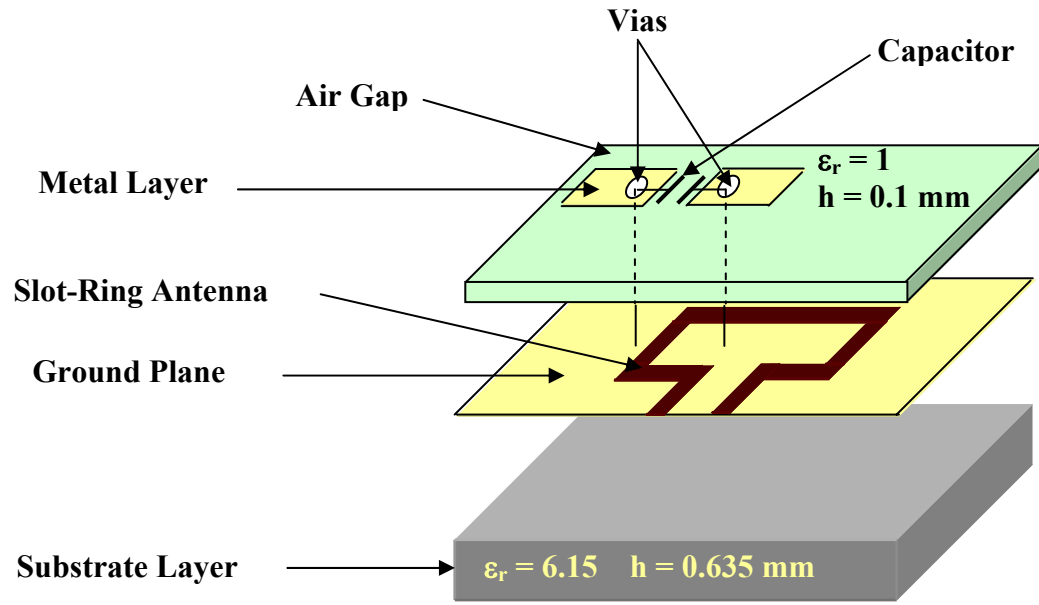


Figure 3.2.2. Slot-ring antenna configuration with a capacitor

The capacitor was simulated as a two-port element in Advanced Design System (ADS) software, where its scattering parameters were calculated for a specific range of frequencies and saved as an .s2p touchstone file. Once the file is created, Ensemble allows the user to set up a black box from the touchstone file, which is attached on top of the metal layer. The procedure described in this section was repeated for every desired capacitance between 1 pF and 3 pF in order to cover the range provided by the SMV1405 tuning varactor.

3.2.2. Tuning Analysis With Varactors Connected at Both Side Slots

Tests described in Section 3.1.4 suggested a significant frequency shift at the second resonance when dimensions w_2 and w_4 were equally changed. Therefore, the slot-ring antenna was simulated with a variable capacitor connected at each slot, as illustrated in Figure 3.2.3, to verify if the same tuning effect can be achieved. In each simulation, the varactors were set to have the same capacitance (1-6 pF) since the same voltage is applied to each varactor. The experiment was performed for a 2.9 GHz-slot-ring antenna having a perimeter λ_g obtained from equation 3.1.1, $w_2 = w_3 = w_4 = \lambda/50$, and $w_1 = \lambda/50 + 4$ mm.

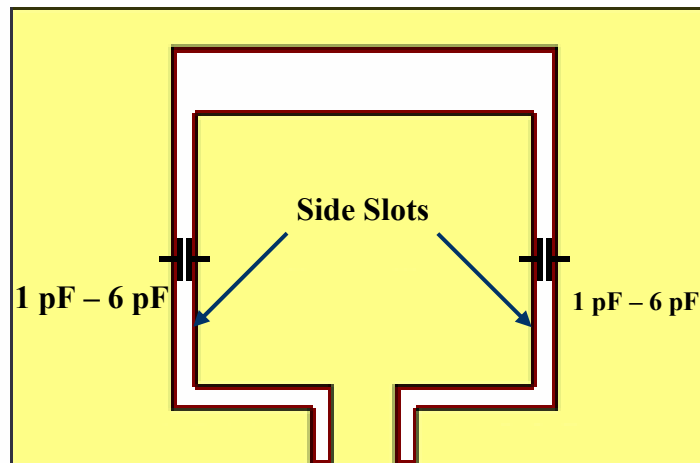


Figure 3.2.3. Slot-ring antenna layout with varactors connected on side slots

3.2.3. Tuning Analysis With Varactors Connected at the Bottom Slots

The tuning effect observed at the first resonant frequency with changes made to dimension w_3 was also simulated with varactors. Two variable capacitors were connected to the bottom slot; varying its capacitance from 1 pF to 3 pF, as represented in

Figure 3.2.4. The experiment was performed over a 2.9 GHz-slot-ring antenna with an upper slot width of $\lambda/50 + 3\text{mm}$ and $w_2 = w_3 = w_4 = \lambda/50$. The perimeter was calculated using equation 3.1.1, each slot contributing with one-quarter of a wavelength.

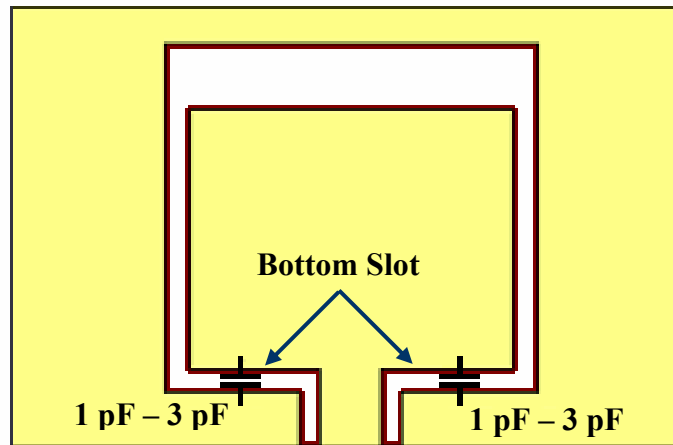


Figure 3.2.4. Slot-ring antenna layout with varactors connected on bottom slots

3.2.4. 2.4 GHz Rectangular Slot-Ring Antenna

For a robust analysis, every experiment must be implemented and measured in order to validate the obtained results. However, a slot-ring antenna with a width of $\lambda/50$, which is equivalent to 2.069 mm at 2.9 GHz, is not a convenient model to fabricate because the width of the slot is wider than the tuning varactor SMV1405 length. Therefore, another slot-ring antenna was designed.

The slot-ring antenna was designed on a substrate with a relative permittivity of 6.15 and a width of 0.635 mm at 2.4 GHz. The antenna was fed with a CPW transmission line for a simpler configuration. The feedline dimensions were calculated using ADS LineCalc program for a CPW having a slot spacing of 0.5 mm. A first

perimeter value was calculated using equation 3.1.1, and then manipulated in order to have the first resonance at 2.4 GHz. The widths w_2 , w_3 , and w_4 were chosen to be 0.25 mm to make possible the varactor connection during the implementation. The first resonant frequency was matched to 50Ω with the help of an open stub after performing several simulations in which the width and length of a short and open-circuited stub were varied. A $50\text{-}\Omega$ matching at the second resonant frequency was obtained by increasing the width of the slot, resulting in a multiband slot-ring antenna.

Simulations with varactors connected at the bottom slot were performed to verify the tuning effect at the first resonant frequency as the capacitance is varied from 1 pF to 3pF. Other simulations were performed with varactors connected at the side slots to tune the second resonant frequency as the capacitance is varied from 1 pF to 3 pF. Furthermore, both experiments were combined on the same antenna to see if it was possible to obtain a tunable dual mode slot-ring antenna. Four varactors were connected to the slot-ring antenna, one on each side slot and two on the bottom slot. Two additional slots were incorporated to the design in order to apply different voltages to both sets of varactors and; therefore, tune both frequencies independently. Figure 3.2.5 shows the Rectangular slot-ring antenna configuration.

The three slot-ring antenna configurations described in this section were implemented in a microwave laminate with a milling machine. Its scattering parameters were measured with a Network Analyzer. In addition, the radiation pattern was measured in the anechoic chamber. All measurements were performed at the UPRM Radiation Laboratory.

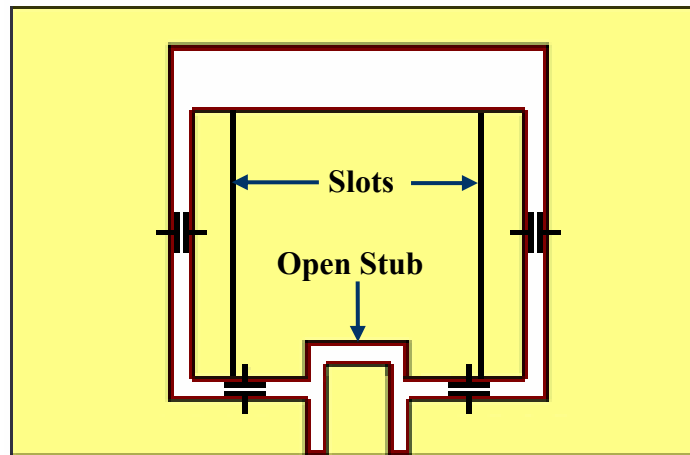


Figure 3.2.5. Tunable dual mode slot-ring antenna configuration

The three different antenna configurations were biased in different ways. A 1.8-nH inductor was attached to the open stub of the slot-ring antenna configuration with varactors connected to the bottom slot, as shown in Figure 3.2.6a. The inductor allowed DC voltage to pass through the open stub and bias the varactors while still having RF coupling between both central conductors. The DC voltage was then applied directly through the Network Analyzer.

The implementation of an inductor in the design worked perfectly for the configuration in which the first resonant frequency was tuned. Nevertheless, the reflections around the second resonant frequency were 30 dB higher than expected. For this reason, no inductance was connected to the slot-ring antenna configuration with varactors connected at the side slots; a gold wire bonding was implemented instead. Figure 3.2.6b. The wire was attached from the central conductor to an additional

connector through which the DC voltage was externally applied. The same technique was applied to the slot-ring antenna with varactors connected at the bottom and side slots.

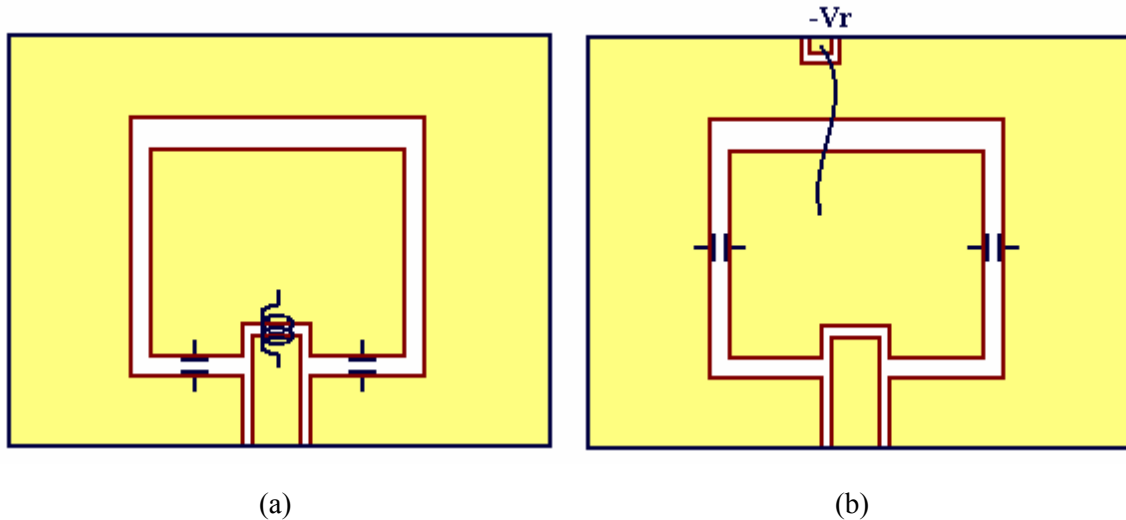


Figure 3.2.6. Bias implementation with (a) an inductor, and (b) a thin gold wire

3.2.5. 6 GHz Rectangular Slot-Ring Antenna

Following the procedure described in Section 3.2.4, a 6 GHz Rectangular slot-ring antenna was designed and analyzed to check if this antenna has the tunable dual mode characteristic as the 2.4-GHz slot-ring antenna. However, the SMV1405 works for frequencies up to 4 GHz; reason for which a GVD90001 super hyperabrupt tuning varactor diode was introduced. The GVD90001 has an efficient performance from VHF to 8 GHz. Its nominal capacitance varies from 0.35 pF to 36 pF approximately when a reversed voltage from 0 V to -12 V is applied.

3.3 Summary

The methodology for a partial characterization of a rectangular slot-ring antenna was presented in this chapter. This partial characterization methodology included physical variations of each antenna dimension such as widths and lengths of each slot. Each section explains how each antenna dimension was changed and what details were taken into account in order to separately analyze the effect of each dimension in the antenna response.

Based on the partial characterization results, simulations in which varactors were connected to the bottom and side slots were performed in order to achieve tuning at the first and second resonant frequencies. No varactor was attached to the upper slot because this width controls the second resonant frequency matching.

A 2.4-GHz slot-ring antenna and a 6-GHz slot-ring antenna were simulated but only the 2.4-GHz antenna was implemented. Input impedance matching at the first resonant frequency was achieved with an open stub while the upper slot width matched the second resonant frequency. In addition, three configurations of the 2.4-GHz antenna were tested: with varactors placed on the bottom slot to control the first resonant frequency, with varactors placed on the side slot to control the second resonant frequency, and a combination of the last two experiments to control both resonant frequencies on the same antenna configuration. Besides, this chapter also explains how and why each antenna was biased in a different way.

Chapter 4. Results and Discussions

4.1 Partial Characterization of Rectangular Slot-Ring Antennas

A full characterization of a rectangular slot-ring antenna has not been yet presented in the literature; therefore, it is of great importance to evaluate how variations on the dimensions affect the antenna's response. A complete characterization includes an exhaustive evaluation of how each antenna dimension affects not only the antenna resonant frequency and input impedance but also the polarization, gain, efficiency, radiation pattern, and establishes a mathematical relationship between the varied dimension and the antenna parameter. In this section a partial characterization of the slot-ring antenna is presented since every experiment was focused only in those parameters that strongly contribute to a resonant frequency shift. But, which are these parameters?

When a varactor is connected in series with a microstrip line, the electrical length of the line is increased or decreased whenever a difference in voltage is applied. If a varactor is attached across a slot in a rectangular slot-ring antenna, between the central conductor and the ground plane, the electrical width of the slot will be varied. Therefore, a partial characterization based only on changes in the widths of the four slots that form the antenna will reveal a possible tuning of the resonant frequency if variable capacitors are used. Moreover, it will specify where to attach the varactor in order to achieve tuning.

4.1.1. Effect Produced by Variations to the Width of the Four Slots

The widths of the four slots that form the antenna were varied to see if there was a tuning effect at the resonant frequency. An antenna with λ_g corresponding to a slot width of $\lambda/75$ was evaluated when the width, w , of the four slots was set to $\lambda/50$, $\lambda/75$, and $\lambda/100$. Dimensions of the three antenna configurations, which are shown in Table 4.1.1, were calculated for an operational frequency of 2.9 GHz. The CPW transmission line dimensions, w_f , s_f , and L_f , were calculated using LineCalc from ADS.

Table 4.1.1. Slot-Ring Antennas Dimensions with Same Perimeter and Different Slot Width

Dimension	$w = \lambda/100$ (mm)	$w = \lambda/75$ (mm)	$w = \lambda/50$ (mm)
w	1.034	1.379	2.069
L_1	19.5189	19.5189	19.5189
L_2	19.5189	19.5189	19.5189
w_f	5.92	5.92	5.92
s_f	0.5	0.5	0.5
L_f	2	2	2
$\lambda_g(w=\lambda/75)$	78.0756	78.0756	78.0756

The reactance shown in Figure 4.1.1, revealed a resonant frequency shift at the first and second resonances, suggesting that frequency tuning can be achieved if varactors are connected to the slots. There was a frequency shift from 2.98 GHz to 3.1 GHz (120 MHz) at the first resonance and from 4.36 GHz to 4.69 GHz at the second resonance (1.5λ) when the width of the slot is varied from $\lambda/100$ to $\lambda/50$.

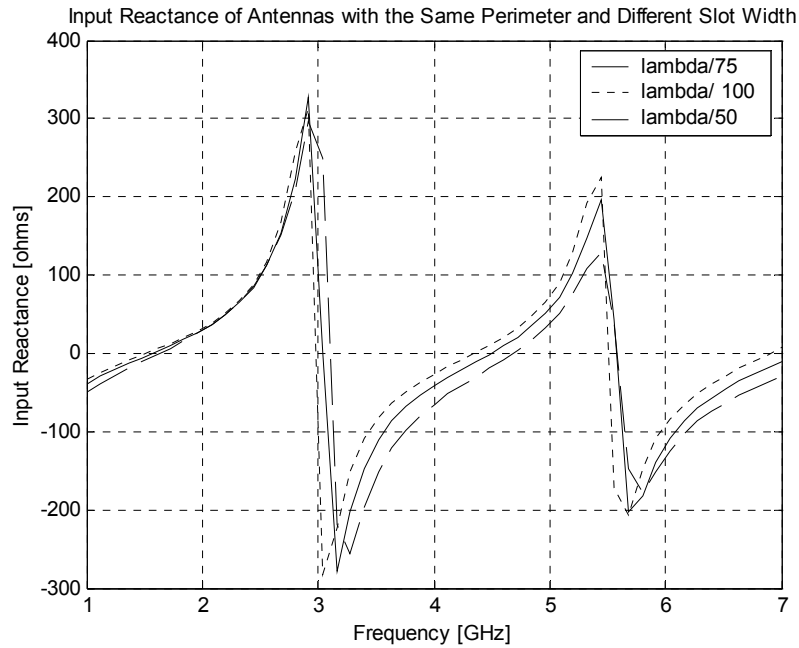


Figure 4.1.1. Input reactance of slot-ring antennas with the same perimeter but different slot widths

This behavior can be explained using equation 3.1.1, which establishes that a one-wavelength slot-ring antenna perimeter will decrease as the width of the slot is decreased. Thus, if the width of the slots is reduced while the perimeter remains unchanged, the resonant frequency must decrease. For example, in the experiment, when the width of the slot was decreased from $\lambda/75$ to $\lambda/100$ the first resonant frequency decreased, since the actual perimeter of the antenna is 1.8 mm longer than the one-wavelength perimeter corresponding to an antenna with a slot width of $\lambda/100$, as shown in Table 4.1.2. But, how much will the resonant frequency decrease? To predict the frequency shift, the ratio between the one-wavelength perimeter corresponding to a slot width of $\lambda/100$ and the one corresponding to $\lambda/75$ was calculated and multiplied by the resonant frequency of the reference antenna.

Table 4.1.2. Frequency Shift Calculations for Antennas with Different Slot Widths but Having the Same Perimeter $\lambda_g(w = \lambda/75)$

w	λ_g (mm) Corresponding to Each w	Wavelength with Respect to $\lambda_g(w = \lambda/75)$	Expected Resonant frequency (GHz)	Resonant frequency in Ensemble (GHz)
$\lambda/100$	76.2675	$0.97\lambda_g$	2.97	2.98
$\lambda/75$	78.0755	λ_g	3.04	3.04
$\lambda/50$	81.0304	$1.04\lambda_g$	3.16	3.10

The resistance at the second resonant frequency, shown in Figure 4.1.2, is lower than the resistance at the first resonance making easier a 50- Ω impedance matching around 4.5 GHz. In addition, as the width of the slot is increased the input resistance decreases.

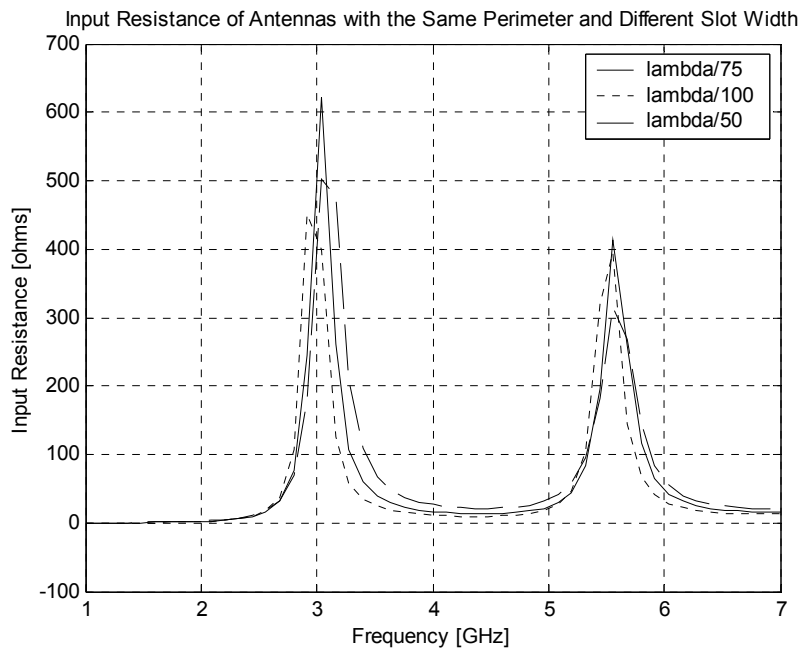


Figure 4.1.2. Input resistance of slot-ring antennas with the same perimeter but different slot widths

4.1.2. Effects on the Antenna Resonant Frequency due to Variations of λ_g

The resonant frequency of the rectangular slot-ring antenna was analyzed when the four widths, w , were varied along with the corresponding perimeter λ_g . The dimensions of the three different configurations are shown in next table.

Table 4.1.3. Slot-Ring Antenna Dimensions with Variations in Width and Perimeter

Dimension	$\lambda_g = \lambda/75$ $w = \lambda/75$ (mm)	$\lambda_g = \lambda/100$ $w = \lambda/100$ (mm)	$\lambda_g = \lambda/50$ $w = \lambda/50$ (mm)
w	1.379	1.034	2.069
L_1	19.5189	19.0669	20.2576
L_2	19.5189	19.0669	20.2576
λ_g	78.0756	76.2676	81.0304

No frequency shift was observed at the first and second resonance because each configuration has the one-wavelength perimeter that corresponds to its width. Therefore, according to equation 3.1.1, the slot-ring antennas must resonate at the same frequency, as shown in Figure 4.1.3. The first and second resonant frequencies were located at 3 GHz and 4.5 GHz, respectively.

On the other hand, graphs of the return loss, shown in Figure 4.1.4, revealed a decrease in reflections as the width of the slot is increased, particularly around the second resonant frequency. In other words, the input resistance at the second resonant frequency is getting closer to 50Ω as the width of the slot is increased. Hence, the slot-ring antenna might be matched to 50Ω by making adjustments to the width of the slots.

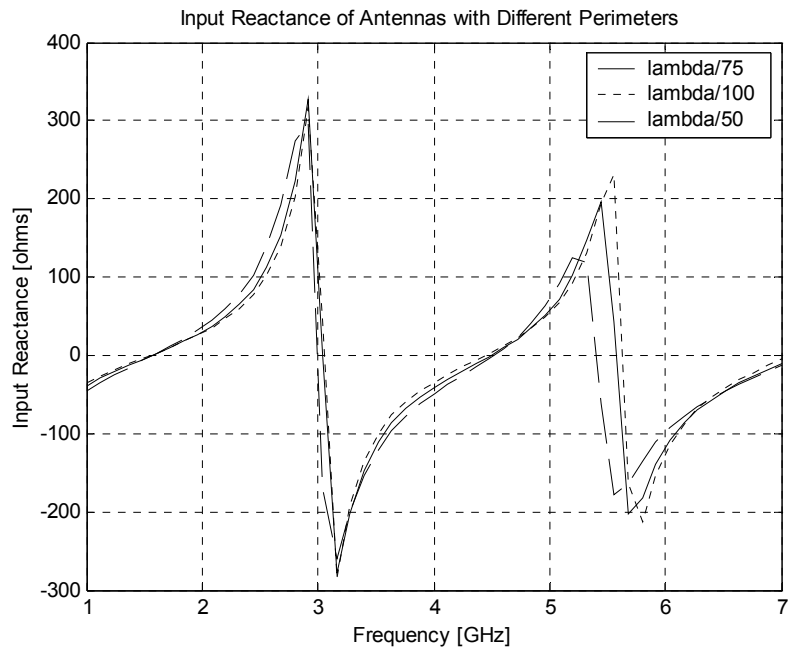


Figure 4.1.3. Input reactance for slot-ring antennas with a physical perimeter corresponding to λ for each width.

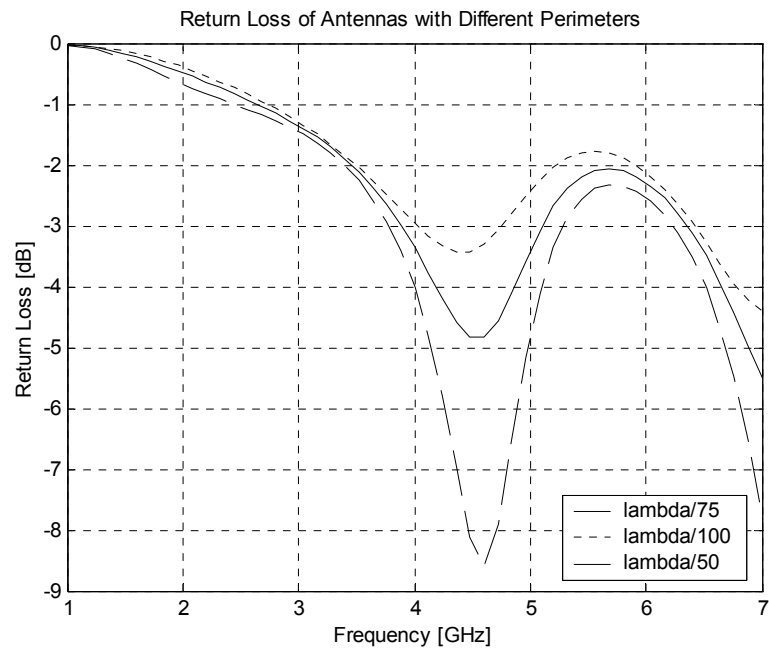


Figure 4.1.4. Return loss for antennas with different perimeters and widths

4.1.3. Effects produced by variations in w_1

According to the graphs of the return loss in the experiment of section 4.1.2, the input resistance around the second resonant frequency approaches 50Ω as the width of the slots is increased. However, if the width of all the slots strongly contributes to the antenna input matching then, which dimension will be varied for tuning? In [19], the input impedance matching of a folded slot antenna could be achieved by controlling the width of the upper slot only. If this technique applies to a slot-ring antenna, w_1 could remain constant for impedance matching while the other slots could be varied for tuning. The antenna's variations are described in Table 4.1.4.

Table 4.1.4. Description of the Slot-Ring Antenna Dimensions

Parameter	Antenna Dimensions (mm)			
	w_1	2.069	3.069	5.069
w^\dagger	2.069	2.069	2.069	2.069
L_1	20.25	21.11	22.43	22.96
L_2	20.25	19.83	19.17	18.90

[†] means $w_2 = w_3 = w_4 = w$.

The upper slot of the slot-ring antenna was varied from 2.069 mm to 6.069 mm with an increasing change of 1 mm. Note that the perimeter was adjusted to be one wavelength every time w_1 was increased to make sure that any variation in the results is due only to the upper slot of the rectangular slot-ring antenna. Curves in Figure 4.1.5 showed that a 50Ω input matching was achieved when w_1 is equal to 5.069 mm at the second resonant frequency only.

Impedance Smith Chart with Changes to w_1

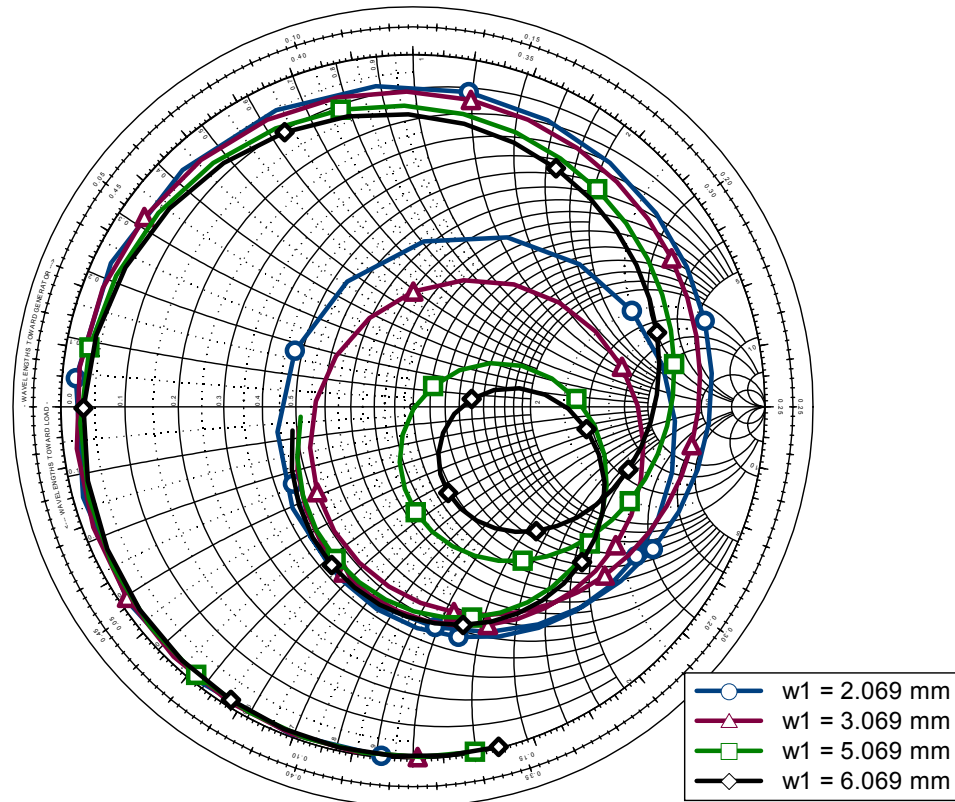


Figure 4.1.5. Representation of the impedance matching of a slot-ring antenna on a Smith Chart

4.1.4. Effects produced by changes to w_2 , w_3 , and w_4

Simulations of the experiment described in Section 4.1.3 suggested that bandwidth enhancement could be achieved as the ratio between the upper slot and the remaining slots increases. Note in Figure 4.1.5, that as the width of the upper slot increased, the input real impedance decreased. Keeping in mind that w_1 provides impedance matching; the width of the remaining slots was changed instead in order to increase the ratio. Hence, leaving w_1 constant and decreasing w_2 , w_3 , and w_4 will provide

a 50Ω matching as well as bandwidth enhancement. Table 4.1.5 shows the dimensions of the slot-ring antennas used to prove this assumption.

Table 4.1.5. Slot-Ring Antennas Dimensions.

Dimension (mm)	Antenna A	Antenna B	Antenna C	Antenna D
w_1	5.069	5.069	5.069	5.069
w^\dagger	2.069	1.50	1.00	0.50
L_1	22.43	22.43	22.43	22.43
L_2	19.17	18.28	17.31	16.00
w_f	5.92	5.92	5.92	5.92
s_f	0.50	0.50	0.50	0.50
L_f	2.00	2.00	2.00	2.00

[†] means $w_2 = w_3 = w_4 = w$.

Setting the upper slot width to 5.069 mm matched the slot-ring antenna to 50Ω . The dimension w was varied from 2.069 to 0.5 mm to see if bandwidth enhancement could be achieved. Every time w was varied, the perimeter of the antenna was also varied; considering that each slot contributes with one-quarter of the wavelength to keep the second resonant frequency constant.

The Smith Chart in Figure 4.1.6 shows that as w is decreased, the loop around the center of the chart moves towards the middle. In other words, the band of frequencies having reflections less than -10 dB gets wider each time the ratio between the upper slot and the remaining slots is increased.

Figure 4.1.7 shows how the bandwidth increases as the ratio is increased. The bandwidth was measured for frequencies with a return loss below -10 dB around a

central frequency of 4.8 GHz. In this experiment the slot-ring antenna bandwidth could be increased 6% more than that provided by the reference antenna (antenna A).

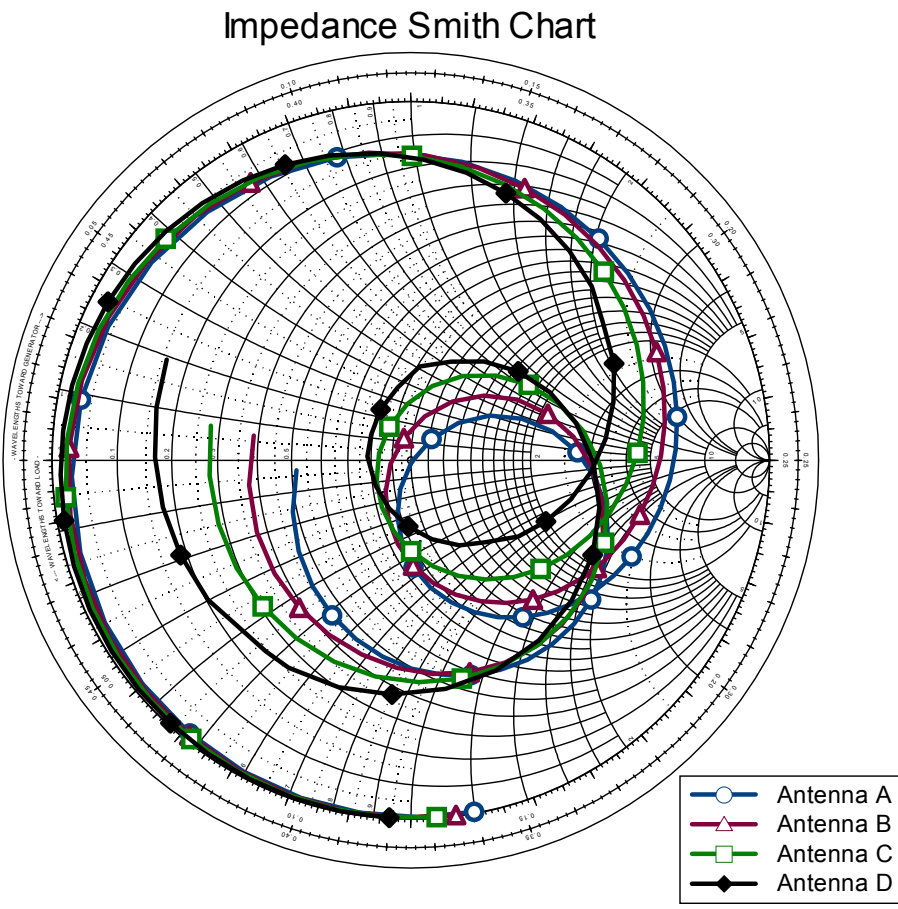


Figure 4.1.6. Input impedance curves with changes in w

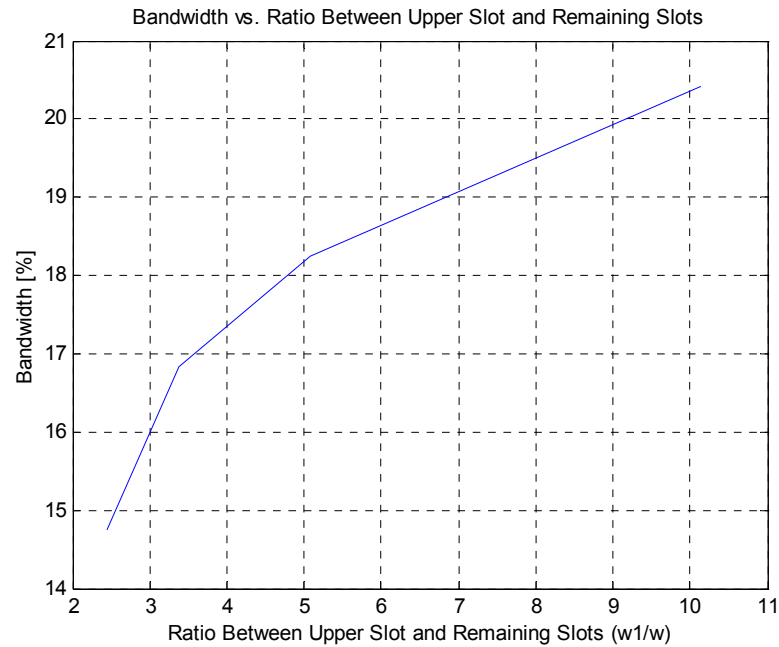


Figure 4.1.7. Graph of bandwidth percent versus ratio between upper slot and remaining slots

Other tests were performed on the slot-ring antenna with dimensions described in Table 4.1.6, where w_2 and w_3 were individually varied. These widths were physically changed in order to attach the varactors in positions where tuning is achieved at both first and second resonant frequencies. When the experiment was made varying w_2 from 1 mm to 2 mm no considerable variation was observed in either resonant frequencies, as shown in Figure 4.1.8. No significant change was either observed on the input resistance, as shown in Figure 4.1.9.

Table 4.1.6. Slot-Ring Antenna Dimensions

Slot-Ring Antenna Dimensions (mm)	
w_1	6.069
w^\dagger	2.069
L_1	22.96
L_2	18.90
w_f	5.92
s_f	0.50
L_f	2.00

[†] means $w_2 = w_3 = w_4 = w$.

On the other hand, when w_3 was physically changed from 1 mm to 2 mm a 70 MHz frequency shift (3.3 - 3.37 MHz) was observed at the first resonant frequency as well as a 100 MHz frequency shift (4.8 – 4.9 GHz) at the second resonant frequency, shown in Figure 4.1.10. In addition, there was a significant decrease of the input resistance, at both the first and second resonant frequencies when w_3 was decreased from 2 mm to 1 mm, as shown in Figure 4.1.11.

The slot-ring antenna was also analyzed when w_2 and w_4 were equally varied. Simulations in Figure 4.1.12 showed 150 MHz frequency shift (4.85 – 5 GHz) at the second resonant frequency when both dimensions were varied from 2 mm to 1 mm, and still a 70 MHz (3.45 - 3.38 GHz) frequency shift was observed at the first resonance. Moreover, as both widths are decreased, the input impedance matching at the second resonant frequency deteriorates, as shown in Figure 4.1.13. This is due to an increase in input impedance, and reduces tuning from 5 GHz down to 4.85 GHz.

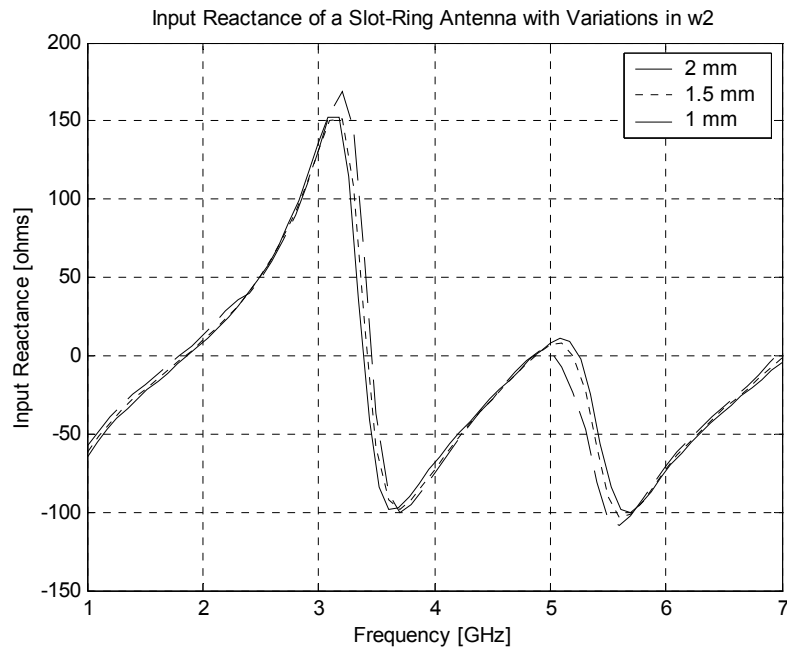


Figure 4.1.8. Graph of the input reactance of a slot-ring antenna when variations to w_2 were performed

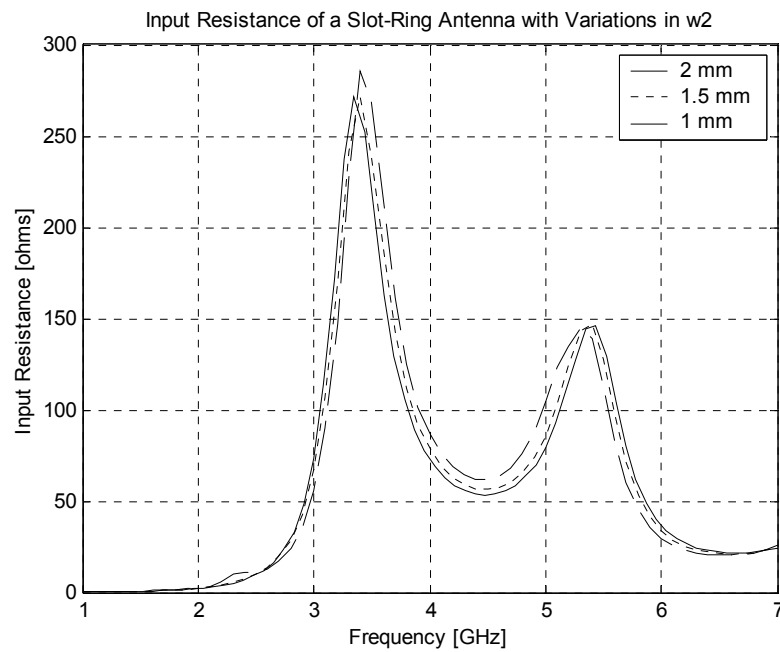


Figure 4.1.9. Graph of the input resistance for a slot-ring antenna when variations to w_2 were performed

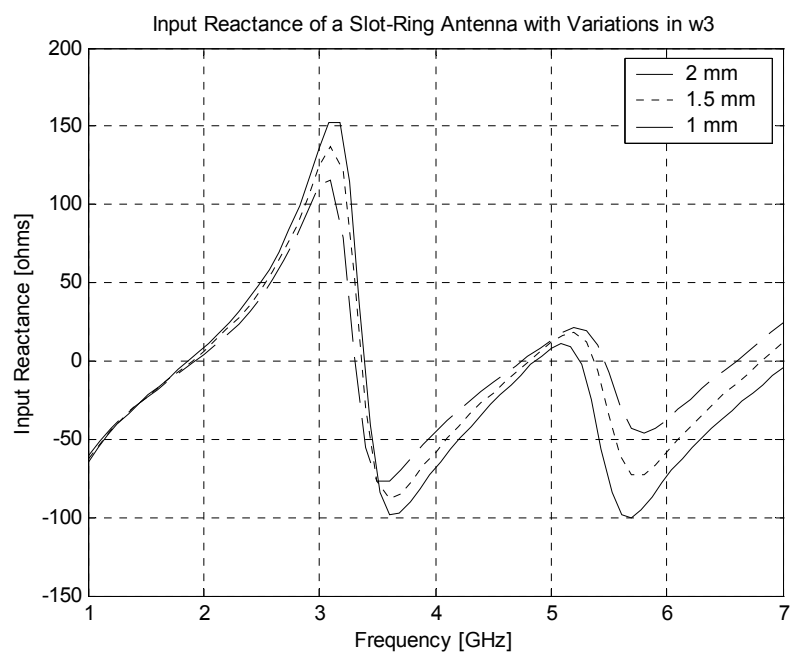


Figure 4.1.10. Graph of the input reactance for a slot-ring antenna when variations to w_3 were performed

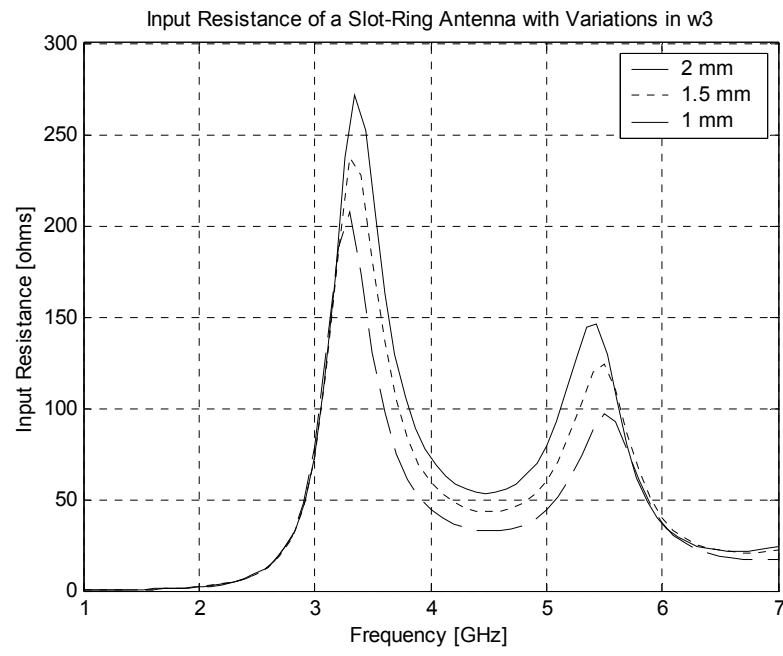


Figure 4.1.11. Graph of the input resistance for a slot-ring antenna when variations to w_3 were performed

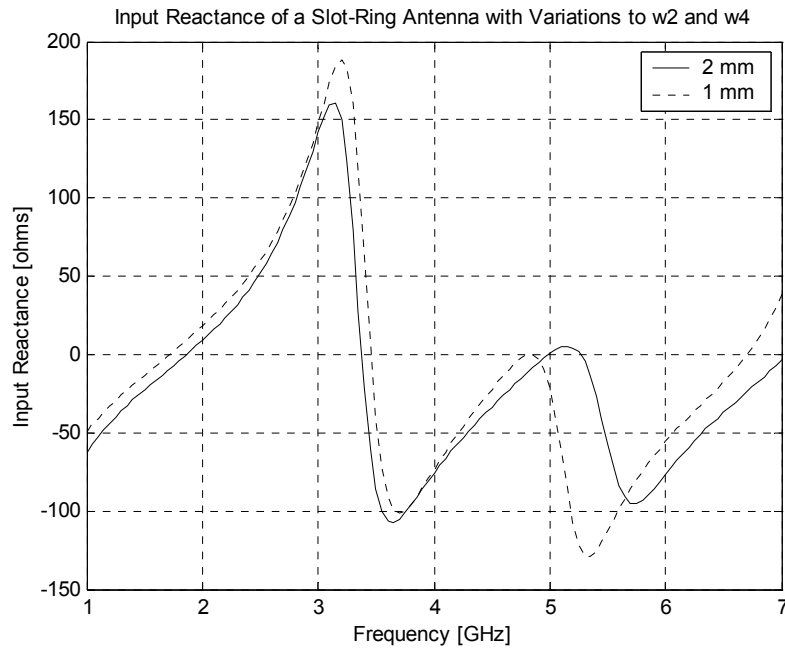


Figure 4.1.12. Graph of the input reactance for a slot-ring antenna when variations to w_2 and w_4 were performed

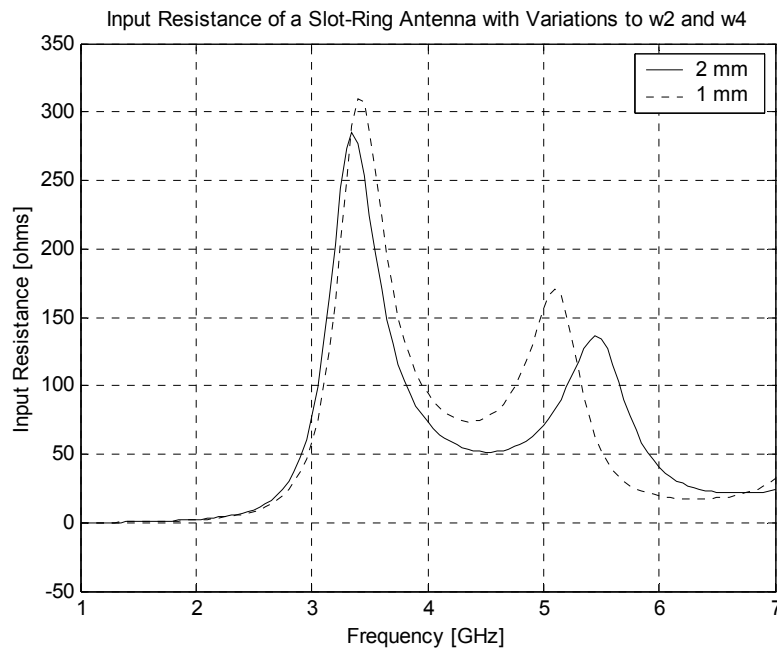


Figure 4.1.13. Graph of the input resistance for a slot-ring antenna when variations to w_2 and w_4 were performed

4.2 Electrical Tuning on the Rectangular Slot-Ring Antenna

The partial characterization of the rectangular slot-ring antenna, described throughout Section 4.1, was of great importance because it revealed the slots that strongly contribute to the frequency shift at the first two resonant frequencies. The results suggested that variations to the width of either the bottom slot or the side slots would tune the first and second resonant frequencies. Based on these results, the experiments described in Section 3.2 consisted of attaching variable capacitors only at the bottom and side slots. No varactor was connected at the upper slot to keep a 50Ω matching at the second resonant frequency.

The results in the following sections will demonstrate that varactors can be used in a rectangular slot-ring antenna configuration to electrically change the width of the slots in order to achieve tuning at the first and second resonant frequencies. Even more, simulations suggested that both frequency shifts could be obtained independently on a same configuration, making the slot-ring antenna a tunable dual mode antenna.

4.2.1 Experiment with Varactors Attached at Both Side Slots

In this test, varactors were connected to each side slot of the slot-ring antenna with the dimensions described in Table 4.2.1. The varactors were set to have the same capacitance because in the antenna configuration they are connected in parallel; and therefore, when the voltage is applied, each of them will have the same capacitance value. For this experiment, the capacitance was varied from 1 pF to 6 pF by connecting

two varactors in parallel to each side slot. Adding more capacitors might allow tuning of the second resonant frequency over a wider band, still having reflections under -10 dB.

Table 4.2.1. Slot Ring Antenna Dimensions

Slot-Ring Antenna Dimensions (mm)	
w_1	6.069
w^\dagger	2.069
L_1	22.96
L_2	18.90

† means $w_2 = w_3 = w_4 = w$.

Curves of the return loss showed that as the capacitance is increased from 1 pF to 3 pF, the second resonant frequency is tuned from a higher to a lower value. This effect was expected since the capacitance and the resonant frequency are inversely proportional. Figure 4.2.1 also shows that there is a decrease in bandwidth from 13.6% around 4.77 GHz to 10.4% around 4.59 GHz as the resonant frequency decreases. In addition, as the capacitance is increased from 3 pF to 6 pF, the bandwidth around the second resonant frequency (6.5% around 4.55 GHz) is completely inside the antenna's bandwidth achieved with a 3-pF capacitor. Therefore, there is no need of a second varactor connected in parallel at either side slot if tuning and bandwidth enhancement is desired.

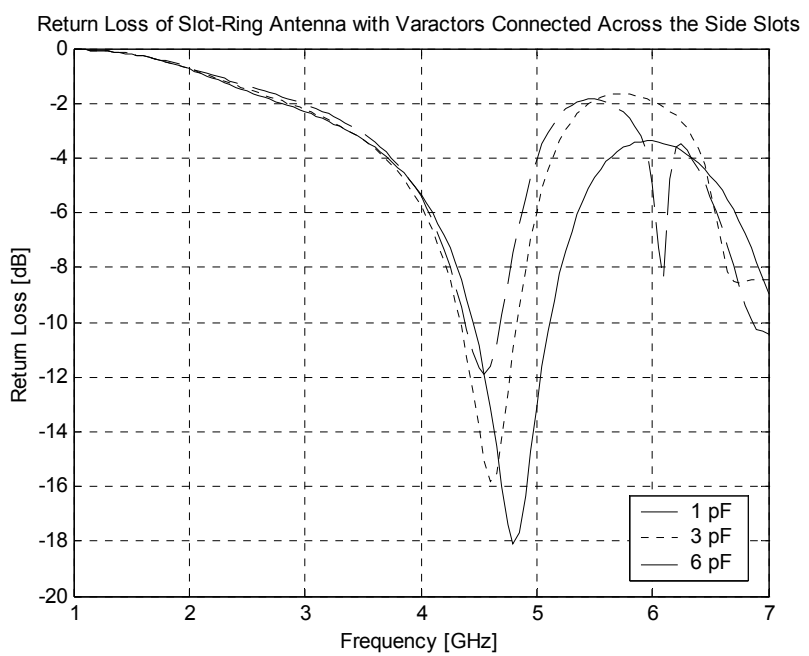


Figure 4.2.1. Graph of the return loss of a rectangular slot-ring antenna when varactors are connected across both side slots

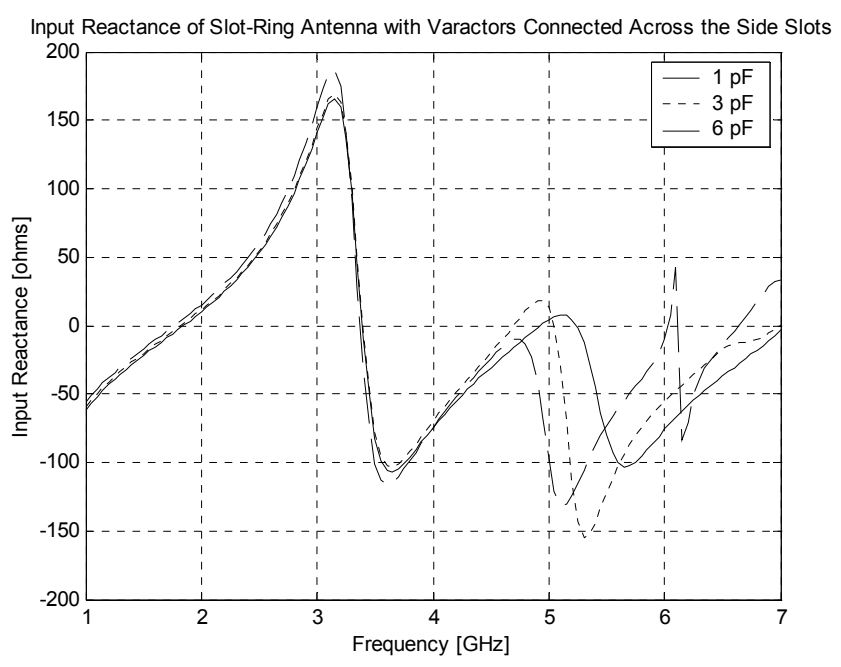


Figure 4.2.2. Graph of the input reactance when varactors are connected at both side slots

The input reactance curves in Figure 4.2.2, better show the resonant frequency shift. No shift at all was observed at the first resonant frequency; however, the second resonant frequency could be tuned from 4.92 GHz to 4.7 GHz (220 MHz); 70 MHz more than the frequency shift predicted by simulations with physical variations described in Section 4.1.4. Besides, as the capacitance is increased from 3 to 6 pF, the second resonance is lost.

The input resistance curves in Figure 4.2.3 illustrate that as the capacitance of the varactor is increased so does the input resistance at the second resonant frequency, reason for which the reflections in Figure 4.2.1 increased.

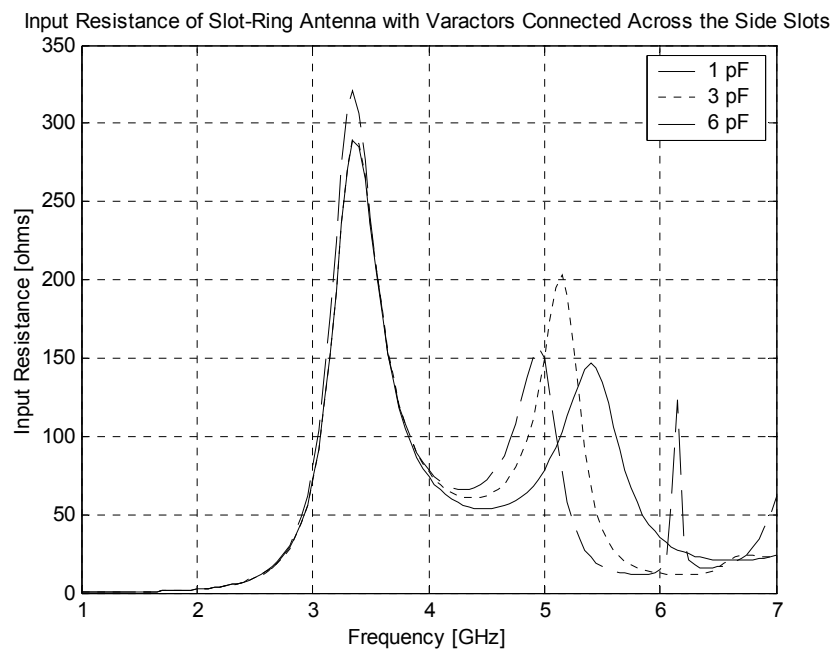


Figure 4.2.3. Graph of the input resistance of a slot-ring antenna with varactors connected at both side slots

4.2.2 Experiment with Varactors Attached at the Bottom Slot

In this test, a pair of varactors was connected at the bottom slot of the slot-ring antenna with dimensions described in Table 4.2.2. The varactors were connected in parallel and varied from 1 pF to 3 pF intending to tune the first and second resonant frequencies and analyze the effect in the input impedance.

Table 4.2.2. Slot-Ring Antenna Dimensions

Slot-Ring Antenna Dimensions (mm)	
w_1	5.069
w^\dagger	2.069
L_1	22.43
L_2	19.17

† means $w_2 = w_3 = w_4 = w$.

Return loss curves in Figure 4.2.4 show no significant variation in bandwidth around the second resonant frequency when the capacitance is changed from 1 pF to 3 pF. Simulations present a 15.5 % bandwidth around 4.78 GHz. In addition, reflections increased as the capacitance increased, meaning that the input resistance at the second resonant frequency gets farther away from 50 Ω , as shown in Figure 4.2.5, while the input resistance at the first resonant frequency did not suffer any change.

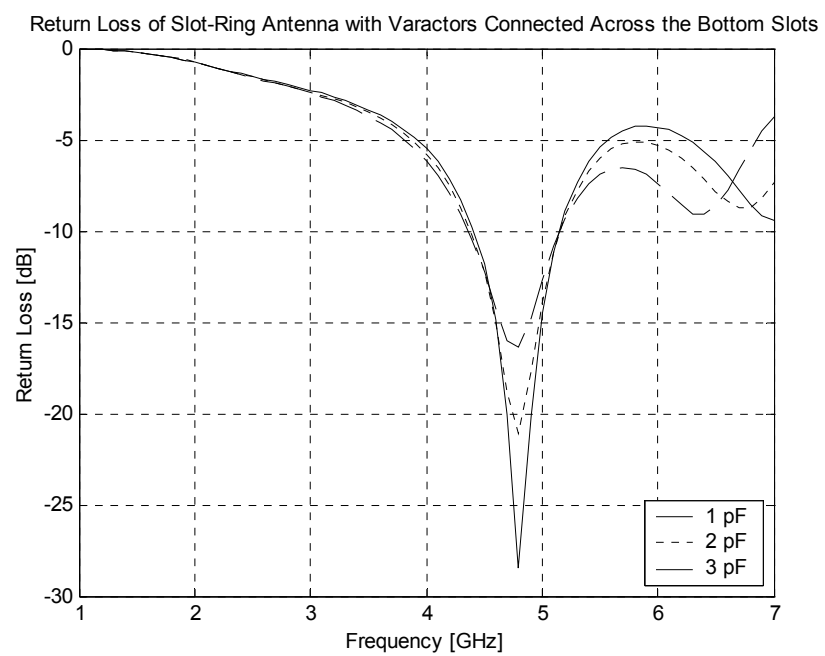


Figure 4.2.4. Return loss graph of a slot-ring antenna with varactors connected at the bottom slot

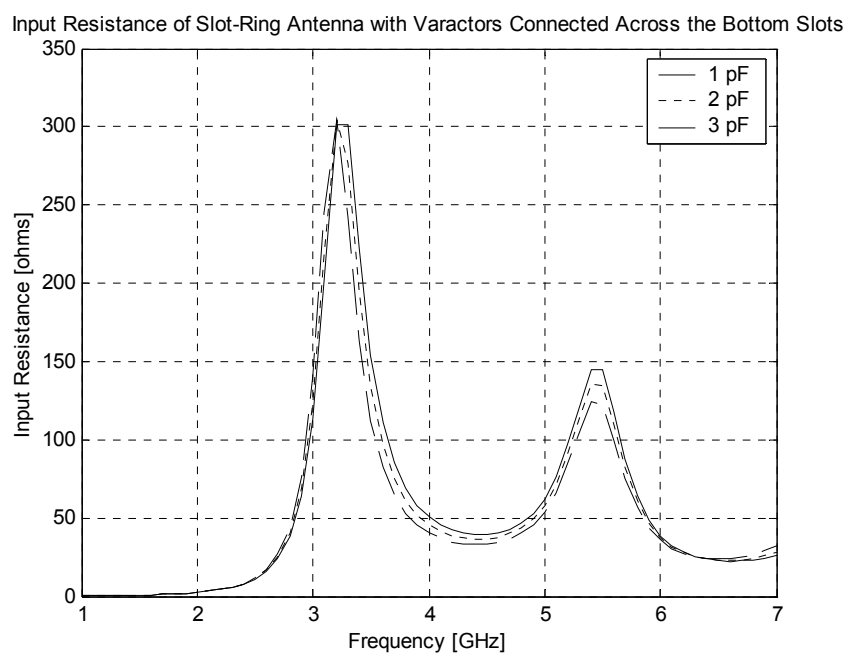


Figure 4.2.5. Input resistance curves of a slot-ring antenna with varactors connected at the bottom slot

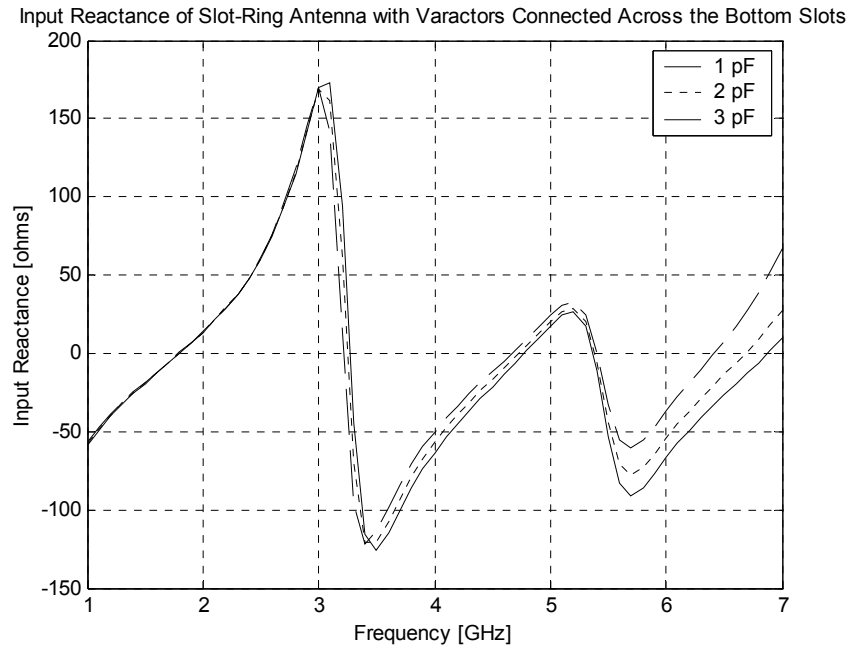


Figure 4.2.6. Input reactance curves of a slot-ring antenna with varactors connected at the bottom slot

The input reactance curves in Figure 4.2.6 illustrate a frequency shift at the first resonant from 3.26 GHz to 3.21 GHz (50 MHz) when the capacitance is increased from 1 pF to 3 pF. Moreover, another frequency shift was observed at the second resonance. The resonant frequency moved from 4.8 GHz to 4.66 GHz as the capacitance was increased from 1 pF to 3 pF.

4.2.3 Experiments with Varactors on a 2.4-GHz Rectangular Slot-Ring Antenna

The implementation of an antenna prototype is a robust step in order to validate the results obtained on the previous two sections. Nevertheless, the slot-ring antenna with a $\lambda/50$ width at 2.9 GHz is an inconvenient model to build since the width of the slot (2.069 mm) is wider than the SMV1405 varactors length (1.60 mm). Therefore, a 2.4-GHz slot-ring antenna was simulated and implemented instead, in which the width of the

slot was chosen to be 0.25 mm. The dimensions of the prototype are listed on Table 4.2.3.

Table 4.2.3. 2.4-GHz Slot-Ring Antenna Dimensions

2.4-GHz Slot-Ring Antenna Dimensions (mm)	
w_1	2.00
w^\dagger	0.25
L_1	26.1
L_2	26.1
w_f	6.22
s_f	0.50
L_f	2.00

† means $w_2 = w_3 = w_4 = w$.

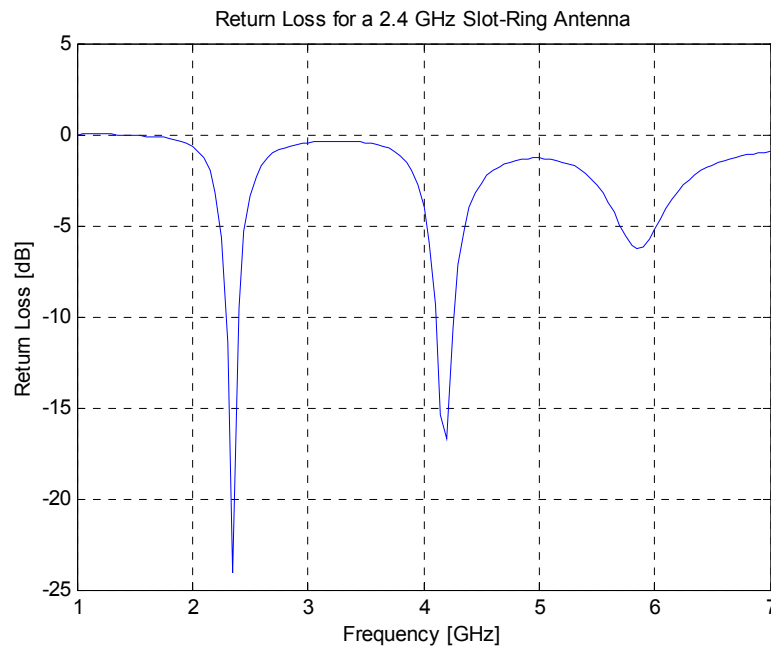


Figure 4.2.7. Graph of the return loss for the 2.4-GHz slot-ring antenna with matching stubs and without varactors

Setting the width of the upper slot to 2 mm, allowed the antenna to have a 50Ω -impedance matching around the second resonant frequency, but no matching was observed at the first resonant frequency. Hence, an open stub was included in the feed in order to also match the first resonant frequency. This results in a multiband slot-ring antenna design. The reason why an open-circuited stub was used over a short-circuited stub is explained in Section 4.3. Figure 4.2.7 locates the first resonant frequency at 2.4 GHz with a 4.7 % bandwidth around 2.35 GHz and the second resonant frequency at 4.25 GHz with a 3.8 % bandwidth around 4.18 GHz.

This antenna was taken as a reference of a set of experiments in which varactors were connected to the side and bottom slots. First, a varactor was connected at each side slot. Results predicted that when the capacitance is changed from 1 pF to 3 pF, it creates a tuning effect only at the second resonant frequency. Return loss results in Figure 4.2.8 illustrate a frequency shift from a higher value to a lower value at the second resonant frequency when the capacitance was increased. Meanwhile, the first resonant frequency remained unchanged. The second resonant frequency was tuned over a 22 % bandwidth around 3.7 GHz.

The input reactance curves shown in Figure 4.2.9 demonstrate that as the capacitance is increased the second resonant frequency decreases until it is lost. Nevertheless, low reflections are still seen at the 3-pF curve around 3.3 GHz because the input resistance is near $50\ \Omega$ around that band, as shown in Figure 4.2.10.

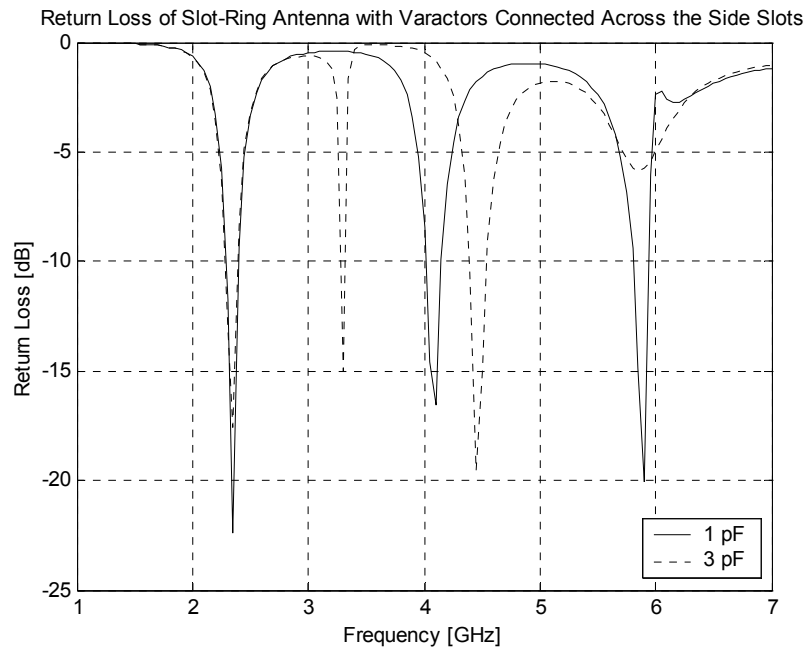


Figure 4.2.8. Graph of the return loss of the 2.4-GHz slot-ring antenna with varactors connected at each side slot

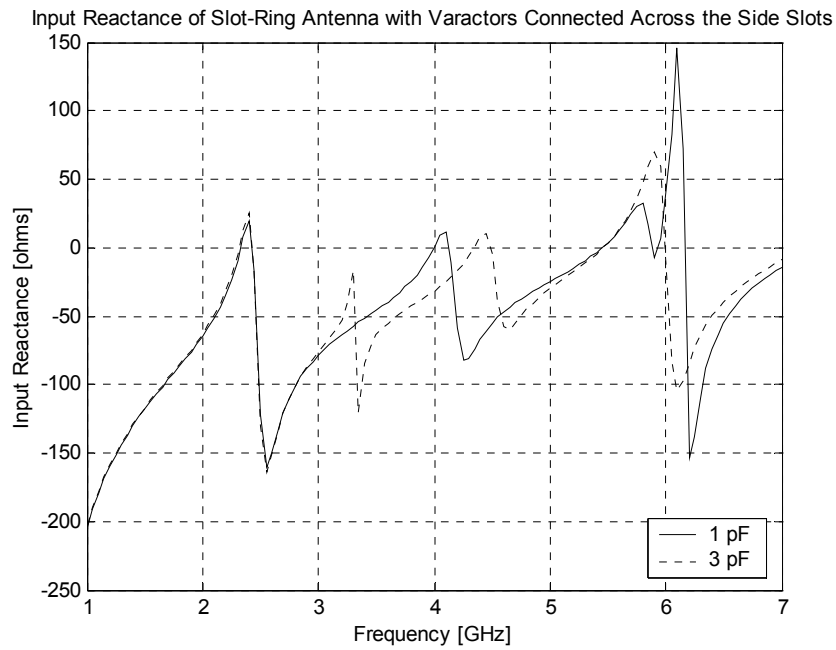


Figure 4.2.9. Graph of the input reactance curves of a 2.4-GHz slot-ring antenna with varactors connected at each side slot

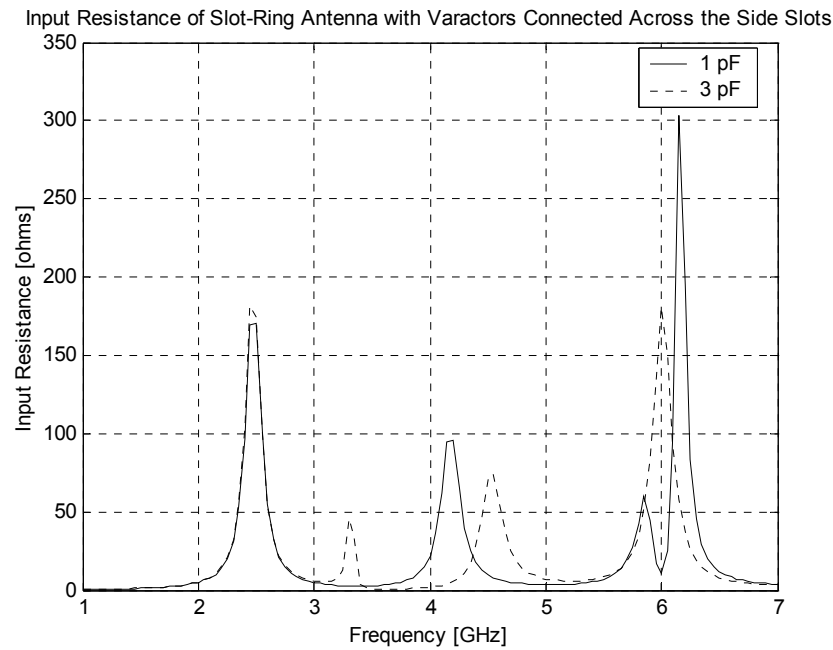


Figure 4.2.10. Graph of the input resistance curves of a 2.4-GHz slot-ring antenna with varactors connected at each side slot

The antenna with the varactors connected at the side slots was fabricated and its input impedance matching and frequency response were measured. Return loss results shown in Figure 4.2.11 illustrate a shift at the second resonant frequency only, as suggested by simulations. Nevertheless, the reactance curves shown in Figure 4.2.12, revealed a loss of the second resonance throughout the whole capacitance tuning range. When the antenna was measured, the connector and the transmission line effects were removed with a phase offset, which might be responsible for the disagreement between impedance measurements and simulations. However, a wider w would recover the second resonant frequency, as suggested in Figure 4.1.12. The measured resistance approaches 50Ω as the voltage is decreased or in other words, as the capacitance is increased, as shown in Figure 4.2.13.

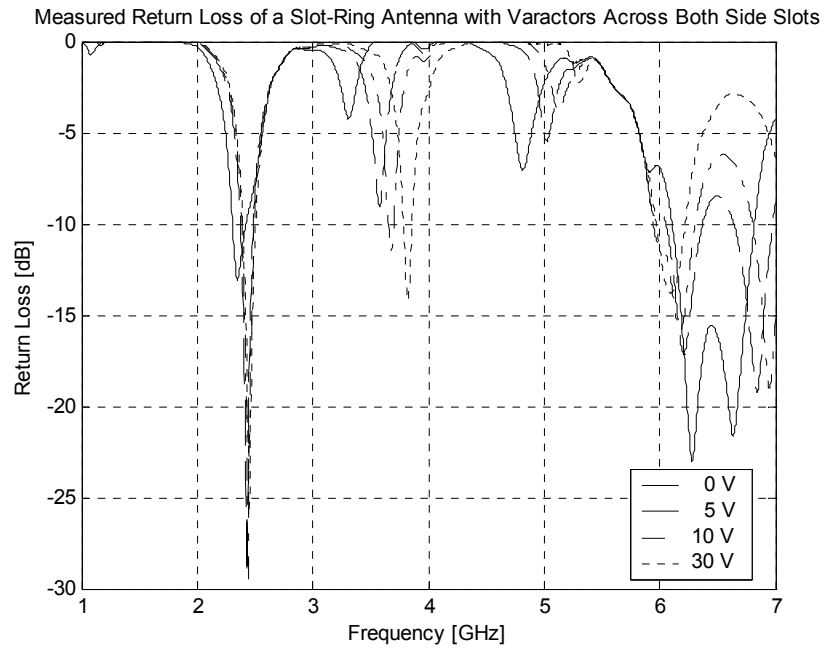


Figure 4.2.11. Graph of the measured return loss of the 2.4-GHz slot-ring antenna with varactors connected at each side slot

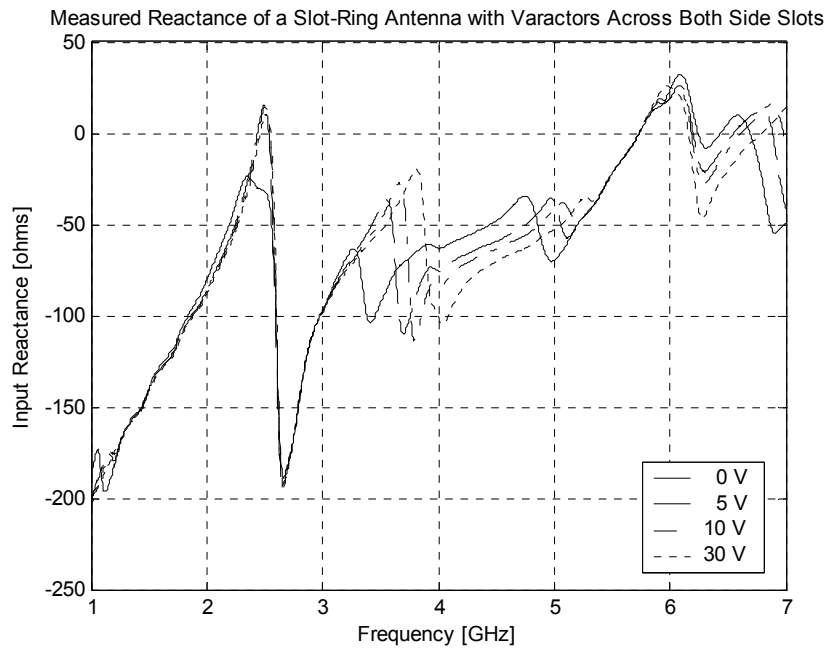


Figure 4.2.12. Graph of the measured reactance of the 2.4-GHz slot-ring antenna with varactors connected at each side slot

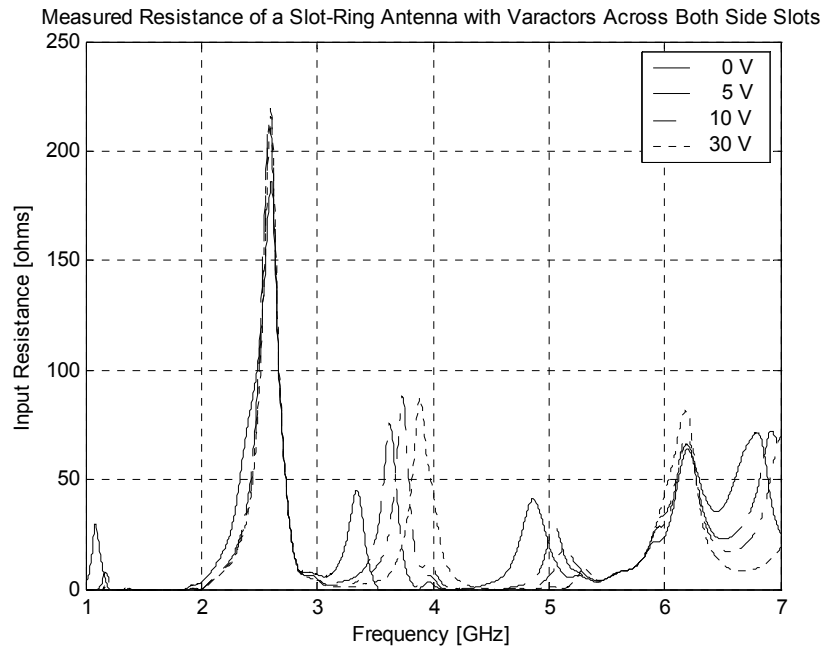


Figure 4.2.13. Graph of the measured resistance of the 2.4-GHz slot-ring antenna with varactors connected at each side slot

Then, another experiment was performed but with a set of varactors connected at the bottom slot of the 2.4-GHz slot-ring antenna. Simulations registered a 4.4 % frequency shift around 2.25 GHz as the capacitance is changed from 1 pF to 3 pF still having less than -10 dB reflections, as shown in Figure 4.2.14. However, an increase in capacitance resulted in an increase in reflections around the second resonant frequency.

The simulated input reactance curves in Figure 4.2.15 illustrate the frequency shift at the first resonance going from 2.3 GHz to 2.2 GHz when the capacitance is increased. Meanwhile, the second resonant frequency is lost because the capacitive reactance around 3.7 GHz increases and the input resistance gets farther away from 50Ω , as shown in Figure 4.2.16.

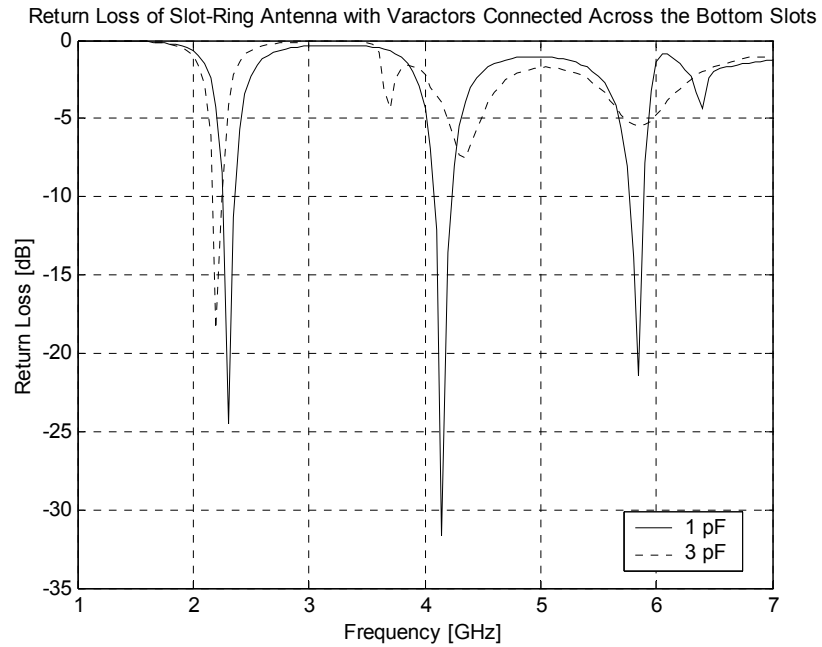


Figure 4.2.14. Graph of the return loss of the 2.4-GHz slot-ring antenna with varactors connected to the bottom slot

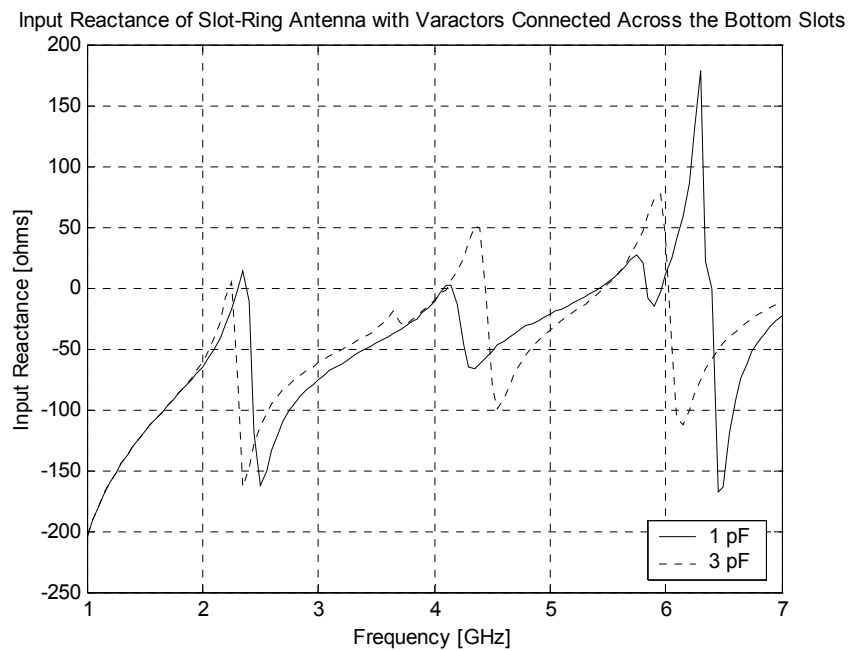


Figure 4.2.15. Graph of the input reactance curves of a 2.4-GHz slot-ring antenna with varactors connected to the bottom slot

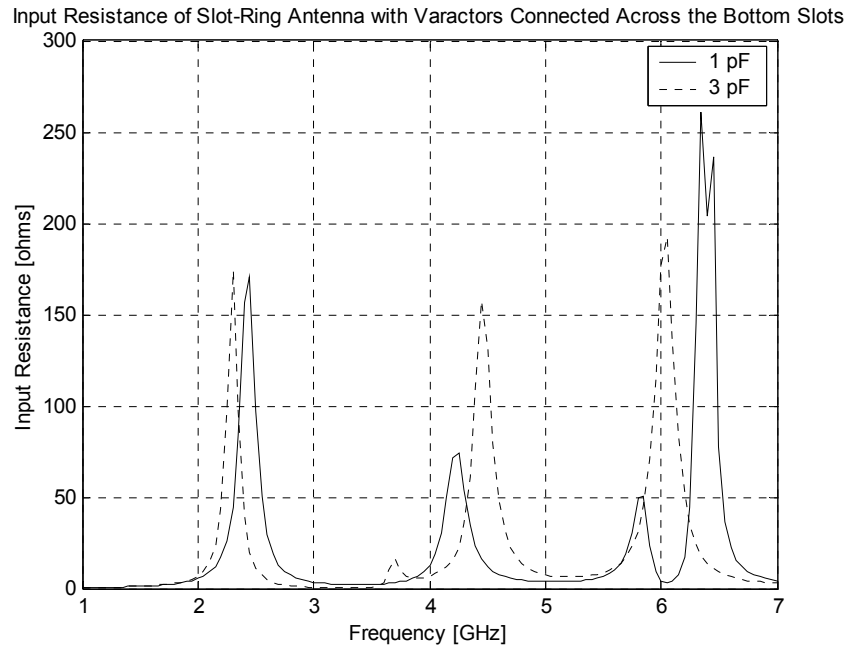


Figure 4.2.16. Graph of input resistance curves of a 2.4-GHz slot-ring antenna with varactors connected to the bottom slot

The antenna with varactors attached across the bottom slot was also implemented and measured. The return loss curves shown in Figure 4.2.17, illustrate a frequency shift at the first and the second resonant frequency. As the capacitance increases so do the reflections, limiting the tuning range. The measured reactance curves revealed a 2.5% frequency shift around 2.35 GHz, and an 8.1 % frequency shift around 2.46 GHz, as shown in Figure 4.2.18. An inductor was added to the design in order to bias the varactors, which was not included in the simulations. In addition, a phase offset was performed to remove effect of the transmission line and the connector, causing disagreements between measurements and simulations. The resistance along both tuning ranges stays near the vicinity of 50 Ω , as illustrated in Figure 4.2.19.

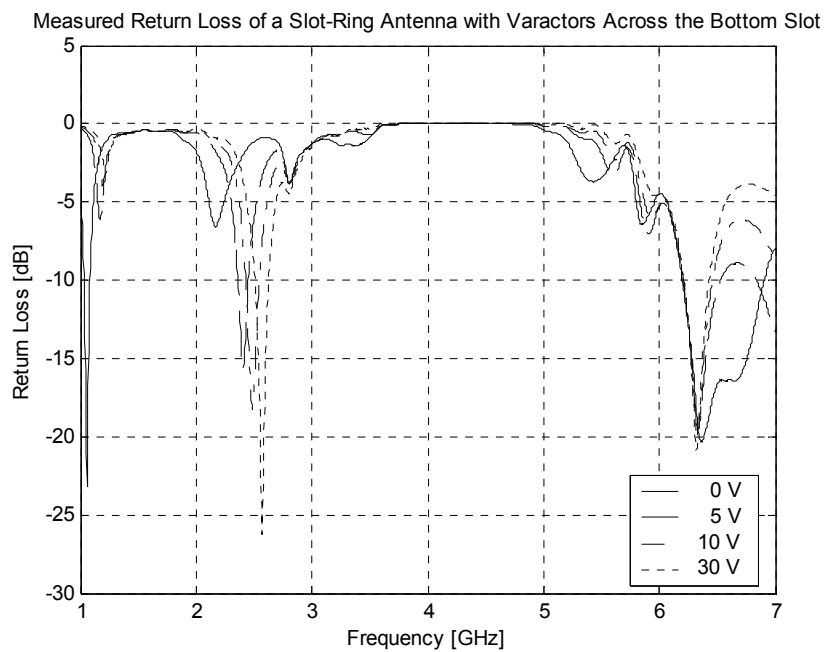


Figure 4.2.17. Graph of the measured return loss of the 2.4-GHz slot-ring antenna with varactors connected to the bottom slot

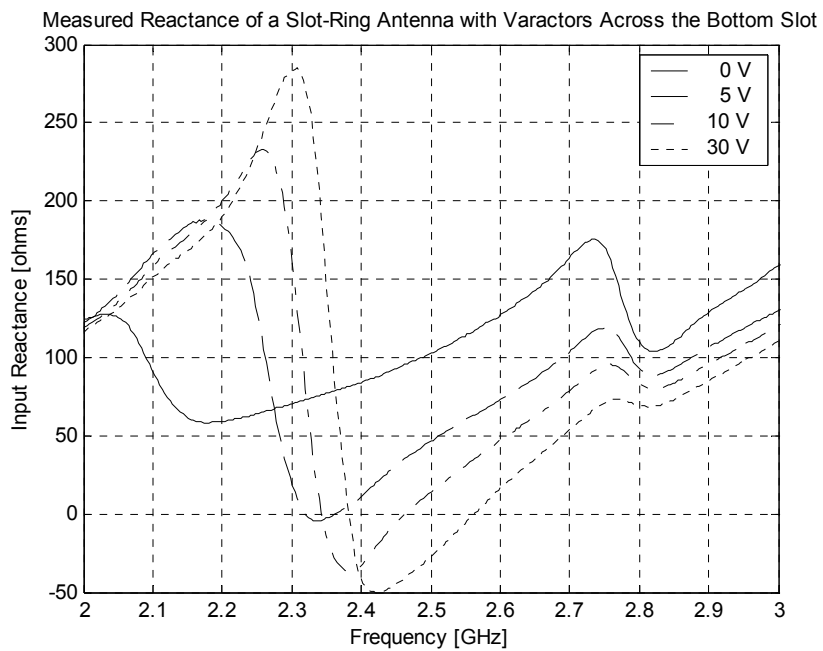


Figure 4.2.18. Graph of the measured reactance of the 2.4-GHz slot-ring antenna with varactors connected to the bottom slot

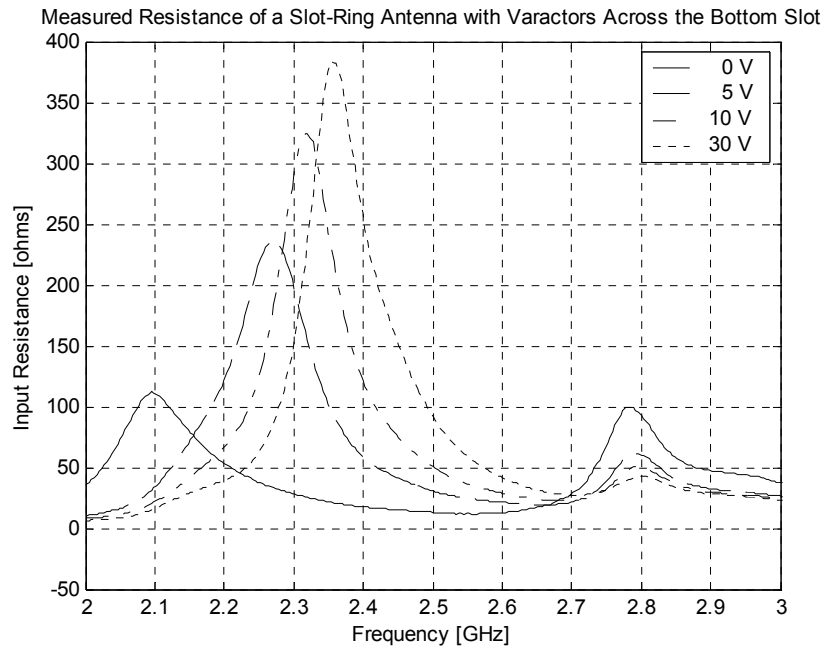


Figure 4.2.19. Graph of the measured resistance of the 2.4-GHz slot-ring antenna with varactors connected to the bottom slot

The experiments in which the varactors were attached to the antenna's side slots and the one in which the varactor was attached to the antenna's bottom slot were combined on the same antenna configuration to see if it was possible to obtain a tunable dual mode slot-ring antenna. Just one modification was made to the antenna, which consisted of adding two very thin slots on the central conductor. Without the additional slots, the four capacitors would have had the same capacitance whenever a voltage is applied, avoiding tuning of the first and second resonant frequency in an independent manner.

The input reactance curves shown in Figure 4.2.20 illustrate a frequency shift at the second resonance clearer than the return loss curves, reason for which the return loss

curves are not included. The reactance curves revealed a 12.3 % frequency shift around 4.05 GHz, and no shift of the first resonant frequency was observed when the varactors attached to the side slots are varied from 1 pF to 3 pF while the ones connected at the bottom slot are set to 3 pF.

In addition, the simulations revealed a decrease of the input resistance around 4.05 GHz as the capacitance of the varactors attached to the side slots increases while the capacitance of the varactors attached to the bottom slot remains constant at 3 pF, as shown in Figure 4.2.21. There was no change observed in the input resistance at the first resonant frequency.

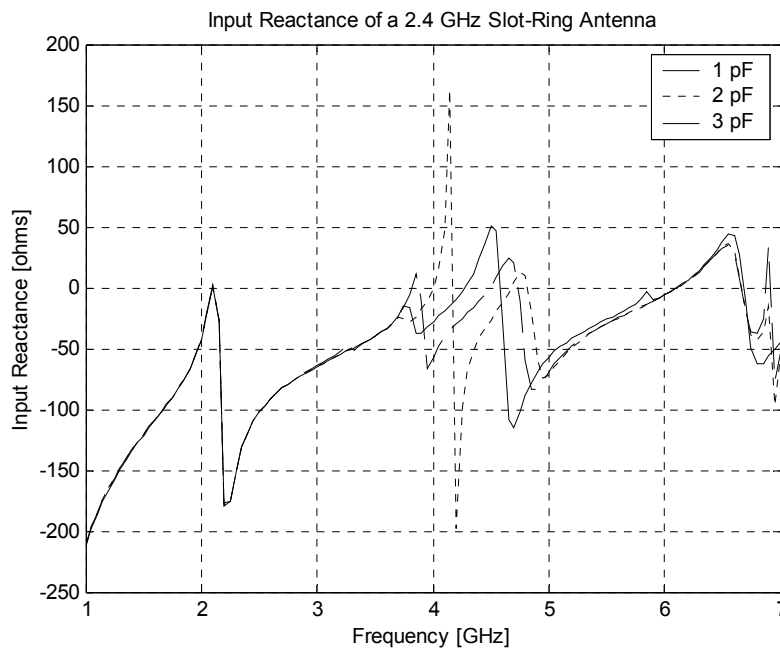


Figure 4.2.20. Input Reactance curves for a 2.4 GHz slot-ring antenna having a 3-pF capacitance at the bottom slot while the varactors on the sides varied from 1 pF to 3 pF.

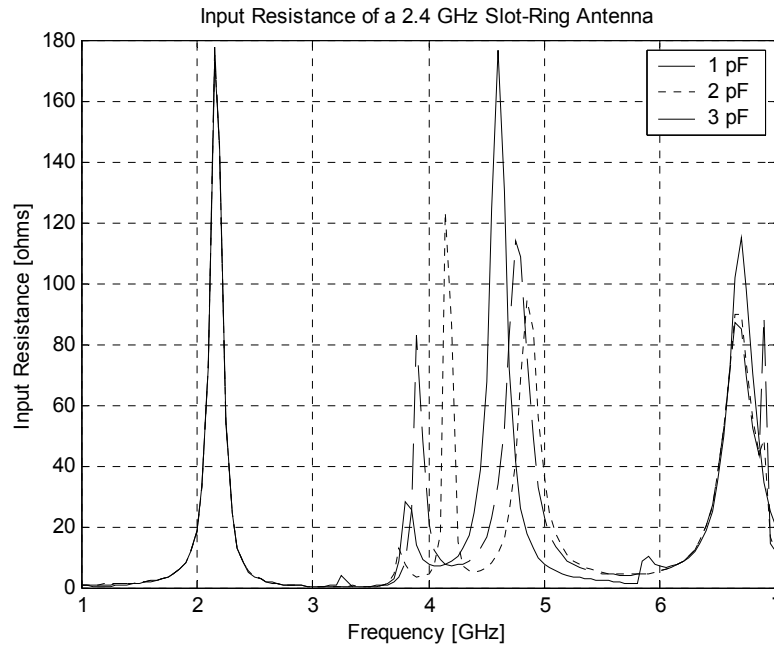


Figure 4.2.21. Input resistance curves for a 2.4 GHz slot-ring antenna having a 3-pF capacitance at the bottom slot while the varactors on the sides varied from 1 pF to 3 pF

The varactors attached to the side slots were set to 3 pF while the varactors at the bottom slot were varied from 1 pF to 3 pF to see if the first resonant frequency could be tuned. Simulations revealed a 7.3 % frequency shift around 2.18 GHz, as shown in Figure 4.2.22; nevertheless, the second resonant frequency is lost with an increase in the capacitance at the bottom slot. In addition, reflections at the second resonant frequency increased since the input resistance gets farther away from 50Ω , as shown in Figure 4.2.23.

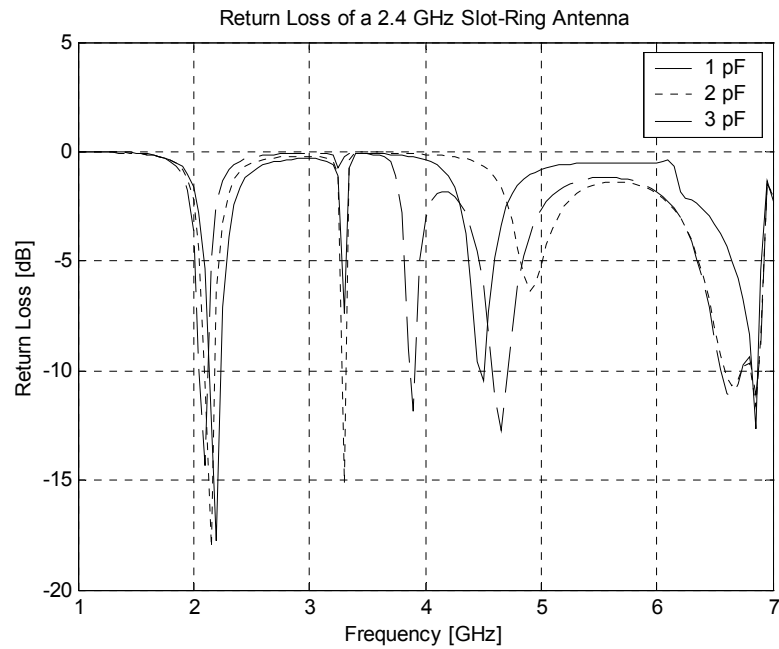


Figure 4.2.22. Return loss curves for a 2.4 GHz slot-ring antenna having a 3-pF capacitance at the side slots while the varactors on the bottom slot varied from 1 to 3 pF

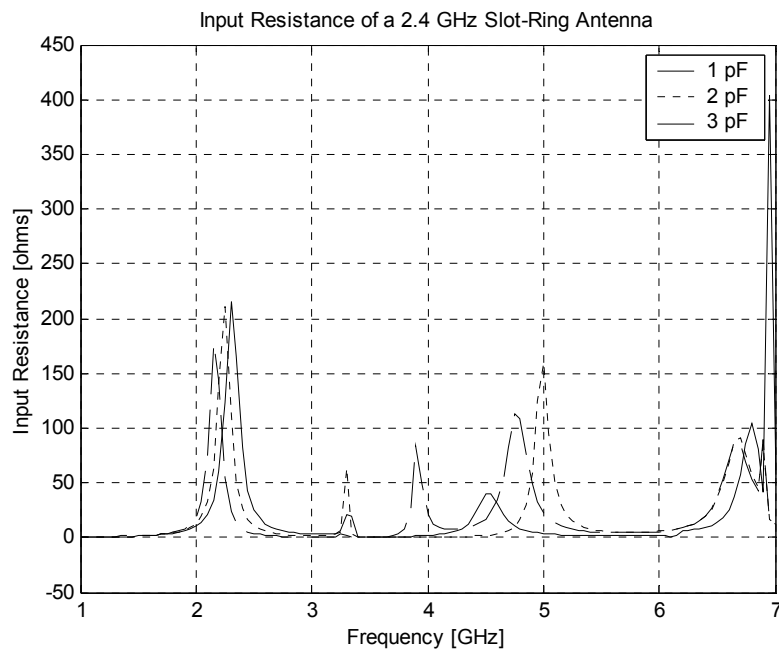


Figure 4.2.23. Input resistance curves for a 2.4-GHz slot-ring antenna having a 3-pF capacitance at the side slot while the varactors on the bottom varied from 1 pF to 3 pF.

4.2.4 Experiments with Varactors on a 6-GHz Rectangular Slot-Ring Antenna

To verify the tunable dual mode characteristic of a slot-ring antenna, another antenna was designed with the same procedure described in Section 3.2.4. The antenna was designed to operate at 6 GHz over a substrate with a relative permittivity of 6 and a thickness of 0.635 mm. It was tested in three different configurations: with varactors attached to the side slots, to the bottom slot, and to the side and bottom slots in the same configuration. The GVD90001 was used since the SMV1405 works for frequencies up to 4 GHz. The dimensions of the 6-GHz slot-ring antenna are described in Table 4.2.4.

Table 4.2.4. 6-GHz Slot-Ring Antenna Dimensions

6-GHz Slot-Ring Antenna Dimensions (mm)	
w_1	1.00
w^\dagger	1.00
L_1	9.75
L_2	9.75
w_f	1.82
s_f	0.25
L_f	2.00

[†] means that $w_2 = w_3 = w_4 = w$.

With the help of an open stub the first resonant frequency of the antenna was matched to 50 Ω , as shown in Figure 4.2.24. Simulations predicted the first resonant frequency at 6 GHz with a 5.5 % bandwidth. Return loss curves also predicted low reflections not only at the first but also at a second resonant frequency (11 GHz); therefore, the input resistance at the second resonance is close to 50 Ω . The input

resistance curve in Figure 4.2.25 revealed 10Ω at 10.1 GHz, which suggest that an increase of the upper slot width will increase the resistance up to 50Ω .

Once the antenna was designed, a set of varactors was attached to each side slot to see if tuning of the second resonant frequency could be achieved. The second resonance was matched with an upper slot width of 1.75 mm. The varactor used for the experiments, a GVD90001 super hyperabrupt varactor, has a capacitance range from 1 pF to 36 pF when a reversed voltage is varied from 1 V to 12 V.

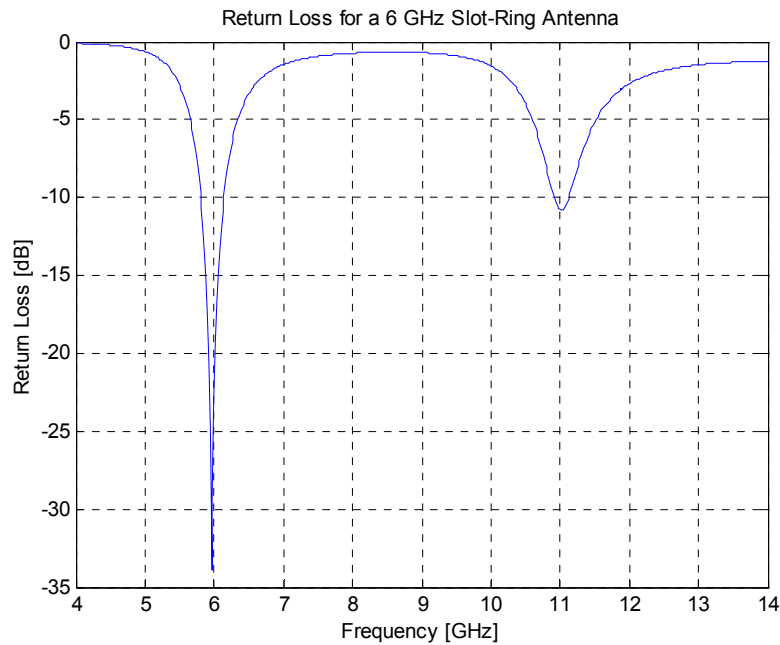


Figure 4.2.24. Graph of the return loss for the 6-GHz slot-ring antenna without varactors

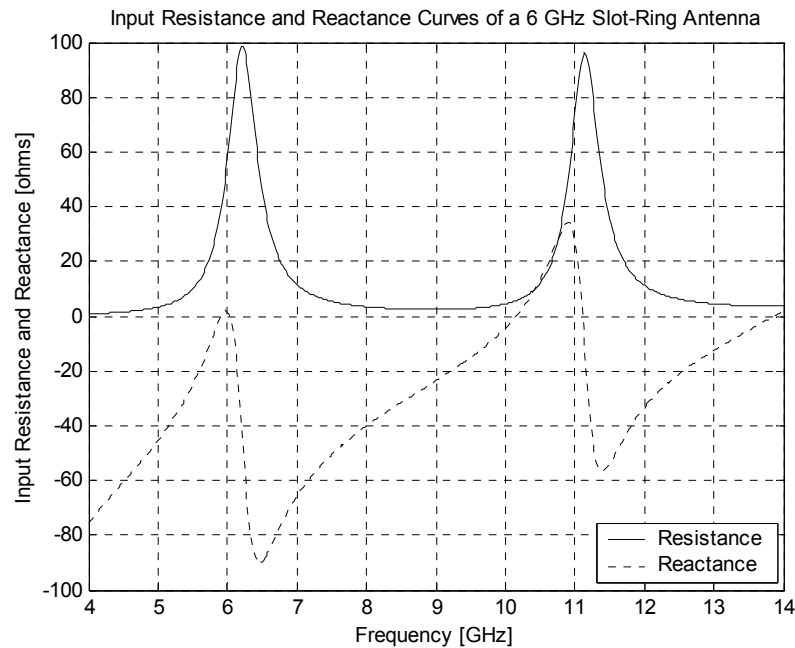


Figure 4.2.25. Resistance and reactance curves of the 6-GHz slot-ring antenna without varactors

Results predicted that when the capacitance is changed from 1 pF to 4 pF, it creates a tuning effect only at the second resonant frequency. Return loss results in Figure 4.2.26 illustrate a frequency shift from a higher value to a lower value at the second resonant frequency when the capacitance was increased from 1 pF to 3 pF. As the capacitance increases from 3 pF to a higher value the second resonant frequency mixes with the first resonant frequency. The second resonant frequency was tuned over a 40 % bandwidth around 8 GHz. Meanwhile, the first resonant frequency remains unchanged.

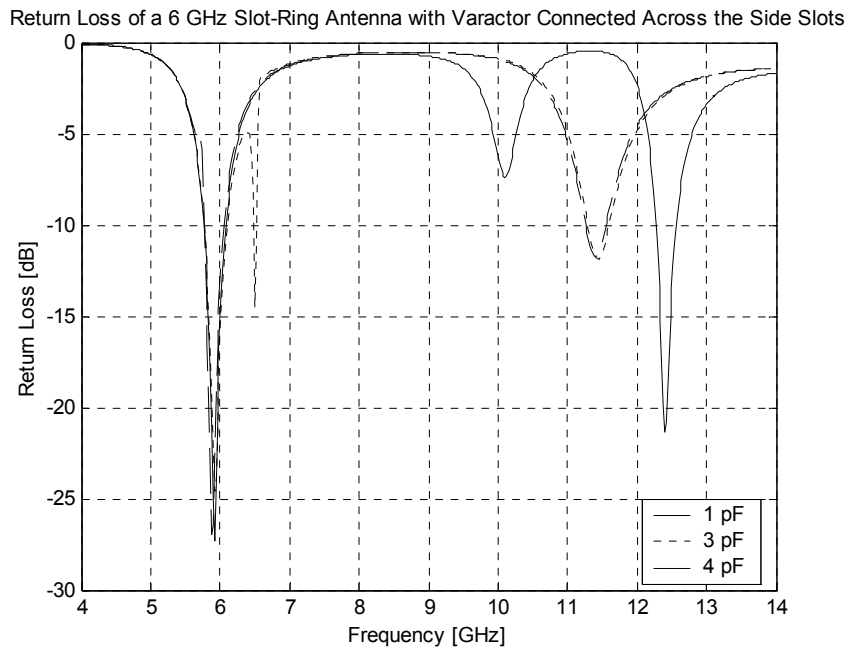


Figure 4.2.26. Graph of the return loss of the 6-GHz slot-ring antenna with varactors connected at each side slot

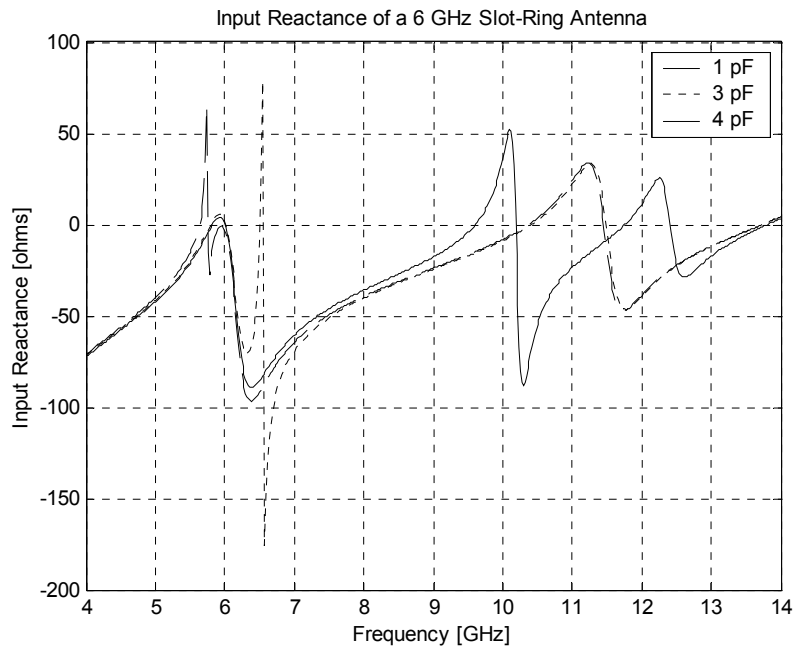


Figure 4.2.27. Graph of the input reactance curves of a 6-GHz slot-ring antenna with varactors connected at each side slot

The input reactance curves in Figure 4.2.27 give a better look of the second resonant frequency shift, going from 9.6 GHz to 6.4 GHz as the capacitance is increased from 1 pF to 3 pF. The first resonant frequency remained constant just like the 2.4 GHz slot-ring antenna behaved. On the other hand, the input resistance around the first resonant frequency did not change either, but it did around the second resonant frequency, as shown in Figure 4.2.28. Nevertheless, the input resistance at exactly the resonant frequency decreased, getting closer to 50 Ω since the reflections decreased as the capacitance increased.

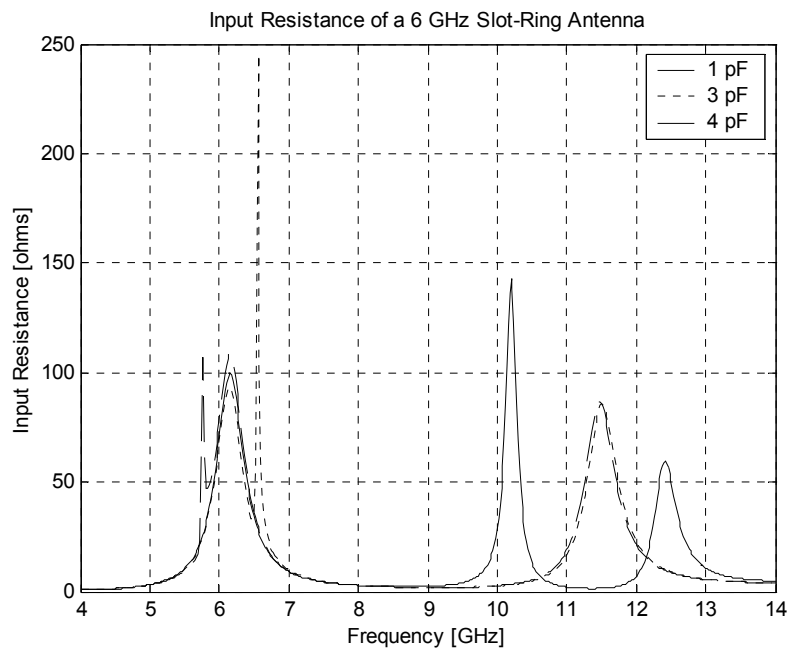


Figure 4.2.28. Graph of the input resistance curves of a 6-GHz slot-ring antenna with varactors connected at each side slot

Then, a set of varactors was attached to the bottom slot to check if the first resonant frequency could be tuned behaving just like the 2.4-GHz slot-ring antenna. The return loss curves in Figure 4.2.29 predicted such frequency shift not only at the first resonance but also at the second resonant frequency with reflections below -10 dB at both bands as the varactors were varied from 1 pF to 6 pF. However, as the capacitance increased so did the reflections, reason for which simulations with higher capacitance values were not performed.

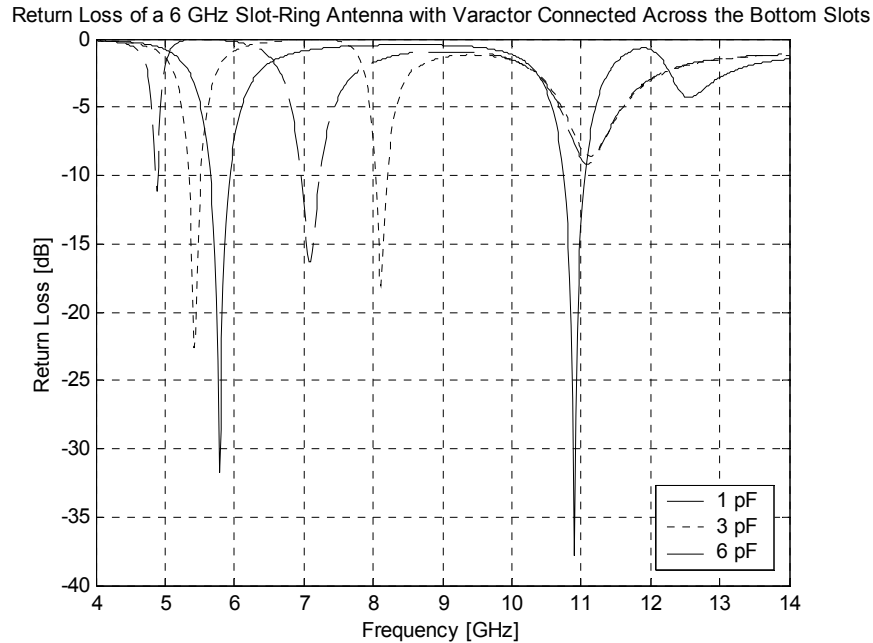


Figure 4.2.29. Graph of the return loss of the 6-GHz slot-ring antenna with varactors connected to the bottom slot

The input reactance curves in Figure 4.2.30 recorded a 16.8 % frequency shift around 5.35 GHz as well as 25 % frequency shift around 7.2 GHz. However, as the capacitance is increased the first resonant frequency is lost, making it tunable only in the 1 pF to 6 pF capacitance range. Besides, the input resistance in Figure 4.2.31 kept values around 50Ω at both frequency bands as suggested by the return loss curves.

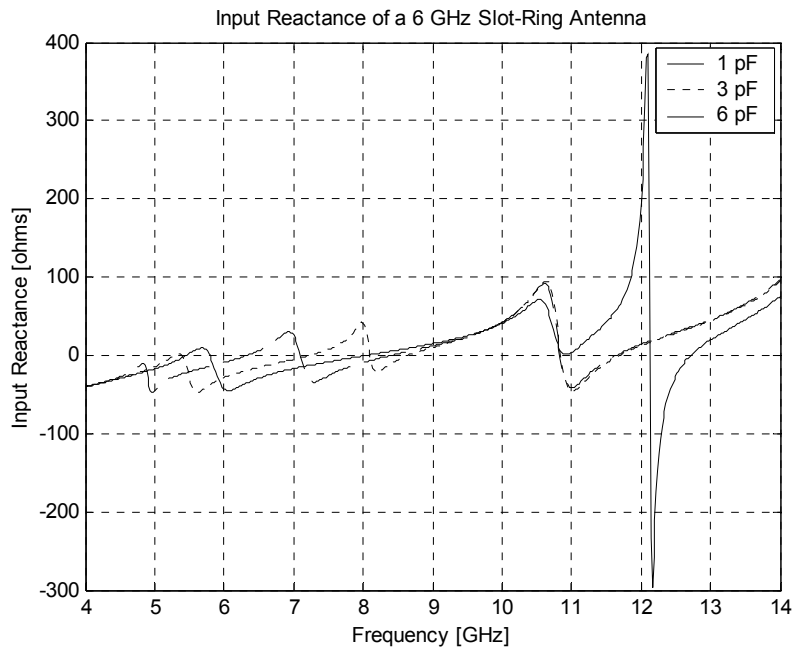


Figure 4.2.30. Graph of the input reactance curves of a 6-GHz slot-ring antenna with varactors connected to the bottom slot

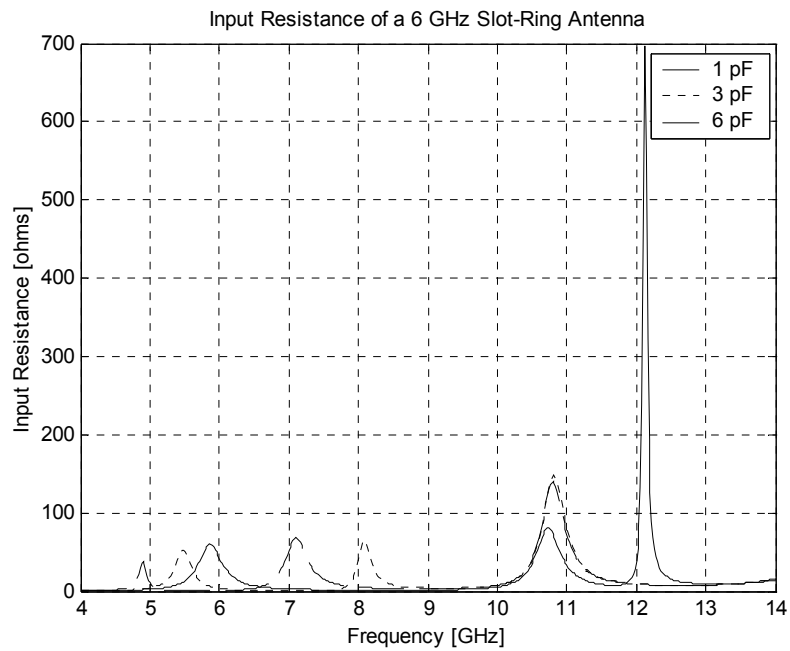


Figure 4.2.31. Graph of the input resistance curves of a 6-GHz slot-ring antenna with varactors connected to the bottom slot

4.3 Effect of a Short and Open-Circuited Stub on a Slot-Ring Antenna

Short and open-circuited stubs have been a powerful matching technique used on slot and microstrip antenna designs. The stub is designed to match the real input impedance of an antenna to a certain resistance value in order to eliminate reflections at a specific frequency. This effect can be achieved by the use of either a short or an open-circuited stub. However, in the 2.4-GHz slot-ring antenna and the 6-GHz slot-ring antenna design, the use of an open-circuited stub was chosen. Why an open stub was used instead?

Certain simulations were performed on the 2.4-GHz antenna, in which the first resonant frequency could be matched as the length of the short-circuited stub was increased. The antenna layout is shown in Figure 4.3.1. As the length of the stub, l_s , was increased so did the reflections at the second resonant frequency. Return loss curves in Figure 4.3.2 illustrate short-circuited stub effect on the antenna response. The lowest reflections at the first resonant frequency were recorded with a short-circuited stub length of 10 mm; however, matching at the second resonant frequency was completely lost. Note that as the stub length is increased from 10 to 13 mm the reflections around 2.7 GHz start to increase as the reflections at the second resonant frequency decreased again.

The input resistance curves in Figure 4.3.3 show a high increase in resistance at the second resonant frequency as l_s is increased which explains the high reflections observed at the return loss curves. Zooming in the input resistance from 2 GHz to 3 GHz in Figure 4.3.4, it can be seen that the resistance at 2.7 GHz, where the lowest reflections were recorded, approaches 50Ω with l_s equal to 10 mm. The input impedance curves, in

Figure 4.3.5, shows a frequency shift from 3.2 to 4.4 GHz as the length of the stub decreases while the first resonant frequency remains unchanged.

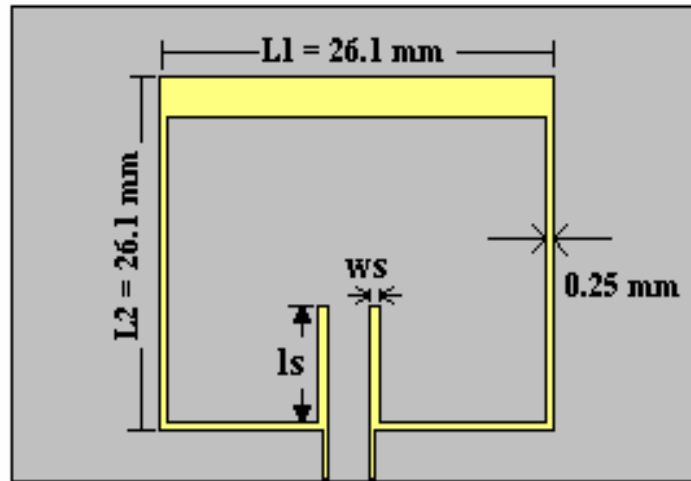


Figure 4.3.1. 2.4 GHz antenna layout matched to 50Ω with a short-circuited stub

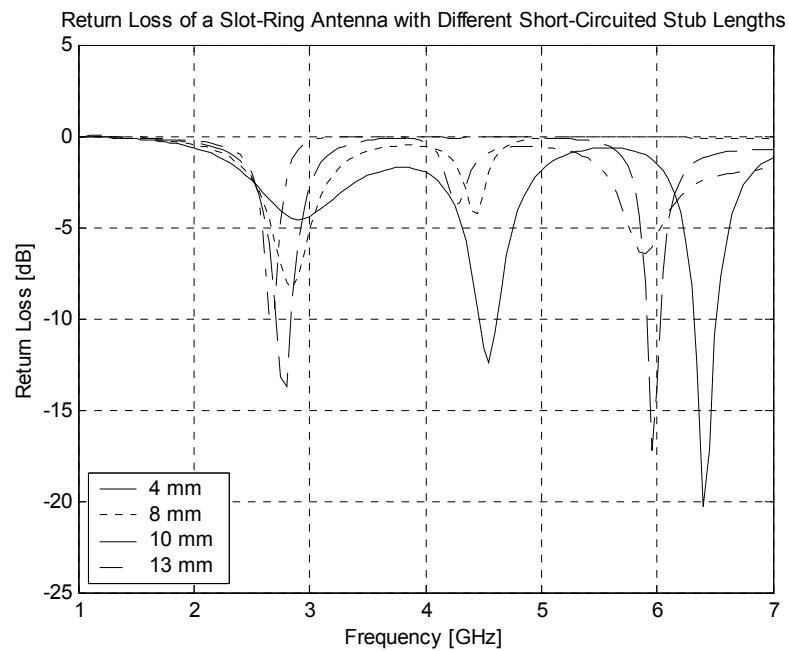


Figure 4.3.2. Return loss curves of a slot-ring antenna with different short-circuited stub lengths

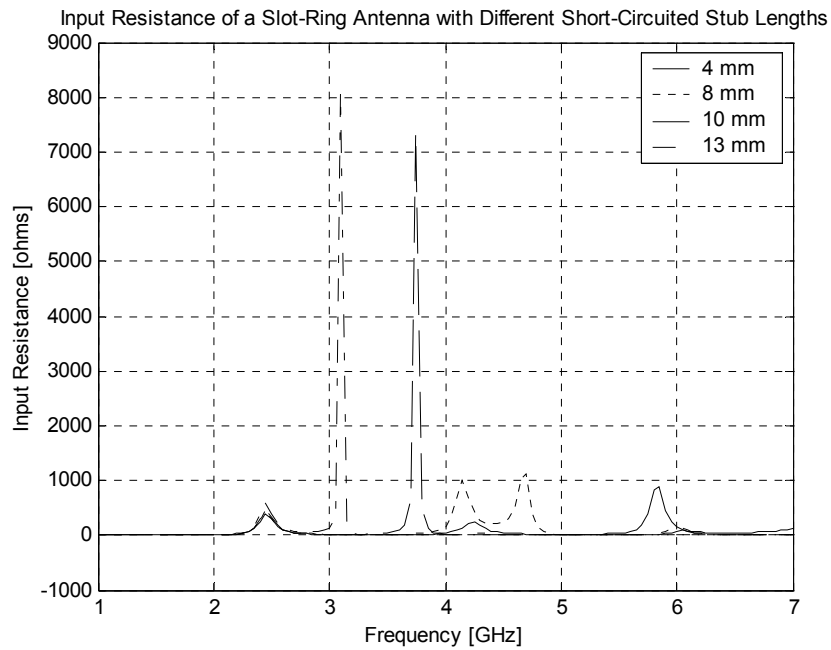


Figure 4.3.3. Input resistance curves of a slot-ring antenna with different short-circuited stub lengths

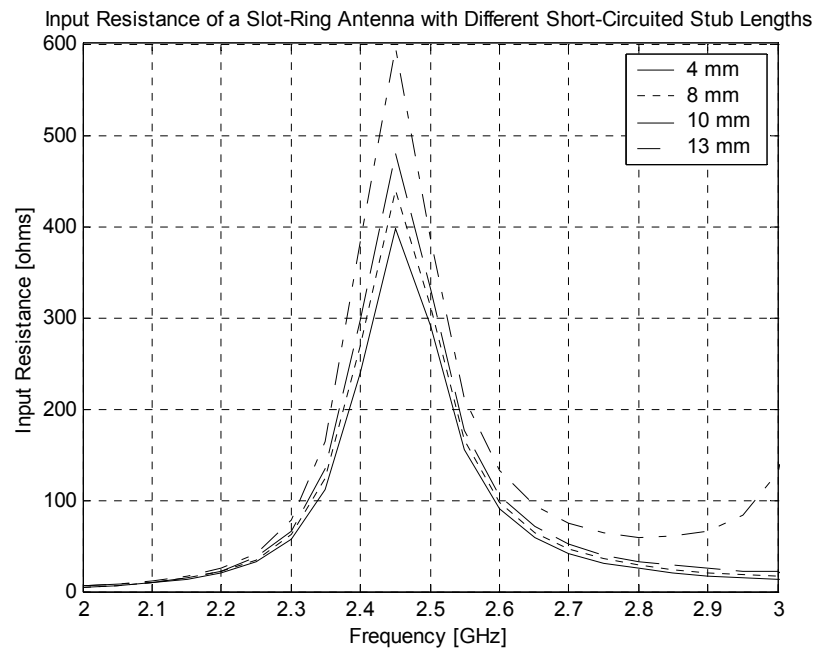


Figure 4.3.4. Input resistance curves around the first resonant frequency of a slot-ring antenna with different short-circuited stub lengths

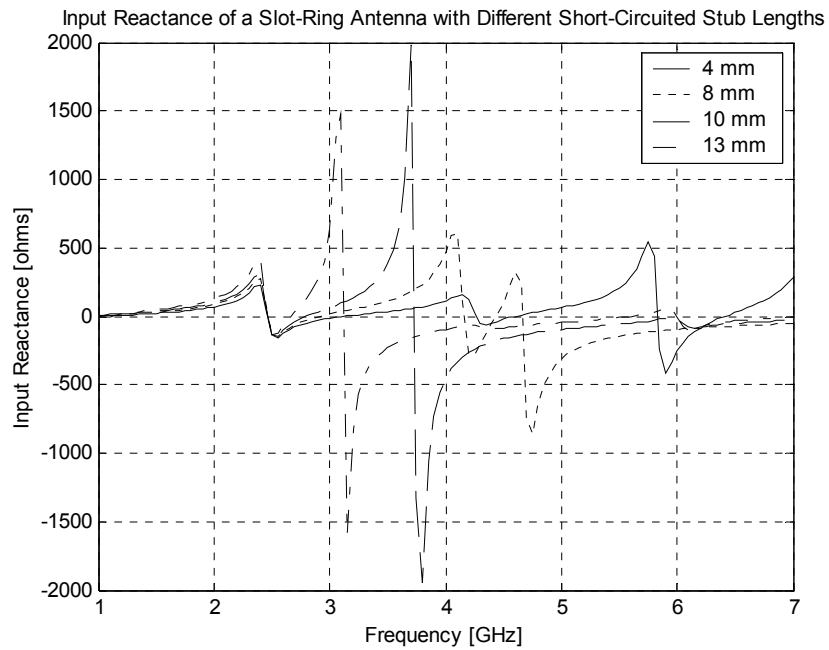


Figure 4.3.5. Input reactance curves of a slot-ring antenna with different short-circuited stub lengths

Taking as a reference the 2.4-GHz slot-ring antenna with l_s equal to 10 mm, several simulations were made in which the width of the short-circuited stub, w_s , was changed to check the effect in the antenna response. In Figure 4.3.6, return loss curves revealed a decreased in reflections around 2.7 GHz as the width is varied from 0.50 mm to 1.25 mm. In other words, the input resistance at 2.7 GHz is approaching 50Ω . Moreover, the resistance curves in Figure 4.3.7 revealed a decrease of $2.5 \text{ k}\Omega$ at the second resonance with a 0.75-mm w_s change.

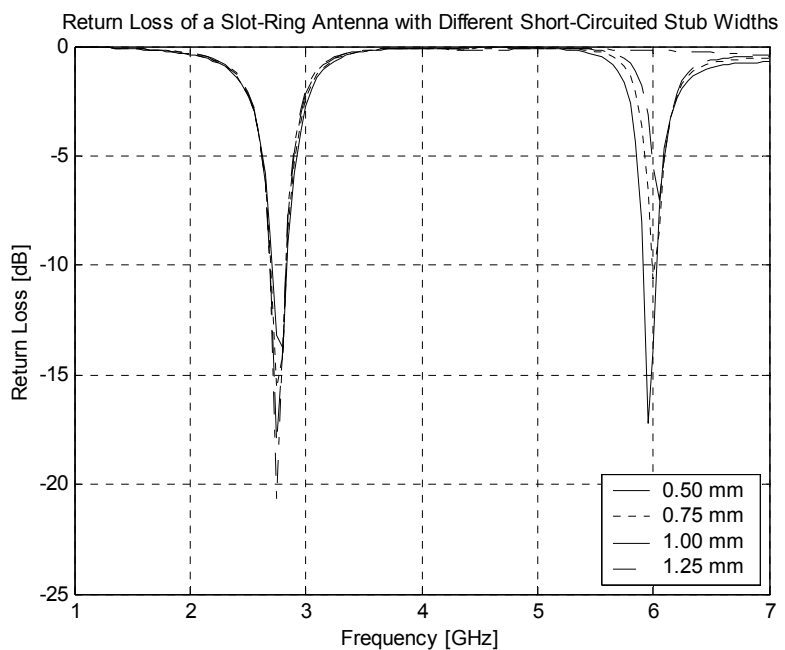


Figure 4.3.6. Return loss curves of a slot-ring antenna with different short-circuited stub widths

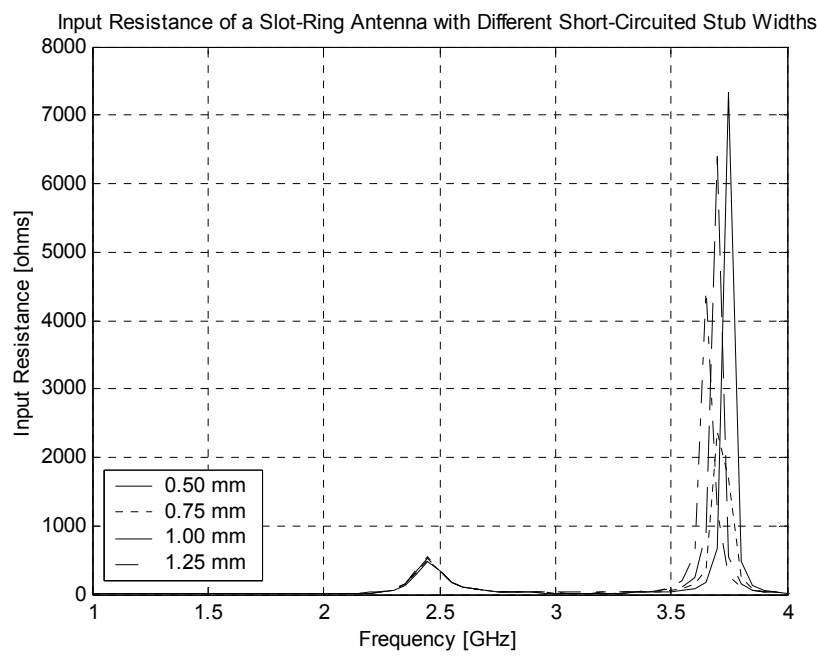


Figure 4.3.7. Input resistance curves of a slot-ring antenna with different short-circuited stub widths

On the other hand, the employment of an open-circuited stub in the 2.4-GHz slot-ring antenna design provided good input matching around 2.4 GHz without deteriorating the input matching around the second resonant frequency. As l_s is increased from 1 mm to 3 mm, reflections around 2.4 GHz decrease; however, they start to increase for l_s greater than 3 mm, as illustrated in Figure 4.3.8. There is a trade off between the reflections at the first and second resonant frequencies but matching at both frequencies can still be achieved with relatively small dimensions, l_s and w_s . The width of the stub was kept constant at 0.5 mm for all simulations. The input resistance around the first and second resonant frequencies remains close to the vicinity of 50Ω , which explain the low reflections, observed in the return loss curves. In addition, Figure 4.3.9 revealed that as l_s is increased, the resistance at both frequencies also increased. Meanwhile, the first and second resonances are lost as l_s decreases, as shown in Figure 4.3.10.

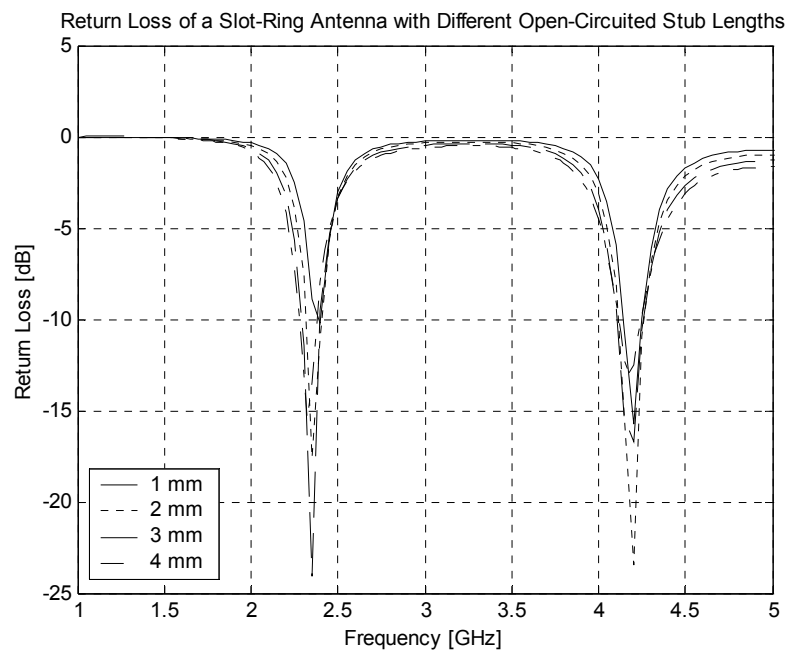


Figure 4.3.8. Return loss curves of a slot-ring antenna with different open stub lengths

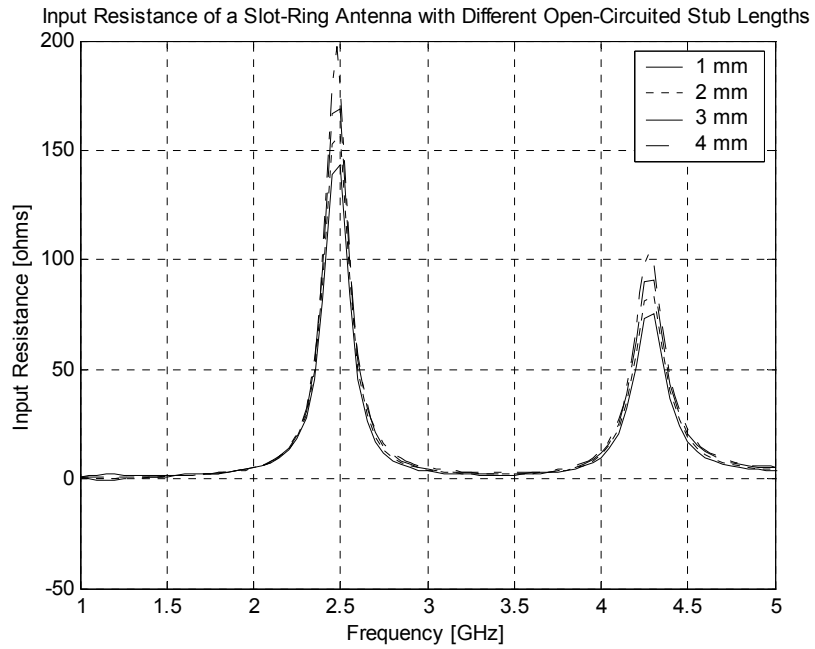


Figure 4.3.9. Input resistance of a slot-ring antenna with different open stub lengths

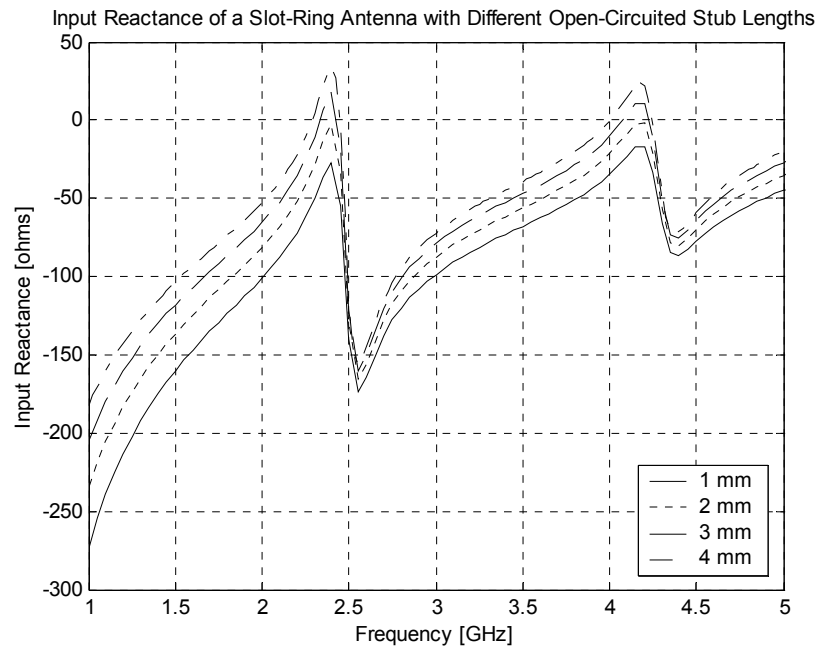


Figure 4.3.10. Input reactance of a slot-ring antenna with different open stub lengths

The slot-ring antenna response with a 3-mm open stub length was analyzed for different stub width values. The antenna layout is shown in Figure 4.3.11. The stub width, w_s , was increased from 0.25 mm to 0.75 mm. Simulations in Figure 4.3.12 revealed an increase in reflections around the second resonant frequency but still below -10 dB. Meanwhile, reflections at the first resonant frequency had its lowest value with a 0.5-mm w_s . Figure 4.3.13 illustrates the input resistance close to 50Ω around 2.4 and 4.2 GHz. For this reason, the open-circuited stub, with a 3-mm l_s and a 0.5-mm w_s , was implemented in the slot-ring antenna design.

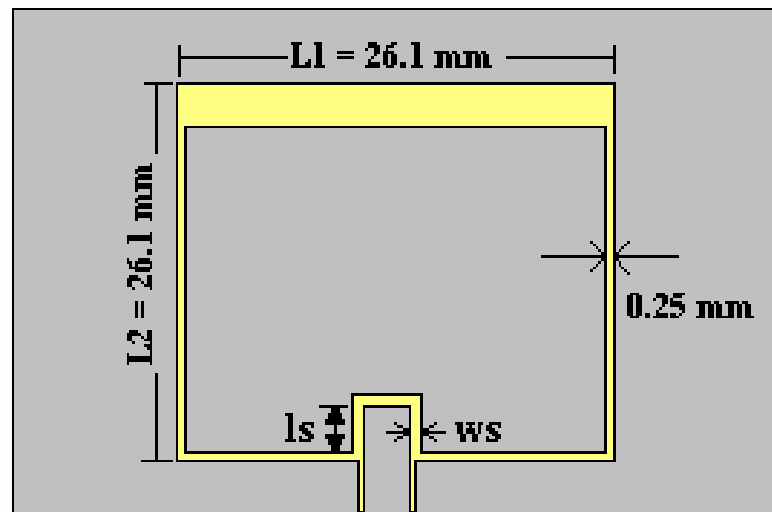


Figure 4.3.11. 2.4 GHz antenna layout matched to 50Ω with an open-circuited stub

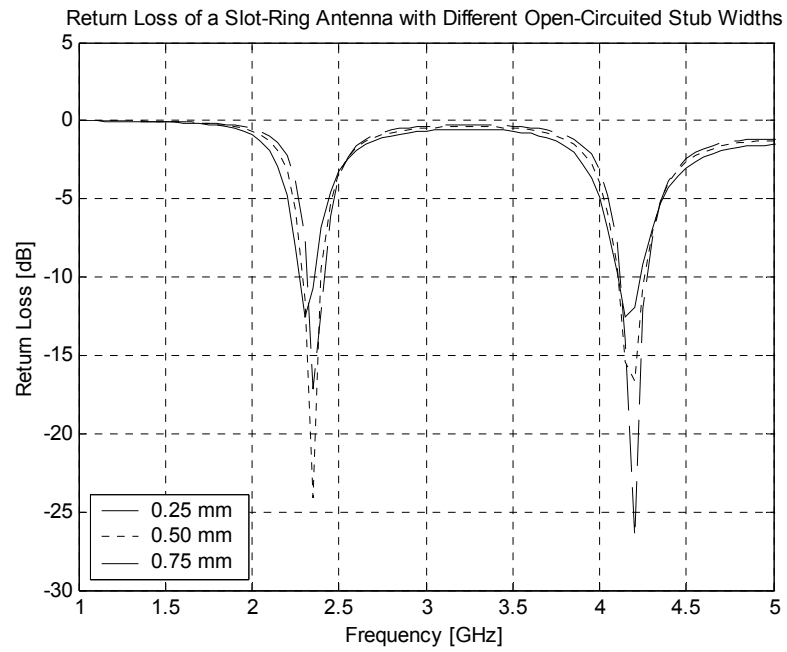


Figure 4.3.12. Return loss curves of a slot-ring antenna with different open stub widths

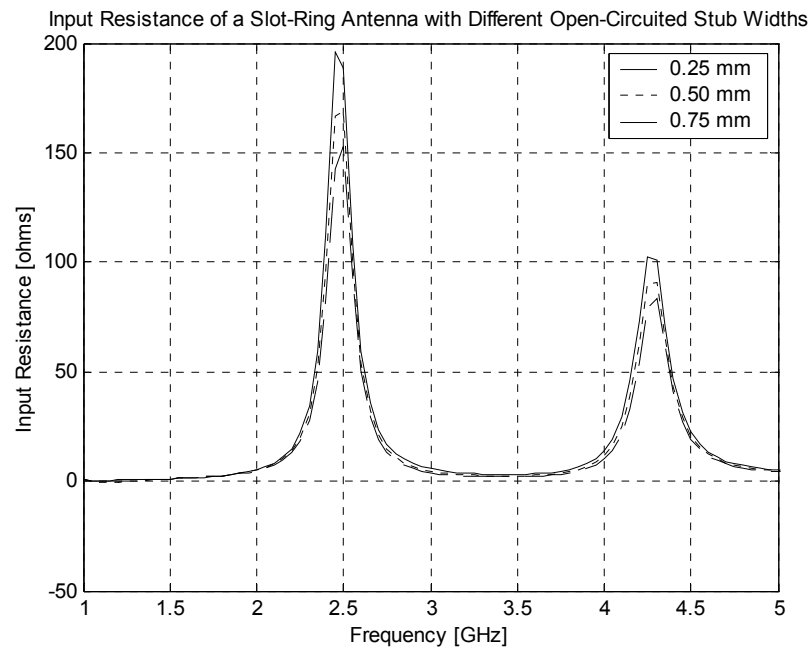


Figure 4.3.13. Input resistance curves of a slot-ring antenna with different open stub widths

4.4 Gain, Polarization and Radiation Pattern

Gain, polarization and radiation pattern were also taken into account when analyzing the rectangular slot-ring antenna response. Due to the electric field distribution at the first resonance (2.3 GHz), shown in Figure 4.4.1, the electric fields at the side slots were canceled, obtaining the major field component in the y-direction. Therefore, when the radiation pattern is plotted in the plane of $\phi = 0^\circ$, the maximum amount of energy will be ϕ -component of the electric field vector, as shown in Figure 4.4.2. The antenna is located along the horizontal axis of the graph with the substrate layer on top of the metallization layer. The graph shows that the slot-ring antenna radiates the same amount of power to both sides of the ground plane. Simulations recorded a 2.4-dB gain at $\theta = 0^\circ$.

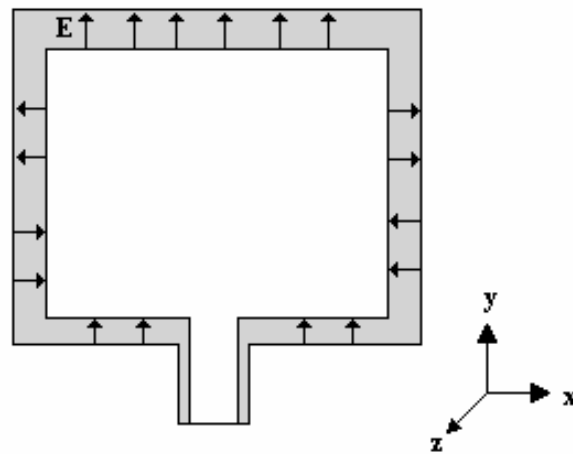


Figure 4.4.1. Electric field distribution of the slot-ring antenna at 2.3 GHz

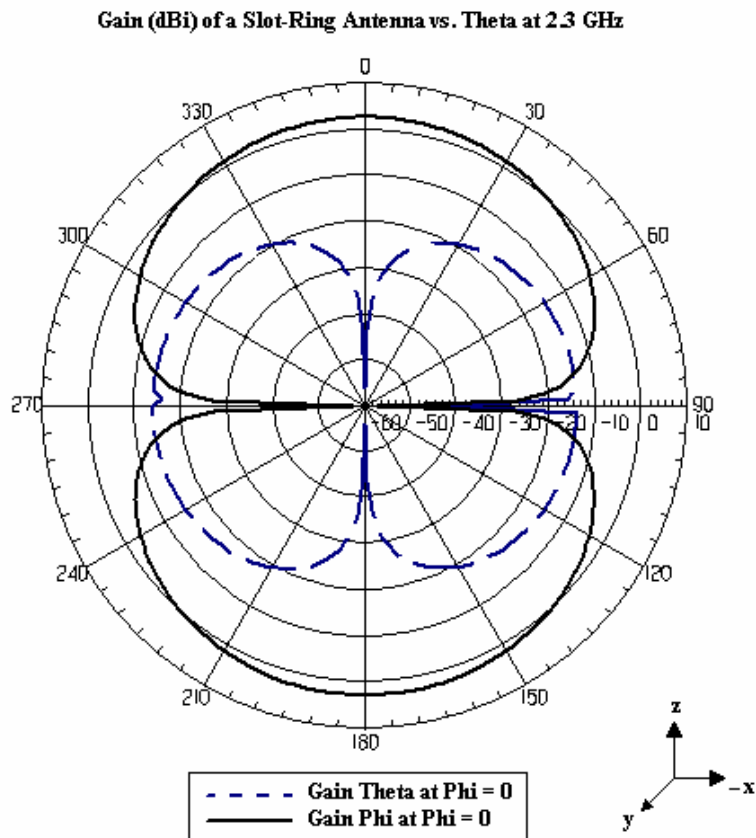


Figure 4.4.2. Gain (dBi) of a slot-ring antenna vs. theta at 2.3 GHz and $\phi = 0^\circ$

The radiation pattern plotted in the plane $\phi = 90^\circ$ has the major field component oriented in the θ -direction. The maximum recorded gain is 2.56 dBi at $\theta = 0^\circ$, as shown in Figure 4.4.3. Note that the electric field has only one component, suggesting that the antenna is linearly polarized. No change in the radiation pattern was recorded at all whenever the capacitance and the varactor position were changed.

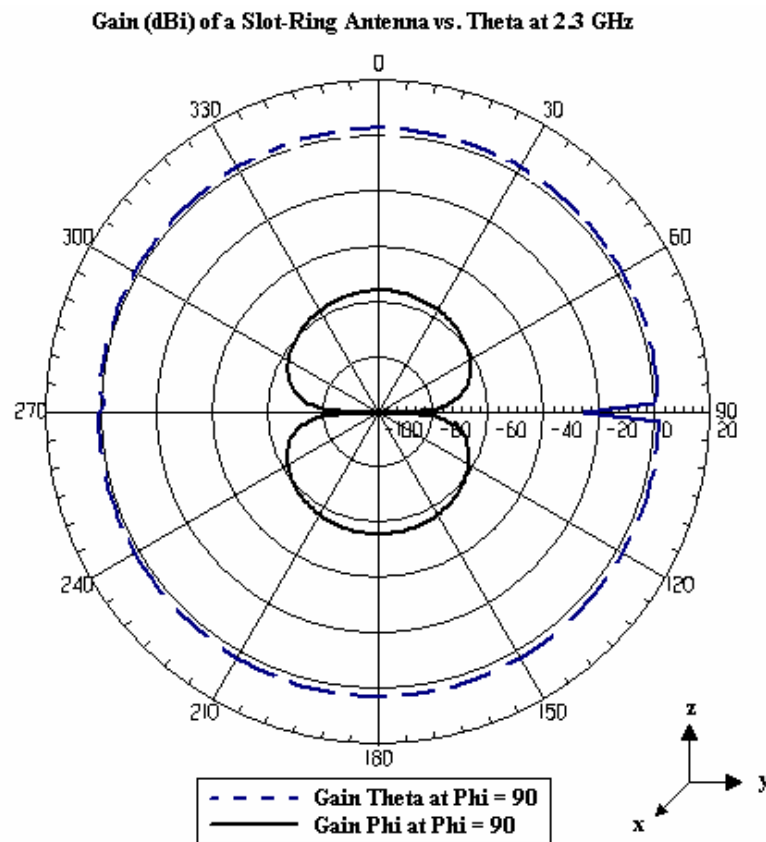


Figure 4.4.3. Gain (dBi) of a slot-ring antenna vs. theta at 2.3 GHz and $\phi = 90^\circ$

On the other hand, at the second resonant frequency (4.15 GHz), the antenna presents a different electric field distribution, as shown in Figure 4.4.4. Even though the electric fields across the bottom and upper slots are directed in opposite directions, these fields do not cancel out since the magnitude of the electric field at the bottom slot is greater than the fields at the upper slot. Thus, there is a field component in the ϕ -direction at $\phi = 0^\circ$ and $\theta = 0^\circ$, as shown in Figure 4.4.5. Again, the electric fields at the side slots canceled out.

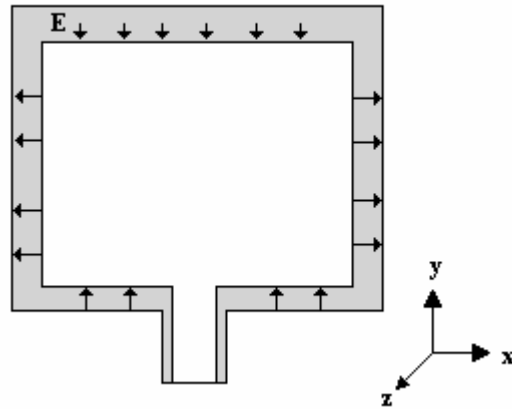


Figure 4.4.4. Electric field distribution of the slot-ring antenna at 4.15 GHz

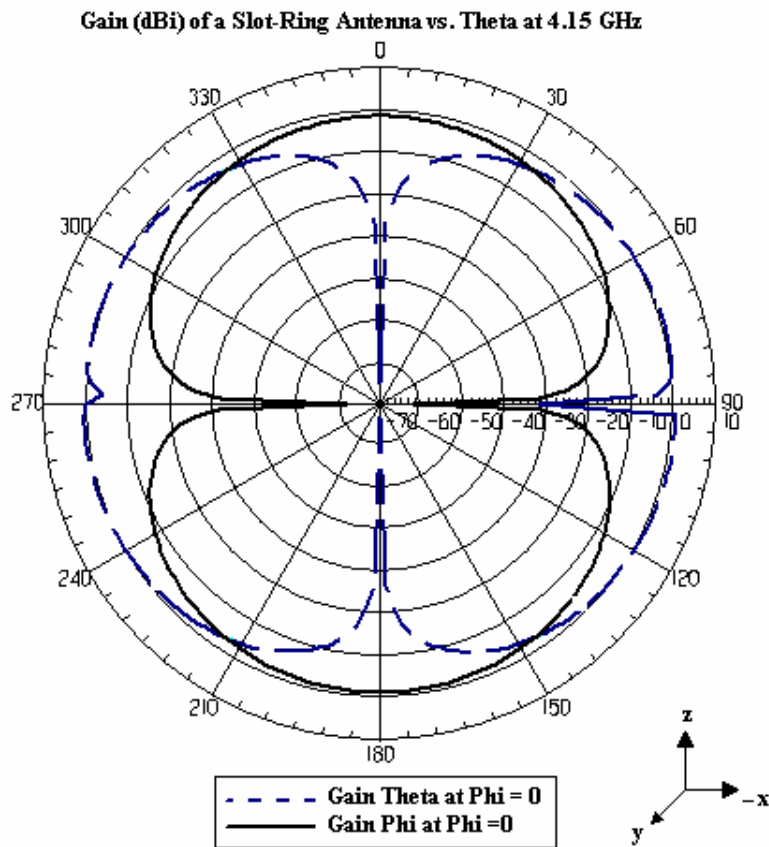


Figure 4.4.5. Gain (dBi) of a slot-ring antenna vs. theta at 4.15 GHz and $\phi = 0^\circ$

The maximum gain at the second resonant frequency was observed in the plane where $\phi = 90^\circ$. As illustrated in Figure 4.4.6, the maximum radiation recorded is 3.76 dBi at $\theta = 74^\circ$ and $\theta = 94^\circ$.

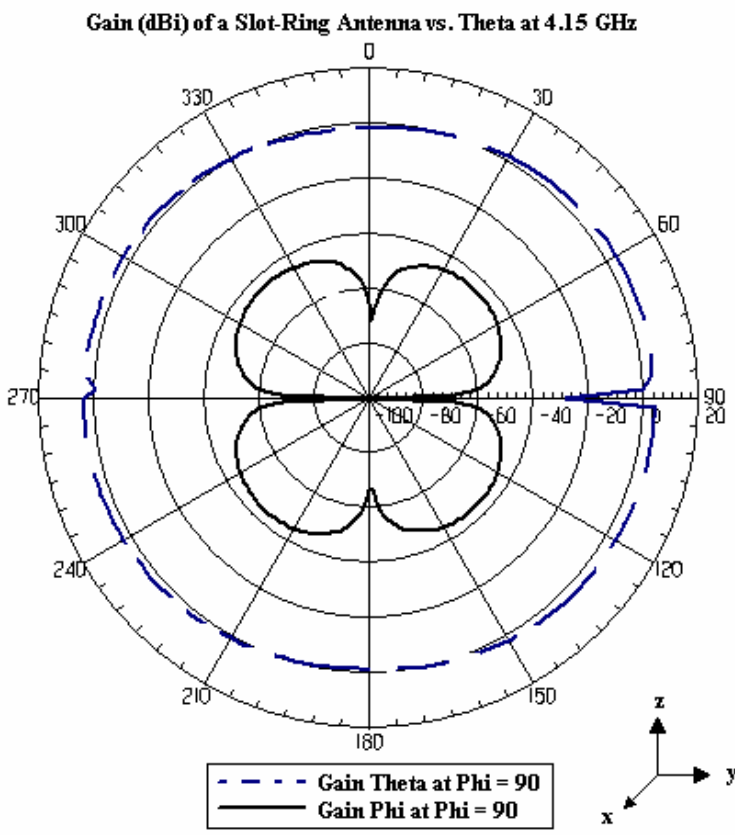


Figure 4.4.6. Gain (dBi) of a slot-ring antenna vs. theta at 4.15 GHz and $\phi = 90^\circ$

The gain was also plotted in the plane where $\phi = 45^\circ$ since at this position the electric fields change direction. No positive gain was achieved in either direction since all the fields canceled out, as shown in Figure 4.4.7.

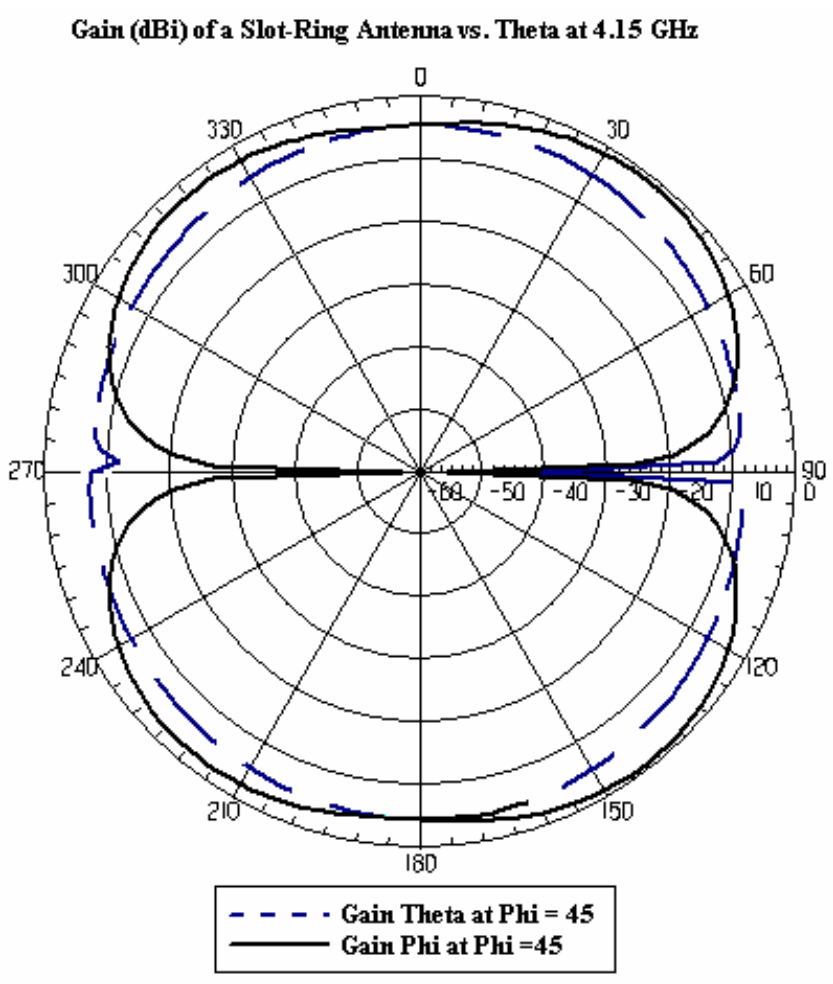


Figure 4.4.7. Gain (dBi) of a slot-ring antenna vs. theta at 4.15 GHz and $\phi=45^\circ$

4.5 Summary

Throughout this chapter, the tuning ability of a slot-ring antenna was physically and electrically analyzed. First, a partial characterization of a rectangular slot-ring antenna was performed in order to predict the dimensions that strongly contribute with a frequency shift. It was possible to match the second resonant frequency of the slot-ring antenna by simply adjusting its upper slot. Meanwhile, the first resonant frequency was

matched to 50Ω with an open-circuited stub. Matching of both frequencies made possible the design of a multiband slot-ring antenna.

Two different slot-ring antenna designs proved that it is possible to tune both resonant frequencies with the implementation of varactors. Tuning of the first resonant frequency was achieved when varactors were attached to the bottom slot. The second resonant frequency was tuned when varactors were placed at both side slots. Prototypes were fabricated and compared with simulated results. In addition, gain, polarization and radiation pattern were also taken into account when analyzing the rectangular slot-ring antenna response.

Chapter 5. Conclusions and Recommendations

5.1 Conclusions

A rectangular slot-ring antenna was tuned over a band of frequencies using varactors as the tuning element. A partial characterization of the rectangular slot-ring antenna was done, in which the antenna dimensions were changed to identify those dimensions that strongly contribute with a frequency shift. If the four slots widths of slot-ring antenna are varied at the same time while the perimeter remains unchanged, tuning will be achieved at the first and second resonant frequencies. As the width of the slots is reduced, the first and second resonant frequencies will decrease. On the other hand, if the four widths are varied along with their corresponding perimeter λ_g no frequency shift will be observed at the first and second resonance because each configuration has the one-wavelength perimeter that corresponds to its width. It was found that a 50- Ω input impedance matching around the second resonant frequency is achieved by adjusting the width of the upper slot only. The input impedance at the first resonant frequency was matched introducing an open-circuited stub at the feeding line. A short-circuited stub was not used because as the length of the stub was increased to match the impedance at the first resonance, matching at the second resonance was completely lost.

In addition, bandwidth enhancement is achieved if the ratio between the upper slot and the remaining slots width increases. Therefore, if the width of the upper slot is kept constant while the width of the remaining slots is decreased input impedance

matching will be accomplished as well as bandwidth enhancement. If only one of the side slots is varied, no variation will be observed in either resonant frequencies or input resistance. On the other hand, if the width of the bottom slot is changed, there will be a shift at the first and second resonant frequencies. Moreover, the second resonant frequency could be tuned if both side slots are equally changed.

Based on these results a 2.4-GHz rectangular slot-ring antenna and a 6-GHz rectangular slot-ring antenna were designed and tuned with the help of varactors. A first set of varactors was connected across both side slots. The second resonant frequency of the 2.4-GHz slot-ring antenna was tuned over a 22 % bandwidth around 3.7 GHz, while the first resonant frequency remained unchanged. A similar behavior was observed with the measured prototype the second resonance was lost. The second resonant frequency of the 6-GHz slot-ring antenna was tuned over a 40 % bandwidth around 8 GHz. The varactors connected across the bottom slots tuned the first resonant frequency of the 2.4-GHz slot-ring antenna over a 4.4 % bandwidth around 2.25 GHz. The antenna prototype registered a 2.5 % frequency shift around 2.35 GHz and an 8.1 % tuning around 2.46 GHz. The 6-GHz rectangular slot-ring antenna recorded a 16.8 % frequency shift around 5.35 GHz as well as 25 % frequency shift around 7.2 GHz. The tunable dual mode slot-ring antenna configuration registered 12.3 % frequency shift around 4.05 GHz was achieved, while no shift of the first resonant frequency was observed when the varactors attached to the side slots were varied. In addition, a 7.3 % frequency shift around 2.18 GHz could be achieved when the varactors attached the bottom slot were varied.

5.2 Recommendations

Still, a full characterization of rectangular slot-ring antennas has not yet been elaborated. A Design of Experiments (DOE) could be a helpful tool to be used in a full characterization process. In addition, to switch from a linear to a circular polarization, diodes could be included in an antenna configuration fed with two coplanar waveguide transmission lines with 90-degree phase shift. This tunable dual mode rectangular slot-ring antenna promises to offer good performance in many wireless applications. It can be used in applications where access to multiple systems through the same device is required, providing tuning around both operating frequencies in a simple antenna configuration.

References

- [1] Balanis, C. A., *Antenna Theory Analysis and Design*, John Wiley & Sons, Inc., New York, NY, pp. 64.
- [2] Carrasquillo-Rivera I., Popović, Z., and Rodríguez Solís, R. A., "Tunable Slot Antenna Using Varactors and Photodiodes," *IEEE Antennas and Propagation Society International Symposium 2003*, vol. 4, 2003, pp. 532-535
- [3] Forman, M. and Popović, Z., "A Tunable Second-Resonance Cross-Slot Antenna," *IEEE Antennas and Propagation Society International Symposium 1997*, vol. 1, 1997, pp. 18-21
- [4] Raman, S. and Rebeiz, G., "Single and Dual Polarized Millimeter-Wave Slot-Ring Antennas," *IEEE Transactions on Antennas and Propagation*, Nov. 1996, pp. 1438-1444
- [5] Gupta, K.C., Garg, R., Bahl, I., and Bhartia, P., *Microstrip Lines and Slotlines*. Artech House, Inc., Norwood, MA, pp. 269-274
- [6] Chang, K., *Microwave Ring Circuits and Antennas*. John Wiley & Sons, Inc., New York, NY, pp. 252-255
- [7] Minard, P., and Louzir, A., "A New Wide Frequency Band Feeding Technique of Annular Slot Antenna," *IEEE Antennas and Propagation Society International Symposium 2002*, vol. 1, 2002, pp. 406-409
- [8] Fries, M. K., Gräni, M., and R. Vahldieck, "Slot-Antenna with Switchable Polarization," *Antennas and Propagation Society International Symposium 2002*, vol. 2, 2002, pp. 440-443
- [9] Filipović, D. S. and Volakis, J. L., "Design of a multi-functional slot aperture (combo-antenna) for automotive applications," *Antennas and Propagation Society International Symposium 2002*, vol. 2, 2002, pp. 428-431
- [10] Misra, I. S. and Chowdry, S. K., "Study of impedance and radiation properties of a concentric microstrip triangular-ring antenna and its modeling techniques using FDTD method," *IEEE Transactions of Antennas and Propagation*, April 1998, pp. 531-537
- [11] Li, K., Cheng, C. H., Matsui, T., and Izutsu, M., "Coplanar patch antennas: principles, simulation and experiment," *Antennas and Propagation Society International Symposium 2001*, vol. 3, 2001, pp.402-405
- [12] Elsherbeni, A. Z., Eldek, A. A., Baker, B. N., Smith, C. E., and Kai-Fong, L., "Wideband coplanar patch-slot antennas for radar applications," *Antennas and Propagation Society International Symposium 2002*, vol. 2, 2002, pp. 436-439

- [13] Chin, P. L., Elsherbeni, A. Z., and Smith, C. E., "Characteristics of coplanar bow-tie patch antennas," *Antennas and Propagation Society International Symposium 2002*, vol. 1, 2002, pp. 398-401
- [14] Gupta, K.C., Garg, R., Bahl, I., and Bhartia, P., *Microstrip Lines and Slotlines*. Artech House, Inc., Norwood, MA, pp. 375-379
- [15] Snyder, H. L., 2000 Coplanar Transmission Line
<http://www.qsl.net/wb6tpu/si-list4/0443.html> Active on April 2000
- [16] Nave, C. R., 2000 Hyperphysics
<http://hyperphysics.phy-astr.gsu.edu/hbase/electronic/varactor.html> Active on 2000
- [17] American Microsemiconductor, Tutorials: Varactor Diode
<http://www.americanmicrosemi.com/tutorials/varactor.htm>
- [18] Gupta, K.C., Garg, R., Bahl, I., and Bhartia, P., *Microstrip Lines and Slotlines*. Artech House, Inc., Norwood, MA, pp. 285
- [19] López-Rivera, N and Rodríguez-Solís, R. A., "Impedance matching technique for microwave folded slot antennas," *Antennas and Propagation Society International Symposium 2002*, vol. 3, 2002, pp. 450-453